A Case Study of Severe Cloudburst Events in Denmark

Master thesis

By *Jonas Hermann Damsbo*

20th May 2021

Supervised by

Aksel Walløe Hansen and Niels Woetmann Nielsen

University of Copenhagen

UNIVERSITY OF COPENHAGEN

NAME OF INSTITUTE:	Niels Bohr Institute
NAME OF DEPARTMENT:	Physics of Ice, Climate and Earth (PICE)
AUTHOR(S):	Jonas Hermann Damsbo
EMAIL:	ftm147@alumni.ku.dk
TITLE AND SUBTITLE:	A Case Study of Severe Cloudburst Events in Denmark -
SUPERVISOR(S):	Aksel Walløe Hansen and Niels Woetmann Nielsen
HANDED IN:	20.05.2021
DEFENCE DATE:	09.06.2021

NAME Jonas Hermann Damsbo

SIGNATURE Jonas Damsbo

DATE 20-05-2021

Abstract

Research shows that extreme rain, including cloudbursts (more than 15 *mm* in 30 minutes), has become more frequent in Denmark. The climate atlas at DMI furthermore shows that in a future climate (year 2100), with expected levels of high CO_2 (RCP8.5) in the atmosphere, the amount of annual cloudbursts in Denmark will have increased by 70 % (the uncertainty ranges from 20 % to 150 %). This thesis investigates how cloudbursts occur under Danish weather conditions. Cloudbursts occur during deep moist convection and can cause major damage, such as floods. This thesis analyses seven different cases of cloudbursts from the past 25 years, and proposes an overview of how these weather phenomena can occur in Denmark. The analysis is primarily based on weather maps, satellite images, radar images and soundings. The analysis shows that cloudbursts in Denmark is a phenomenon that primarily occurs in the period May to September - typically in the afternoon or evening where sun forcing creating favorable conditions for convection during quasi-geostrophic forcing. Jets streaks also prove to be an important trigger for cloudbursts. In case 2, extratropical cyclogenesis in connection with quasi-geostrophic forcing is a factor. In some cases, orographic forcing also affects how the air interacts at the convergence lines. In Denmark, the severe cloudbursts generally organize as multicells, but in case 7 the cloudburst was likely a low-topped supercell. This thesis finds, that the synoptic situation that is particularly favorable for cloudbursts, is a deepening low pressure west of Denmark with cold and dry air, and a high pressure east of Denmark with warm and humid air. These air flows create very good conditions for potential or conditional instability when these air masses collide over Denmark. Thus, the conditions are set for thunder cells to form along a frontal zone. These thunder cells have the potential to develop cloudbursts.

Contents

Preface

This master thesis has been written at the University of Copenhagen at Physics of Ice, Climate and Earth (PICE), which is part of the Niels Bohr Institute. The thesis has been prepared in the period September 2020 to May 2021 and will be defended in June 2021. The thesis is a graduate project in meteorology.
The background for the thesis is an interest in extreme weather - and in particular for extreme precipitation, including cloudbursts, which will be the starting point of the analysis. The purpose is to analyze cloudbursts and extreme rain in Denmark and should provide an insight into how this can develop in Denmark.
The thesis would not have been realized without expert guidance from professor emeritus Aksel Walløe Hansen at the University of Copenhagen and senior scientist Niels Woetmann Nielsen from DMI. Thank you very much for your time and help. In addition, I would like to thank Thomas Bøvith from DMI for providing radar data and Bjarne Amstrup from DMI for help in finding previous soundings from Denmark, Germany and Sweden. I could not have gone through the thesis without good sparring with my mentor, Rusen Kerpic, thank you for your help! A big thank you must also go to my reviewers Patrick Bülow, Kimi Cardoso Kreilgaard, Charlotte Cramer Kristensen, Tobias Thornsen Røhling, Sebastian Pelt and Frederik Guldagger Lund for thorough reading and ideas for corrections. Finally, a big thank to my friends and family for the support and encouragement throughout the period.

1 Introduction

The cloudburst in Copenhagen in 1997 caused fallen trees, flooded streets and chaos in the Danish capital. 14 years later in 2011, the chaos repeated itself in Copenhagen with one of the most intense cloudbursts in the history of Denmark with a rainfall in the Botanical Garden of 135.5 *mm* in the course of 24 hours! A similarly heavy cloudburst hit Gråsten in 2007 with unimaginable amounts of rain and several consecutive cloudbursts. In the same area by Aabenraa, a very unusual phenomenon was experienced in 2019 in Denmark: A real tornado!
All events have, in their own way, an impact on several people's lives with damages for many millions Danish kroner. Characteristic for them all is that they can be characterized as cloudbursts. Climate research shown that cloudbursts over time has become more frequent in Denmark, which is shown by statements from a report prepared by John Cappelen at the Danish Meteorological Institute (DMI) [1]. Cloudbursts can cause floods, that lead to damage to buildings, roads and crops.
The weather in Denmark is expected to become more extreme with wetter summers and winters due to the warmer climate. The result is a warmer atmosphere that may contain more water vapor. The warmer climate is due to the emission of greenhouse gases [2]. This is supported by figure 1, which shows a clear tendency for the annual accumulated rainfall in Denmark to increase. Since the 1870s, precipitation has increased from approx. 650 *mm* to an annual rainfall of around 750 *mm* in recent years. This is an increase of approx. 15%.

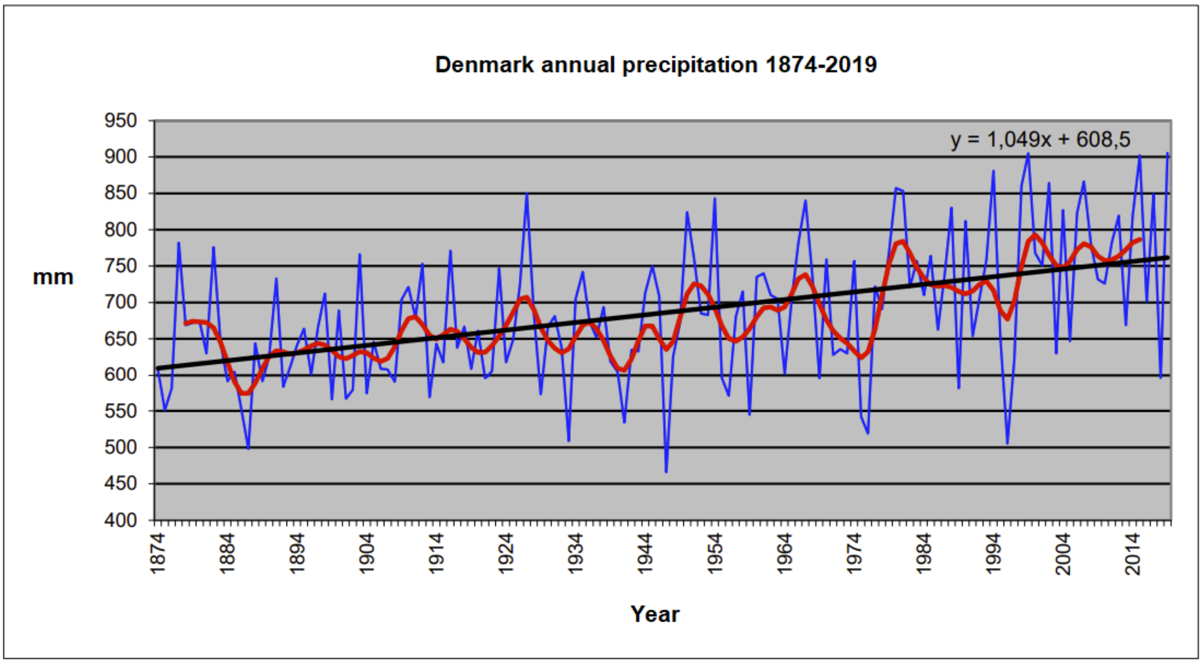

Figure 1: The blue line is the annual accumulated precipitation in Denmark, 1874-2019. The red line is a 9-point Gaussian filter and the black is a linear trend line. [1]

Figure 2 and 3 show the number of days with more than 10 *mm* of precipitation during 24 hours (figure 2) as well as the largest annual 24 hour precipitation at a locality (figure 3). Precisely these two figures give indications that there is more extreme rain in Denmark in a warmer climate. The number of days with a lot of rain is increasing, but perhaps even more notably, the cloudbursts generally become more intense, which could be the indicator in figure 3.

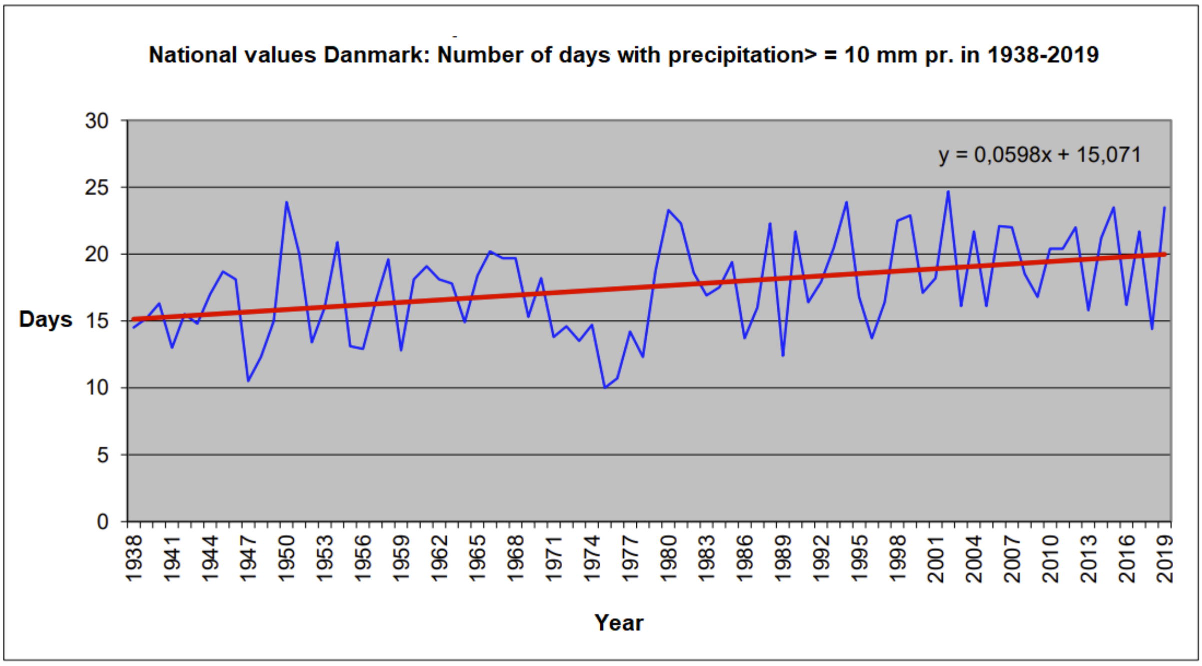

Figure 2: National values Danmark: The blue line is the number of days with precipitation > = 10 mm pr. year 1938-2019. The red line is a linear trend line. [1]

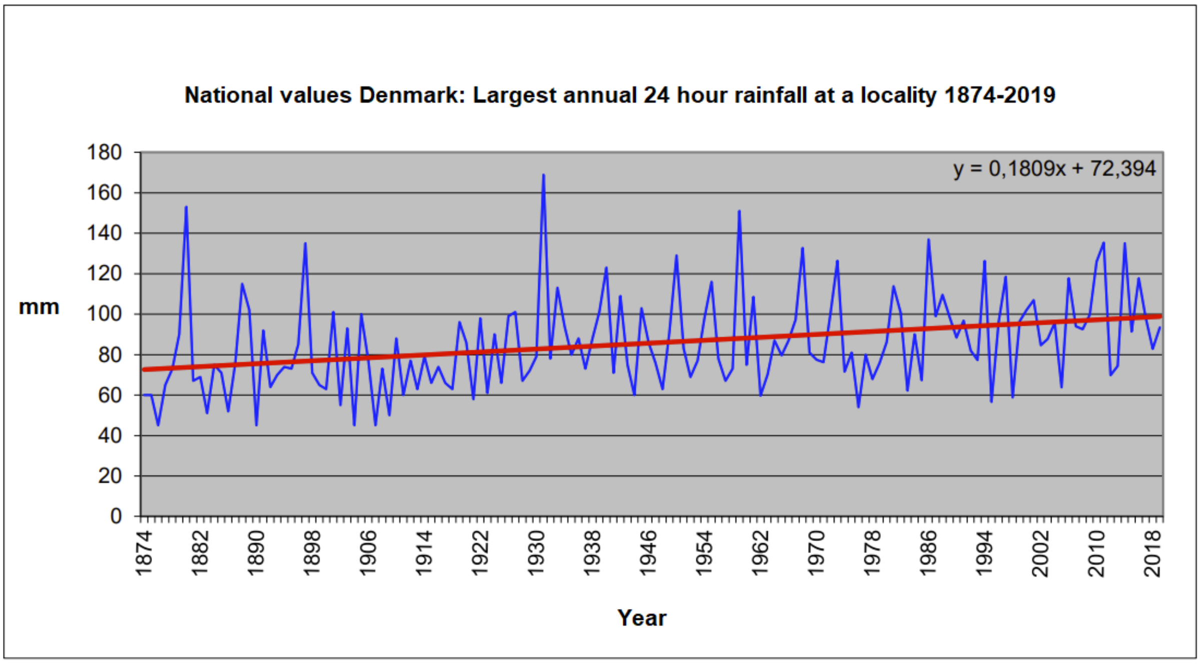

Figure 3: National values Denmark: The blue line is the largest annual 24 hour rainfall at a locality, 1874-2019. The red line is a linear trend line. [1]

Cloudburst events is due to Deep Moist Convection (DMC) which causes severe convection, and in contrast to the daily convection in the planetary boundary layer, reaches all the way up to the tropopause with overshooting tops in the lower stratosphere. Ordinary convection means heating of the Earth's surface due to solar heating. It creates turbulence and thus a convective boundary layer. In severe convection, it is necessary that convective instability (or potential instability) is accompanied by several factors that matter for the development of cloudburst. This includes high values of vertically integrated water vapor, stability conditions (e.g.

CAPE and CIN)[1], wind conditions (especially a significant vertical wind shear) in combination with quasi-geostrophic forcings.

In this thesis, an analysis will be performed on cloudbursts in Denmark, where 7 cases will be analyzed. In addition to the aforementioned 4, the storm Skt. Hans evening in 2003, the multi cloudburst in Copenhagen in 2014 as well as the cloudburst in Copenhagen in the early autumn of 2015 will also be analyzed. For practical reasons, there is only time to analyze a small number of cases selected after severe weather; extremely strong cloudbursts, tornadoes, strong winds during the passage of squall line and so on. As it is only a small selection of cloudburst events in the thesis, this means that the focus is more on the development of the individual cloudburst, more so than the total overview of all 7 cloudbursts. However, it is assessed that the analysis of the 7 cloudbursts is fairly representative of extreme rain and cloudbursts in Denmark and can contribute to provide a general picture for the formation and development of cloudburst events in Denmark.

It is only in the recent years that cloudbursts have been actively measured in Denmark. At The Water Pollution Committee of The Society of Danish Engineers (SVK), measurements began back in the 1980s, while DMI began in 2011. Therefore, only relatively newer cases are included, as availability of data has been over the past 30 to 40 years.

The overall purpose of the thesis is to make an analysis of the development of cloudbursts in Denmark. The thesis will try to form an overview of how cloudbursts occur, under what conditions and in what seasons. The approach is that cloudbursts is primarily a summer phenomenon, as in summer there are large temperature differences from the surface and up through the troposphere, which provides favorable conditions for the formation of heavy showers. The thesis will thus end up providing an understanding of the development of cloudbursts in Denmark, and what the probability of cloudbursts in a future climate is. A categorization of the individual cloudbursts in single cells, multicells or supercells will be made in the analysis.

The structure of the thesis is that section 2 will describe the background theory for cloudburst, which is severe convection. In section 3, the data will be described, where they come from and how they are structured. In section 4, the method for the analysis is reviewed. Section 5 contains the analysis of the 7 cases with small partial conclusions and summaries along the way. Section 6 will contain an overall conclusion for the analysis in the thesis. Finally, section 7 will put cloudbursts in a wider perspective and look a little into a future climate. At the end of the thesis, there is an appendix with additional knowledge and tables as well as references.

[1] Convective available potential energy (CAPE) and Convective Inhibition (CIN)

2 Theory

In this section a reviews of the background theory of cloudbursts is given, which is commonly associated with DMC. First, we must have in place how precipitation in Denmark is generally formed.

2.1 Weather Situations With Precipitation in Denmark

In Denmark, there are mainly two types of precipitation situations. One is frontal precipitation, where the precipitation is typically of relatively uniform intensity. If no fronts are present, then there must be a forcing to raise the air and organization of convective cells can begin. Convective cells can have many different characters in the form of showers or cloudbursts, and occurs disorganized or organized in co-active system, e.g. in a trough, in a polar low or squall lines. In this section, different types of rainfall situations in Denmark will be described.

2.1.1 Frontal Precipitation

Frontal precipitation is associated with cold, warm and occlusion fronts. In cold fronts, cold air displaces warm air at the surface as seen in figure 4, where cold fronts in Denmark typically come from the west and northwest. The characteristic features of a cold front in the northern hemisphere is sharp veering of the wind with the altitude, there is a drop in temperature and dew point - as well as a rise in pressure. Precipitation typically occurs about 100 to 200 *km* in front of or behind the front, but in some cases cold fronts can be without precipitation. Under the right circumstances and a suitably unstable troposphere, thunder cells can organize itself as a squall line along the front, see figure 4.
The steeper slope a cold front has acquired from the surface, the more active is the cold front. Precisely the active cold fronts have the greatest probability that convective clouds and thus thunder cells can be formed if it is warm and humid conditionally unstable air which the cold front replaces on its way across the surface.
Warm fronts are defined by cold air is replaced by warm air because the warm air pushes itself up over the cold air. Warm fronts is associated with a pressure drop occurs while the temperature and dew point rise. The precipitation band in warm fronts are typically a wide band up to 400 *km* ahead of the front. The wind is veering in the warm front passage. The typical precipitation associated with warm fronts is slight moderate rain. Thunder cells are less common along warm fronts, but can occur if the warm air mass is unstable. In that case, they occur among the stratiform cloud ahead of the front and can continue after the front passage.
In the zone between the cool air from the cold front and the warm air from the warm front is a confluence zone available to be formed. A confluence zone is characterized by having a flow toward an axis oriented parallel to the general direction of the flow. The wind often accelerates when they enter a confluence zone, resulting in divergence of the wind.
The last main types of fronts are occlusion fronts. They occur because warm fronts moves slower than cold fronts, as it is easier for the cold and heavy air to push the warm and light air. When the cold front has caught up with the warm front, an occlusion front arises which is accompanied by an occlusion point where both the cold front, the warm front and the occlusion

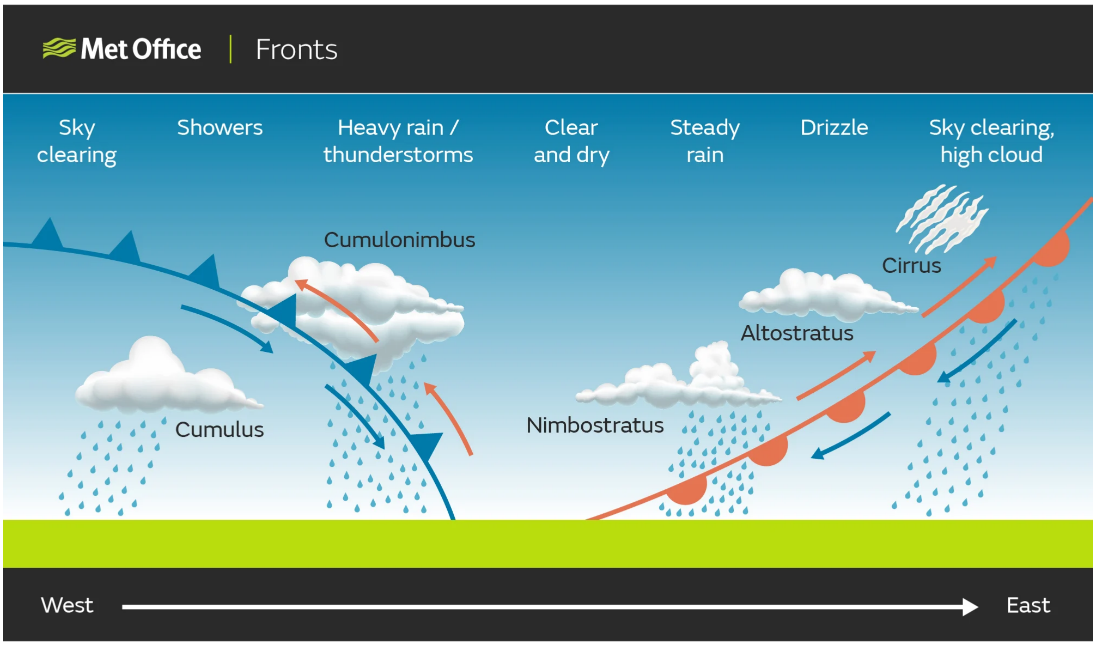

Figure 4: In a low pressure system, the first frontal zone will be associated with a warm front, represented by the red line with arcs. These fronts typically starts with high cirrus clouds and drizzle produced by low stratiform clouds and later these is replaced by high cirrus clouds. The warm front is commonly followed by the cold front, which is the blue line with triangles. Heavy thunder cells can develop in the form of cumulonimbus clouds. On the back there can often be cumulus clouds which in an unstable troposphere can develop into showers. Thunder cells may develop among the stratiform clouds if the warm air mass is unstable. [3]

front meet. These points are associated with heavy rainfall.
The theory in frontal precipitation is important knowledge, because a frontal analysis will be performed in each case in section 5.

2.1.2 Convective Precipitation

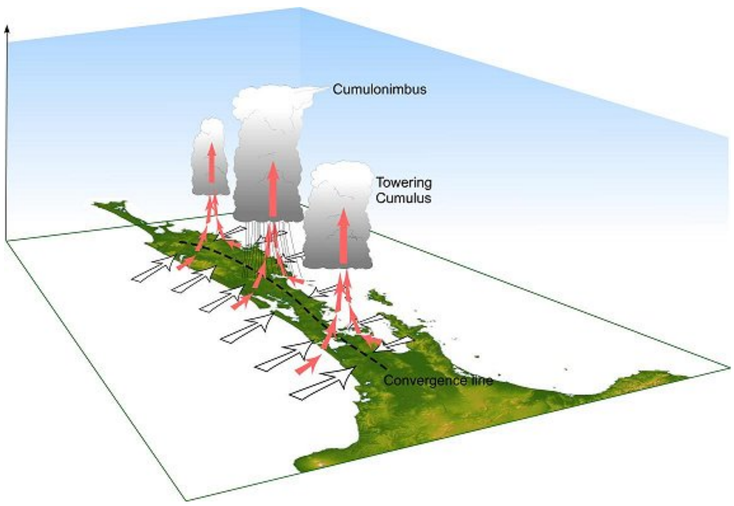

Figure 5: Two air masses meet and form a convergence line where strong showers can form. [4]

Convective showers are another possibility of precipitation in Denmark and these can occur in different situations. They can occur in winter situations with the ocean effect, where cold winds move over the warmer seawater, which can collect water vapor in the air and form showers. The other possibility is the so-called polar lows, that are sometimes experienced in Denmark, where deep convection can develop in a continuous area surrounding the 'eye' with strong vertical updraft. In addition, there are the familiar summer situations where warm and humid air rises to higher altitudes and can form cumulonimbus

clouds. Convection along frontal zones is also quite normal.
Convective showers or cloudbursts can, as previously mentioned (figure 4) , occur along fronts, but also along convergence lines where two air masses meet, see figure 5. It could be in situations with a cold air mass from west and northwest that heads towards east, while a warm and humid air mass from east heads towards west. It provides favorable conditions for an unstable troposphere and the development of cloudbursts and is a case in a couple of the analyzes.
In the next section, the dynamics behind convection are described and how convection can cause buildup of showers.

2.2 Convection

Convection in the atmosphere occurs when the surface is heated from solar radiation. The surface then heats the bottom layer in the atmosphere, which expands and begins to rise because it is less dense than the surrounding air mass. This process is characterized by instability and temperature differences in the different atmospheric layers. If the warm air contains moisture, some of the water vapor will condense as it cools on the way up through the atmosphere. By condensation, latent heat is released and cumulus clouds are forming. This is the basis for the development of convective precipitation and cloudbursts.
In order to understand how convection affects cloudbursts, it is important to understand the basic equations. These equations are not a part of the analysis, but are an important foundation for convection in the atmosphere. The dynamical equations for convective clouds can be written with the frictionless equations of motion:

$$\frac{Du}{Dt} = -\frac{1}{\rho}\frac{\partial p}{\partial x} \tag{1}$$

$$\frac{Dv}{Dt} = -\frac{1}{\rho}\frac{\partial p}{\partial y} \tag{2}$$

$$\frac{Dw}{Dt} = -\frac{1}{\rho}\frac{\partial p}{\partial z} - g \tag{3}$$

Equation 1 and 2 are the horizontal momentum equations and equation 3 is the vertical momentum equation, where u is the zonal velocity, v is the meridional velocity, w is the vertical velocity, ρ is density, p is pressure and g is gravity. Perturbation theory is an important method to understand convective systems due to the importance of perturbation pressure in cumulus convection [5]. For example, the total pressure (p) and density (ρ) field can be divided into a horizontally homogeneous basic state and a deviation:

$$\rho = \overline{\rho}(z) + \rho'(x, y, z, t) \tag{4}$$

$$p = \overline{p}(z) + p'(x, y, z, t) \tag{5}$$

here ρ' and p' are the fluctuation parts whereas $\overline{\rho}$ and $\overline{p}$ are the horizontally homogeneous basic state. The homogeneous part is in hydrostatic balance:

$$\frac{\partial \overline{p}}{\partial z} = -\overline{\rho} g \tag{6}$$

Substituting equation (4) to (6) in equation (1) to (3) yields the following:

$$\frac{Du}{Dt} = -\frac{1}{\overline{\rho}}\left(1 + \frac{\rho'}{\overline{\rho}}\right)^{-1}\frac{\partial p'}{\partial x} \approx -\frac{1}{\overline{\rho}}\frac{\partial p'}{\partial x} + \frac{1}{\overline{\rho}}\left(\frac{\rho'}{\overline{\rho}}\right)\frac{\partial p'}{\partial x} \tag{7}$$

$$\frac{Dv}{Dt} = -\frac{1}{\bar{\rho}}\left(1+\frac{\rho'}{\bar{\rho}}\right)^{-1}\frac{\partial p'}{\partial y} \approx -\frac{1}{\bar{\rho}}\frac{\partial p'}{\partial y} + \frac{1}{\bar{\rho}}\left(\frac{\rho'}{\bar{\rho}}\right)\frac{\partial p'}{\partial y} \tag{8}$$

$$\frac{Dw}{Dt} = -\frac{1}{\bar{\rho}}\left(1+\frac{\rho'}{\bar{\rho}}\right)^{-1}\left(-\bar{\rho}g + \frac{\partial p'}{\partial z}\right) - g \approx -\frac{1}{\bar{\rho}}\frac{\partial p'}{\partial z} + \frac{1}{\bar{\rho}}\left(\frac{\rho'}{\bar{\rho}}\right)\frac{\partial p'}{\partial z} - \frac{\rho'}{\bar{\rho}}g \tag{9}$$

it follows that:

$$\frac{Du}{Dt} = -\frac{1}{\bar{\rho}}\frac{\partial p'}{\partial x} \tag{10}$$

$$\frac{Dv}{Dt} = -\frac{1}{\bar{\rho}}\frac{\partial p'}{\partial y} \tag{11}$$

$$\frac{Dw}{Dt} = -\frac{1}{\bar{\rho}}\frac{\partial p'}{\partial z} + B \tag{12}$$

since $\frac{\rho'}{\bar{\rho}} \ll 1$. The vertical acceleration (12) is induced by the buoyancy:

$$B = -\frac{\rho'}{\bar{\rho}}g \tag{13}$$

$\frac{\partial p'}{\partial x}$, $\frac{\partial p'}{\partial y}$ and $\frac{\partial p'}{\partial z}$ are components of the pressure gradient vector, $\boldsymbol{\nabla} p'$. Equation 10 and 11 tell us about the acceleration above and below the air parcel associated with horizontal perturbation pressure gradient. Equation 12 is the vertical acceleration of the parcel due to the buoyancy and the vertical pressure gradient force. Another important equation in relation to the vertical motion is the quasi-geostrophic omega equation.

2.2.1 The Quasi-Geostrophic Omega Equation

The quasi-geostrophic omega equation is a method to describe the distribution of mid-latitude synoptic-scale vertical motion with a combination of the quasi-geostrophic vorticity, thermodynamic, and continuity equations [6] and is given by:

$$\left(\nabla_p^2 + \frac{f_0^2}{\sigma}\frac{\partial^2}{\partial p^2}\right)\omega = -\frac{f_0}{\sigma}\frac{\partial}{\partial p}[-\mathbf{V_g}\cdot\nabla_p(\zeta_g + f)] - \frac{R}{\sigma p}\nabla_p^2[-\mathbf{V_g}\cdot\nabla_p T]. \tag{14}$$

where f_0 is the Coriolis parameter, σ is the static stability, ω is vertical motion based on geopotential motion, $\mathbf{V_g}$ is the geostrophic velocity vector, ζ_g is the geostrophic relative vorticity, R is the gas contant for dry air and T is temperature. The left hand side is the Laplacian of vertical motion. This term is approximately zero at the surface and at the tropopause and reaches absolute maximum/minimum values in the mid-troposphere.

The first term on the right hand side (RHS) is the differential vorticity advection. This term tell us that vorticity advection increases with height and forces synoptic-scale upward motion and then is able to trigger the formation of thunder cells. The second RHS term is the Laplacian of temperature advection, which relates temperature advection to vertical motion where warm advection is positive temperature advection (upward motion) and cold advection is negative temperature advection (downward motion). Warm advection can trigger cloudbursts to occur due to the upward motion where the vertical motion is largest when the temperature advection is large.

The static stability parameter, σ, is an important parameter. A low (high) static stability parameter results in a more unstable (stable) atmosphere with strong (weak) vertical motion.

The terms on the RHS of equation 14 are the quasigeostrophic forcing terms for synoptic-scale vertical motion and are important parameters in the analysis section due to the dynamic forcing, which is included in these terms and is a trigger for convection. Convection can occur in both a shallow atmosphere and a deep atmosphere, which is crucial for the development of cloudbursts.

2.2.2 Shallow Moist Convection

The most common clouds on Earth are stratocumulus clouds and are the result of moist thermal convection which is a combination of turbulent convection and latent heat release in the lower atmosphere [7]. Characteristics of stratocumulus are low-level clumps of cloud varying from bright white to dark grey and large variations in the lifetime and the shape of clouds, usually in groups, lines or waves. Stratocumulus clouds is formed when a layer of stratus clouds breaking up.

Stratocumulus occurs in Shallow Moist Convection (SMC) which means that the above mentioned condensation processes are formed at low altitudes around 2000 to 3000 m and where vertical lifting is capped around 500 hPa. For SMC, low level convergence is required while relative humidity is not raised higher than 500 hPa in an unstable atmosphere. Shallow cumulus clouds are found all over the globe, but are most frequently in trade wind belts [8] where the thermodynamic background contain more heat and moisture which is triggering parameters.

For a shallow atmosphere the continuity equation is written as:

$$\frac{1}{\rho}\frac{D\rho}{Dt} = 0 = \boldsymbol{\nabla} \cdot \mathbf{v} \tag{15}$$

where $\mathbf{v}$ is the velocity vector. Equation 15 approximates the atmosphere to be incompressible, which means that the density of an air parcel do not change. In a shallow incompressible atmosphere, fractional changes of density, when following an air parcel, are relatively small for vertical velocities. The equations (10) to (12) and (15) are called Boussinesq equations and are an approximation used in convective systems. When the lapse rate of the clouds in the shallow cumulus layer becomes larger than the environment then, over time, the shallow clouds must become buoyant and a gradual transition from SMC to DMC occurs [10].

Figure 6: Cumulus humilis, clouds formed by shallow convection. [9]

2.2.3 Deep Moist Convection

Unlike in a shallow atmosphere, the density varies with altitude in a deep atmosphere, and there may be relatively large fractional changes in density. For a deep atmosphere, the continuity equation can be expressed anelastically:

$$\frac{1}{\rho}\frac{D\rho}{Dt} = \frac{1}{\overline{\rho}(z)} w \frac{\partial \overline{\rho}}{\partial z} = \boldsymbol{\nabla} \cdot \mathbf{v} \tag{16}$$

The anelastic continuity equations are applicable for the dynamics of a deep atmosphere, while the Boussinesq continuity equation are applicable for the dynamics of a shallow atmosphere.

Convective clouds are typically called "deep" when they have a significant vertical extent up through the troposphere and these are associated with heavy rainfall such like cloudbursts. Convective clouds have their base at the boundary layer where much of the potentially unstable air is organized. Cumulus convection can occur where we have conditional or potential instability in the troposphere. Conditional instability is an atmospheric condition where air parcels during lifting changes gradually from being cooler to warmer than their surroundings if these are lifted above the Lifted Condensation Level (LCL) and under the condition of $-\Gamma_d > \Gamma_e > \Gamma_m$ where Γ_d is the dry adiabatic lapse rate, Γ_e is the environmental lapse rate and Γ_m is the moist adiabatic lapse rate. This means that the saturated (unsaturated) parcel will be warmer (cooler) than the environment. Conditional instability is seen e.g. in relation with turbulence.

If the atmosphere is potentially unstable, then the equivalent potential temperature will decrease with altitude and thus a given layer in the atmosphere will gradually go from being stable to being unstable. A lift in a potentially unstable atmosphere is seen e.g. at fronts where the potentially unstable layer is moist at the bottom (clouds) and dry at the top (inversion layer).

Under certain conditions, external forces are required to lift the parcels from the LCL to the next important level, the Level of Free Convection (LFC), where a parcel will begin to rise due to its own positive buoyancy. The energy that must be added to lift this last piece is called Convective Inhibition (CIN), which is the amount of energy it takes to move a parcel from the surface to the LFC and thus overcome the negative buoyancy. Warm advection or Positive absolute Vorticity Advection (PVA) can be the reason for the necessary lifting and for thunder cells to grow.

Above LFC, the parcel is warmer as we know from the conditional instability and thus the parcel has a positive acceleration until it reaches Equilibrium Level (EL), where the parcel has the same temperature as the surroundings. Above EL, the parcel is slowed down by the changed conditions. The acceleration of the parcel is induced by the buoyancy force from equation (13), which can be written in a new from:

$$B = \frac{T_{v,parcel} - T_{v,env}}{T_{v,env}} g \tag{17}$$

where $T_{v,parcel}$ is the virtual temperature of the parcel and $T_{v,env}$ is the virtual temperature of the environments. The virtual temperature is the temperature where the dry air would have the same density as the moist air, at a given pressure. Equation 17 tell us that if the parcel is warmer than the environments, a positive buoyancy force exists on the parcel. The dynamic effects of the buoyancy in equation 12 when w is in steady state can be simplified [11]:

$$B = \frac{Dw}{Dt} = w\frac{dw}{dz} = \frac{d}{dz}\left(\frac{1}{2}w^2\right) \tag{18}$$

The area between the lifting curve in a skew-T diagram and the temperature curve is Convective Available Potential Energy (CAPE), which exists in a conditionally unstable layer in the troposphere. CAPE can be calculated using the temperature for resp. the parcel and the environments:

$$CAPE = \int_{LFC}^{EL} B dz \tag{19}$$

Integrating equation (18) from LFC to EL with respect to height z, the maximum vertical velocity is given by:

$$w_{max} = \sqrt{2CAPE} \tag{20}$$

The maximum vertical velocity is typically found as the updraft at the EL. The work to be done to lift a parcel of air to the LFC level is given by CIN, which is mentioned earlier. CIN is defined by:

$$CIN = -\int_0^{LFC} B dz \tag{21}$$

CIN is by definition the opposite of CAPE and represents the negative value of the buoyancy, while the parcel temperature is colder than the environments. The closer the CIN value is to zero, the more potentially unstable is the atmosphere. Larger CAPE and smaller CIN thus provide potential for the formation of strong DMC (cloudbursts).
All the mentioned parameters in this section will be used in almost all analyzes to analyze the stability of the troposphere and to suggest why severe cloudbursts could form in the individual cases.
When the convective cells are formed, they can organize themselves in different ways which will be described in the next section.

2.3 Organization of Thunder Cells

Thunder cells are very different in size and in distribution, depending on whether they are a single cell, multicells or supercells. Figure 7 shows a spectrum of convective storms as a function of the vertical wind shear. This spectrum tell us that it is the vertical wind shear that matters for the type of convective cell that can be developed. According to figure 7 supercells can occur in a flow with a vertical wind shear of $\geq 18\ m/s$, where the wind shear is the difference in wind speed over a distance. In order for thunder cells and thus cloudbursts to be formed, it is therefore a prerequisite that the troposphere is sufficiently unstable and there is a significant vertical wind shear. The organization of thunder cells is based on the perturbation pressure.

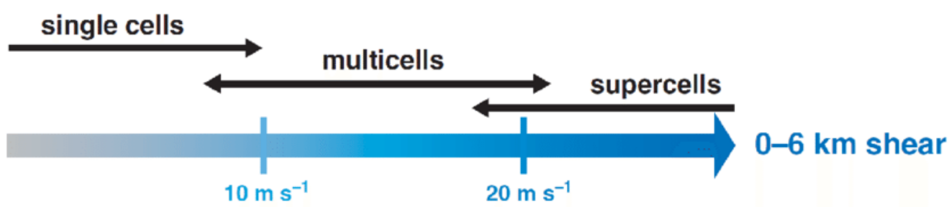

Figure 7: Spectrum of convective storms as a function of vertical wind shear. [12]

2.3.1 The Impact of the Perturbation Pressure

The perturbation pressure occurs in the interaction between the background flow and the vertical wind shear. The perturbation pressure creates areas with horizontal acceleration and vertical acceleration. A self-organizing system of thunder cells has a favorable starting point in areas where the air is accelerated upwards. Such a system is typically seen in conjunction with a moderate to strong wind shear.
A disorganized system occurs in environments with a weak wind shear, where the perturbation pressure is negligible. Here, new single cells emerge if the conditions are right and arise along random gust fronts.

The following equations will not be used in the analysis, but are used to divide the perturbation pressure into a linear part and a non-linear part. In a Boussinesq system, the diagnostic pressure equation can be expressed as:

$$\nabla^2 p' = -\overline{\rho}\left[\left(\frac{\partial u'}{\partial x}\right)^2 + \left(\frac{\partial v'}{\partial y}\right)^2 + \left(\frac{\partial w'}{\partial z}\right)^2 + 2\frac{\partial u'}{\partial y}\frac{\partial v'}{\partial x} + 2\frac{\partial u'}{\partial z}\frac{\partial w'}{\partial x} + 2\frac{\partial v'}{\partial z}\frac{\partial w'}{\partial y}\right] \\ -\overline{\rho}\left(2\frac{\partial \overline{u}}{\partial z}\frac{\partial w'}{\partial x} + 2\frac{\partial \overline{v}}{\partial z}\frac{\partial w'}{\partial y}\right) + \overline{\rho}\frac{\partial B}{\partial z} \tag{22}$$

which is a diagnostic relationship between the perturbation pressure and the gradients in the wind field as well as the vertical derivative of buoyancy. The total perturbation pressure in equation 22 can be simplified as:

$$p' = p'_{dyn} + p'_B = p'_{LPP} + p'_{NPP} + p'_B \tag{23}$$

where p'_{dyn} is the dynamic pressure, which is the perturbation pressure associated with the gradients in the wind field, p'_B is the buoyancy pressure, which is associated with the vertical derivative of buoyancy, while p'_{LPP} is the Linear Perturbation Pressure (LPP) and p'_{NPP} is the Non-linear Perturbation Pressure (NPP). According to equation 23, the dynamic perturbation pressure can be divided into a linear (p'_{LPP}) and a non-linear (p'_{NPP}) contribution. p'_{LPP} and p'_{NPP} are the dynamic part of the perturbation pressure, where LPP is the linear part of the wind field (equation 22):

$$-\overline{\rho}\left(2\frac{\partial \overline{u}}{\partial z}\frac{\partial w'}{\partial x} + 2\frac{\partial \overline{v}}{\partial z}\frac{\partial w'}{\partial y}\right) \tag{24}$$

and NPP is the non-linear part of the wind field:

$$-\overline{\rho}\left[\left(\frac{\partial u'}{\partial x}\right)^2 + \left(\frac{\partial v'}{\partial y}\right)^2 + \left(\frac{\partial w'}{\partial z}\right)^2 + 2\frac{\partial u'}{\partial y}\frac{\partial v'}{\partial x} + 2\frac{\partial u'}{\partial z}\frac{\partial w'}{\partial x} + 2\frac{\partial v'}{\partial z}\frac{\partial w'}{\partial y}\right] \tag{25}$$

where $\left(\frac{\partial u'}{\partial x}\right)^2 + \left(\frac{\partial v'}{\partial y}\right)^2 + \left(\frac{\partial w'}{\partial z}\right)^2$ are the square of the gradient of the wind field and $2\frac{\partial u'}{\partial y}\frac{\partial v'}{\partial x} + 2\frac{\partial u'}{\partial z}\frac{\partial w'}{\partial x} + 2\frac{\partial v'}{\partial z}\frac{\partial w'}{\partial y}$ are the shear terms. LPP are in environments with a moderate wind shear significantly larger than NPP. In a strong wind shear, both contributions have a significant role. In both cases, the thunder cells usually organizes themselves as a multicell system.
For a LPP, an unidirectional wind shear applies, where the wind doesn't change direction with altitude. If the wind grows with height it is called a forward wind shear, while if it decreases with height it is a reverse wind shear, which is illustrated in figure 8.
In a forward wind shear, new cells are formed on the front of the mean wind, where the sum of the control wind and the propagation vector gives a DMC system with cloudbursts that moves quite fast. In a reverse wind shear, new cells are formed on the rear of the mean wind. In such a situation, the cloudburst system can become stationary and result in severe flooding.
The analysis uses warm and cold advection to specifically form an overview of potential cloudburst locations and to determine forcing capabilities in the cases. If the wind is veering (turns clockwise) with the height, then we have warm advection, while if it backs (turns counterclockwise) with the height, then there is cold advection. In figure 9 it is outlined that in the case of temperature advection there are favorable conditions for the development of cloudbursts. In this figure, the quadrants represent a forward and reverse wind shear in environments with cold and warm advection. In figure 9, the control wind is the movement of the mature cell,

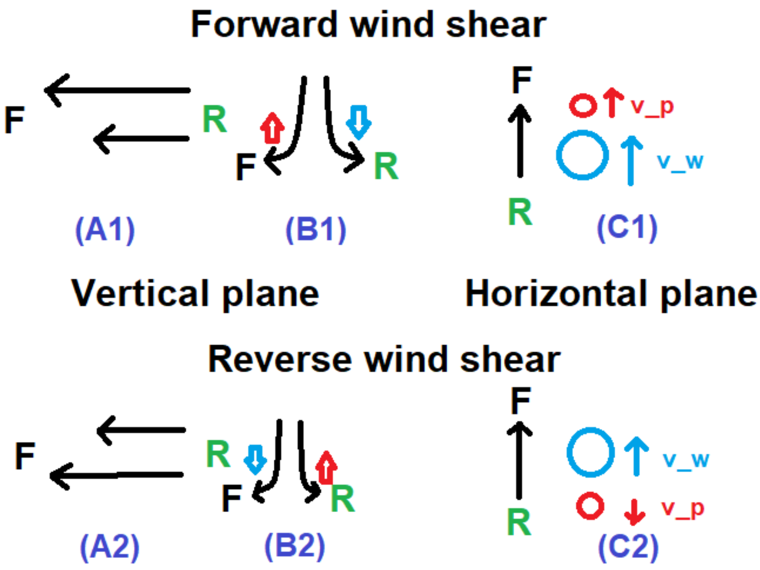

Figure 8: Displays a forward wind shear (top) and a reverse wind shear (bottom). In A1 and A2 are a vertical section of the background flow, while in B1 and B2 are a downward diverging flow from the mature cell. F is the front and R is the rear of the mean wind. The spatial variation of LPP generates a vertical buoyancy upward in B1 (downward in B2) on the front side of the mature cell in the case of forward (reverse) wind shear. In C1 and C2 are a horizontal section where new cells are formed relative to the mature cell. The mature cell is the blue ring and growing cells is the red ring.

while the wind shear vector has the same direction as the propagation vectors. Along the black lines, the shear vector is in warm and cold advection, perpendicular to the right and perpendicular to the left of the steering wind, respectively. The small circles symbolize new cells in resp. a forward wind shear and a reverse wind shear. New cells arise along the large circle at the end of the propagation vector. In warm advection, LPP creates upward acceleration to the right of the mature cell, favoring the growth of new cells. To the left of the mature cell, LPP creates a downward acceleration that slows the development of new cells. In cold advection, it is with opposite sign [13].
The understanding of how thunder cells organize is important in the effort to find out how a system with a series of cloudbursts has been able to become powerful and continue to be able to be formed, thus providing high amounts of precipitation.
The following three subsections will describe the classification of thunder cells which will be used in the analysis to classifies each case. Thunder cells can be divided into three types; single cells, multicells and supercells.

2.3.2 Single Cell Convection

Single cell convection consist of only one updraft. That said, the cell builds up and dies out and no new cells arise after this, primarily due to weak vertical shear. This results in weak and shallow lifting along the gust front. These types of convection cells are short-lived.
Single cell convection depends on the daily cycle in the boundary layer. At mid-latitudes, they typically occur in warm and humid weather during the summer period and thus occur just

after maximum daytime heating (late afternoon), when CIN is smallest and CAPE is largest. When the convection dies out after sunset, the cell also dies out. Typical CAPE values for single cells range from few 100 $\frac{J}{kg}$ to $> 2000\ \frac{J}{kg}$.

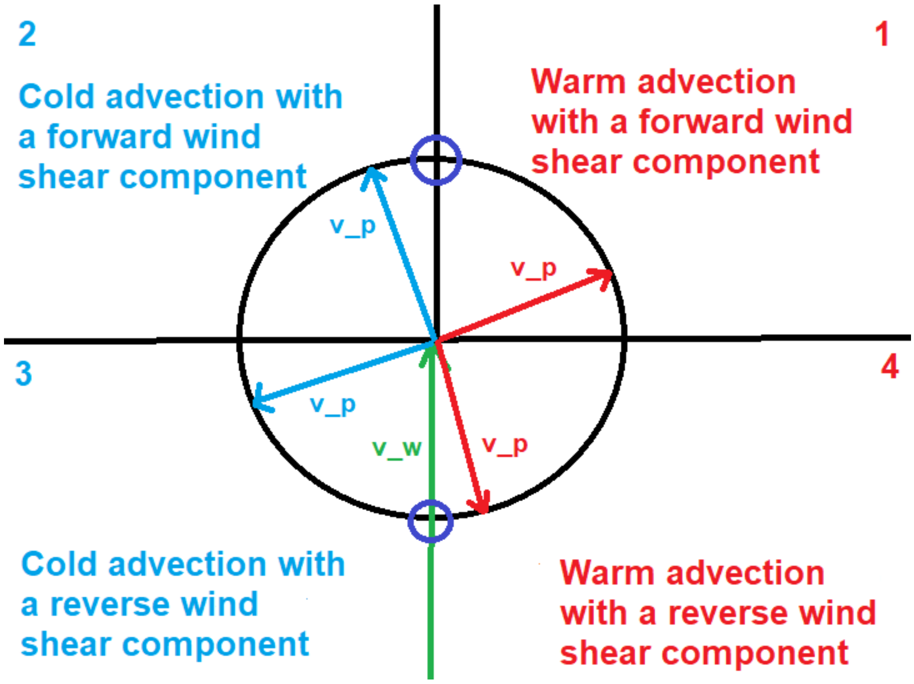

Figure 9: Shows where new cells are formed in relation to temperature advection, which happens along the large circle. The left quadrants (blue) indicate cold advection, while the right indicate warm advection. Forward wind shear (top) and reverse wind shear (bottom). The steering wind from the mature cell is the green vector, while the vectors inside the circle are the direction of the propagating cells. New cells develop to the left of the mature cell by cold advection and to the right by warm advection. The small purple rings indicate if no temperature advection is present, as in figure 8.

Figure 10 shows the three stages of a single cell. In the towering cumulus stage (figure 10a), there is only updraft and the cell builds up. In the mature stage (figure 10b), precipitation is produced, which ”breakthrough” the updraft and forms a downdraft. Likewise, the downdraft is associated with cooling due to evaporation and small raindrops. This reduces the updraft due to loading from the hydrometeor. The downdraft forms a horizontal spread and the leading edge of this is called a gust front, which is a type of cold front. An anvil has also begun to form in the top of the cloud in the mature stage. The anvil is a result of the cloud reaching the level of stratospheric stability. In the dissipating stage (figure 10c), the downdraft dominates and the updraft is cut off and potential buoyancy does not have the opportunity to keep the cell alive and the cell dies out.

The lifetime of a single cell depends on the time it takes for the air to get from the surface to the EL as well as the time it takes for precipitation to reach the ground [12]:

$$\tau \approx \frac{H}{w_0} + \frac{H}{v_t} \tag{26}$$

where H is the scale height of the atmosphere, w_0 is the average updraft speed and v_t is the mean terminal fall speed of the precipitation. This equation tell us that the lifetime for a single cell convection is 30-60 min.

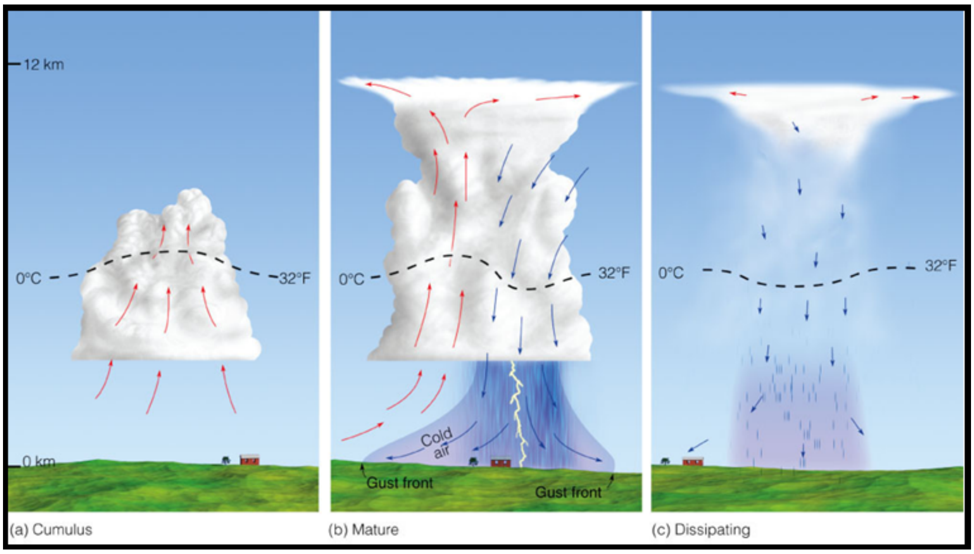

Figure 10: The life cycle of af single cell. The towering cumulus stage (a), the matur stage (b) and the dissipating stage (c). The dashed line is the freezing level, which can change altitude depending on whether there is a updraft or a downdraft. [14]

2.3.3 Multicell Convection

A multicell system is a very common form of convection at midlatitudes. It is a system consisting of a cluster of single cells at different stages of their life cycle and there is a repeated development of new cells. Where single cells have a life cycle of 30 to 60 minutes, a multicell system can last for several hours.

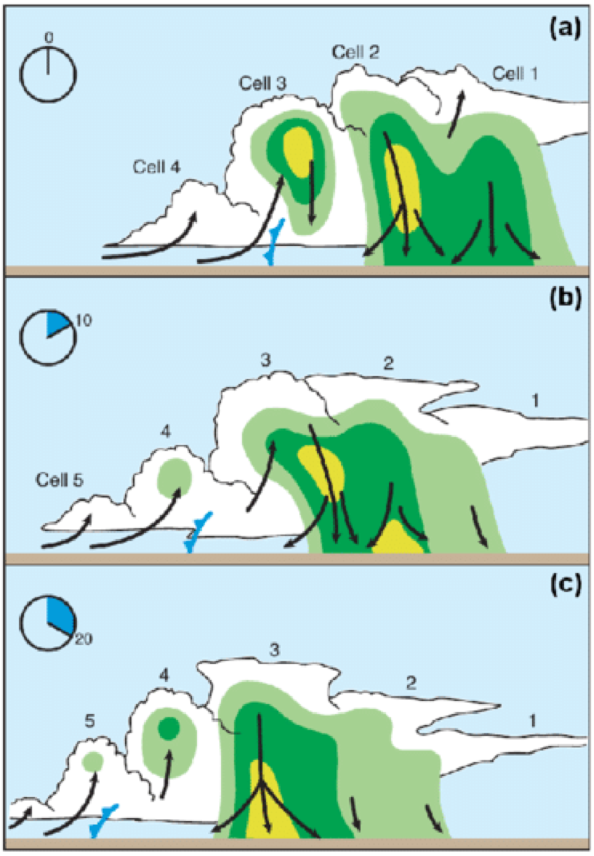

Figure 11: The evolution of a multicell system in 20 minutes (a) to (c). The blue line is the gust front. The black arrows is downdrafts and updrafts. The oldest cell in the system is cell 1 and the newest cell in the system is cell 5. [12]

The temporal development is given in figure 11. In figure 11a, the system consists of 4 different cells. Cell 1 is dominated by downdraft and has reached the dissipating stage. Cell 2 is in the mature stage and cell 3 is dominated by updraft and precipitation has begun to form in this cell. Cell 4 is in the towering cumulus stage. 10 minutes later in 11b, cell 1 is almost dissipated, while cell 2 also enters the dissipating stage, as the buoyancy is weakened due to heavy precipitation and downdraft as a result. Cell 3 begins to form an anvil in the mature stage and cell 4 continues its development and has begun to form precipitation. A new cell 5 is formed due to lifting by the gust front (the blue line). In figure 11c, 20 minutes later has past after the first stage in figure 11a and here both cell 1 and 2 are in the dissipating stage, cell 3 is dominated by downdraft, cell 4 enters the mature stage and cell 5 has begun to form precipitation. This cycle continues as new cells replace cell 5, cell 5 replace cell 4, cell 4 replace cell 3 and so on. The new cells typically occur due to lifting at the gust front as we can see for cell 4 and 5 in figure 11. This lifting is shown in figure 12 for a no-shear single cell environment (figure 12a) and a moderate-shear, multicell environment (figure 12b). For the no-shear single cell environment we had a vertically-stacked structure due to no shear and the outflow boundary (the gust front) is too weak to generate new cells. For the moderate-shear case the gust front is keeping up the updraft and the cell is moving with the cold pool. The cold pool is a blob of cold air under the thunder cell (the dark blue area in figure 12) and is forming due to evaporation of rain. New cells develop along the cold pool and close enough to the old cell that they can interact with each other. Every single cell can develop a cold pool and when cold pools collide with one another they establish circulation which is able to facilitate thunder cell development [15].

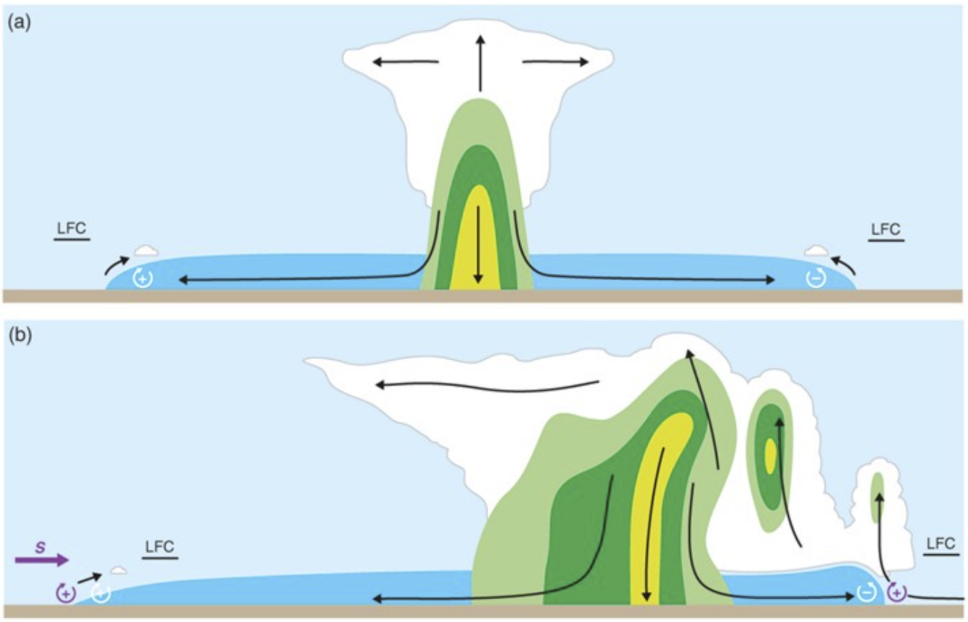

Figure 12: Lifting by the gust front in a no shear, single cell environment (a) and in a moderate shear, multicell (b). S is the environmental shear. [12]

The lifting at the gust front is enhanced where the shear in the outflow points are in the opposite direction to the density gradient. The place where the parcels have a major chance of reaching the LFC (the right part of the picture) is, where the horizontal vorticity of the environmental and the outflow cancels. The lifting shallow is where the horizontal vorticity are in the same direction (the left part of the picture) and the chance of reaching the LFC is small. Multicell systems are self-organizing and research shows that convective events like this produce highest intensities late in the day due to increased surface temperature, which leads to more cloud-cloud interaction and then higher probability of cloudbursts [16]. Sometimes multicells organize themselves into squall lines which is described later in section 2.3.5.

2.3.4 Supercell Convection

Supercells are the most dangerous thunder cells you can experience with a strong vertical wind shear $\geq 20\ ms^{-1}$ in the upper spectrum of storm types (see figure 7). A strong updraft is required and CAPE values in supercell environments tends to be significant and it is common that CAPE values are $\sim 2500\ m^2s^{-2}$ or larger.

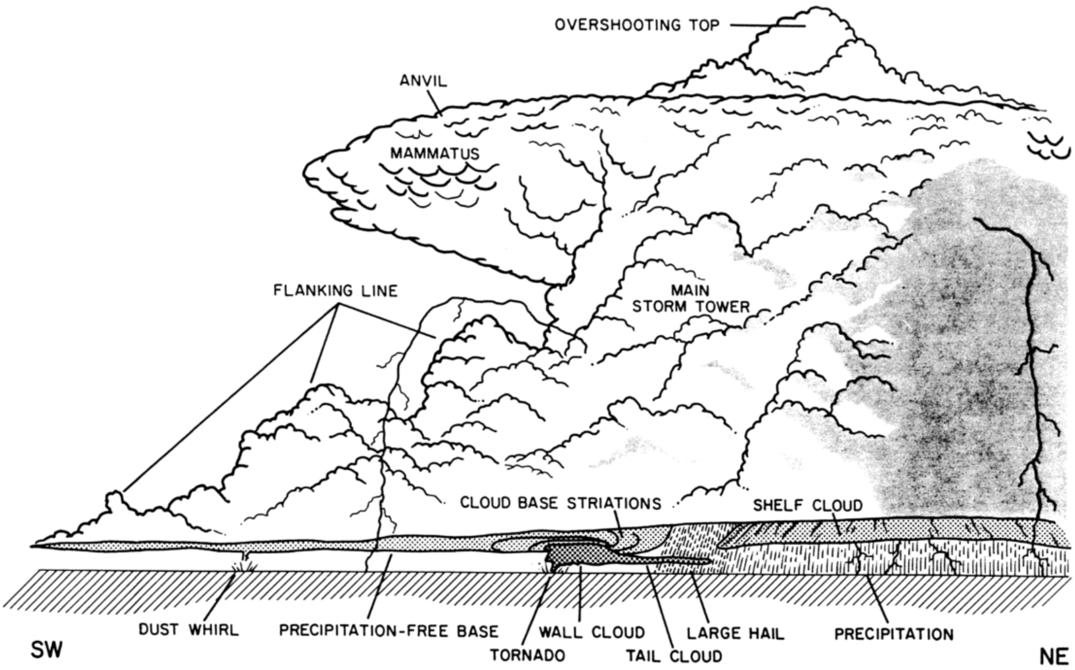

Figure 13: Schematic visual view of a supercell. [17]

The visual characteristics of a supercell are shown in figure 13. Normally during heavy thunder cells an anvil is formed only when the updraft reaches EL and the cloud is formed and spreads horizontally, but due to rapid ascent in the free convective layer there is enough momentum to also form an overshooting top. The flanking line is an area of cumulus congestus that indicates an area of buoyancy in the supercell. This buoyancy comes from warm air being forced upward in the front of the supercell. In the bottom of the supercell we have the wall cloud, which is an abrupt lowering cloud in the base of cumulonimbus clouds. At the wall cloud, moist air converges into the base of the rotating updraft and entrain the cooler air. The most powerful tornadoes occur at the wall cloud. Precipitation that typically consists of rain or hail occurs in areas with downdraft.

In Denmark, there are not the same factors for supercells to develop as there is in the USA. On the other hand, under the right conditions, there may be an opportunity for a low-topped supercell to develop which is a miniature version of the supercell as known from The Great Plains in the USA. The low-topped supercell was identified in the early 1990s by Jon Davies[2] [18] and is very common in Europe. In case 7 with the Aabenraa tornado, it may well have been a low-topped supercell.

Low-topped supercells can be isolated (similar to classic supercells), but can also organize themselves into squall lines. A low EL or a low tropopause is often the reason why deeper

[2]American meteorologist

convection is cut off and the low-topped supercell gets a lower top than the supercell [19].
The instability is weak to moderate with typical CAPE values between 300-1500 jkg^{-1}. However, a moderate to strong wind shear similar to large supercell environments is still required for a mesocyclone to develop. In a sounding, CAPE will be relatively wide, as the CAPE value is contained in a smaller vertical distance between LFC and EL due to the low EL. The result is that the updraft in a low-topped supercell does not reach the same heights as a taller supercell and the updraft peaks around 5-6 km altitude, while large supercell have a updraft that peaks in 10 km altitude. The maximum updraft still has values like large storms. Low-topped supercell has a smaller horizontal extents than supercells, but is still availabe to produce a hook echo as a characteristic. The echo in a low-topped supercell has typical maximum reflectivty around 50 dBZ. Low-topped supercells can still produce tornadoes just like the larger supercells, where tornadoes in a low-topped supercell are of weak to moderate intensity[3]. An example of a low-topped supercell with an associated tornado can be found in appendix B.
It happens that thunder cells (especially multicells) organize themselves into squall lines, as is the situation in case 1 in 1997. Squall lines will be described in the next subsection.

2.3.5 Squall Lines

Squall lines are lines of thunder cells that form along cold fronts. This typically results in heavy rainfall, high frequencies of lightning and strong wind gusts. Tornadoes can also occur. Figure 14 shows a vertical cross section of the airflow and radar echoes in a squall line. The storm motion in figure 14 is to the right, where a low level inflow is lifted to the LFC by the gust front of the squall line. This inflow retains most of its front-to-rear momentum as it follows the convective updraft. A weak subsidence can be observed in the front-to-rear stream in the transition zone from the convective precipitation to the stratiform precipitation in the ascending front-to-rear flow in the trailing stratiform region where trailing stratiform rain is observed beneath this mesoscale updraft.

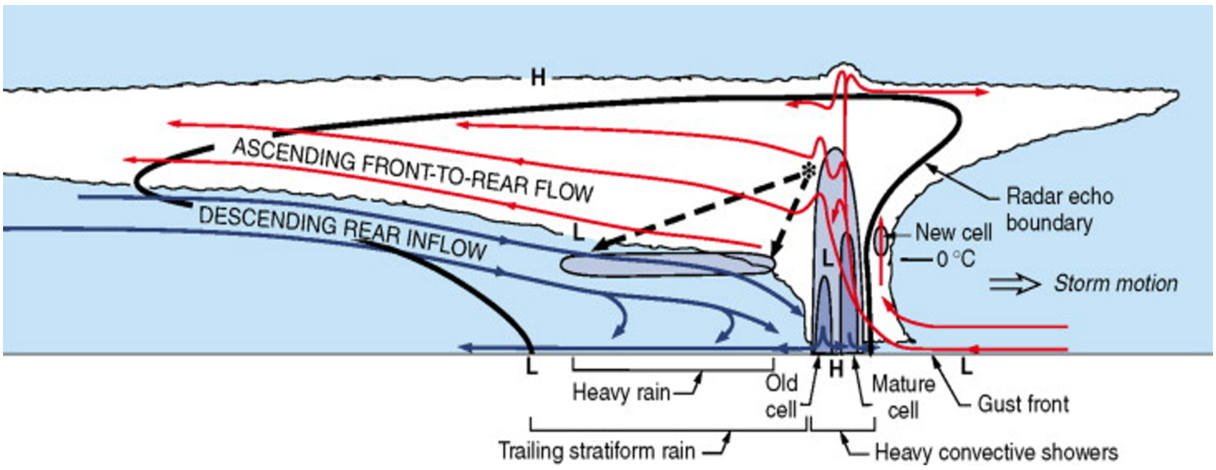

Figure 14: Vertical cross section of a idealized squall line. The blue shading is intense radar echoes. Pressure maxima and minima is indicated with H and L resp. [20]

[3]On the Enhanced Fujita scale: EF0 to EF2 or light damage to considerable damage

The squall line can be divided into three regions. The first is the leading edge with the heaviest precipitation intensities, in the form of convective rain where the strong wind gust is represented. The second is the transition zone with lighter rainfall than the leading zone. The transition zone separates the leading zone from the stratiform region. The third zone is the stratiform region. Precipitation in the stratiform region is typically less intense than in the leading zone but more intense than in the transition zone.
A horizontal section of a squall line is shown in figure 15 where the leading zone is behind the gust front and characterized by a mesohigh, which is a mesoscale high that forms beneath thunderstorms. A mesohigh is mesoscale high-pressure area associated with Mesoscale Convective Systems (MCS) and is formed underneath the downdraft in the squall line. The divergence center is slightly behind the mesohigh center. The rear inflow descends just after the leading zone of the squall line in a region of adiabatic warming within a mesoscale downdraft. The adiabatic warming reduces the hydrostatic pressure and this effect is larger than the effect of rain-cooled air in the stratiform region. Then a wake low is formed to the rear of the mesohigh. The convergence center is just slowing the wake low center. Squall lines can be hundreds of *km* long, but are often not much more than 15 to 40 *km* wide.
It is not enough to know how thunder cells are organized. It is also important to know what severe weather phenomena cloudbursts and strong convection cause, as it can have fatal consequences for the society. In the next section, the three primary weather phenomena that have been experienced during the analysis will be described.

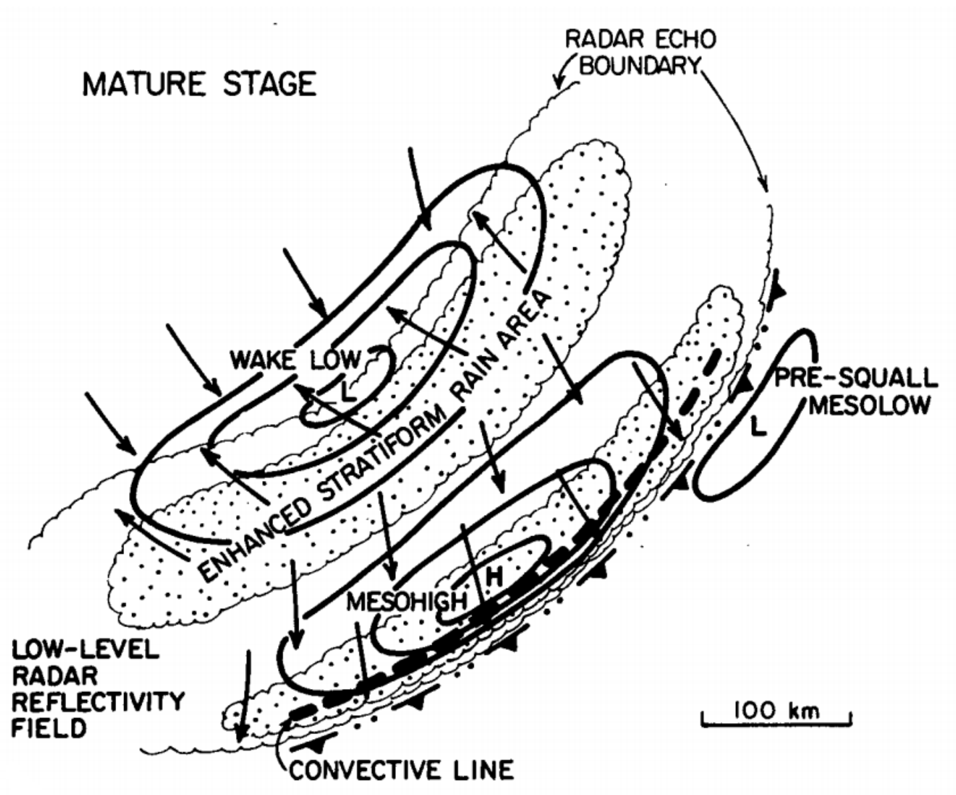

Figure 15: Horizontal cross section of a idealized squall line. The figure represent pressure and precipitation distribution. The dotted area is precipitation [21].

2.4 Weather Phenomena Associated With Strong Convection

2.4.1 Tornadoes

Tornadoes in Denmark are an extremely rare occurrence. Usually it is landspouts or waterspouts that occur at these latitudes, because the preconditions are not for tornadoes. Yet it has happened before that something reminiscent of a tornado-like landspout has formed. In relation with a very mild winter period, a possible tornado was formed on 11th of February 1962 at Holstebro in western Jylland in a frontal zone. 18th of June 2002 in a large thunderstorm where trees at Ilskov in the central Jylland were torn up in a corkscrew-like shape indicated a tornado event. On 10th of August 2009 near Aalborg, a powerful vortex was also observed, which destroyed several houses. It was a vortex during cloudburst-like rain, and therefore may have been a tornado [22]. In 2019, a tornado was filmed in Aabenraa, which in the analysis section is case 7.

Tornadoes are characterized as destructive vortex of rotating winds that can cause severe damage on its way. The description of a tornado could be a rotating column of air that exists downward from the base of a cumulonimbus cloud.

Assuming that the air is incompressible and disregarding baroclinicity and friction, then a three dimensional relative vorticity equation that describes the dynamics behind a tornado can be written as [13]:

$$\frac{\partial \zeta_z}{\partial t} = -u\frac{\partial \zeta_z}{\partial x} - v\frac{\partial \zeta_z}{\partial y} - w\frac{\partial \zeta_z}{\partial z} + \zeta_x\frac{\partial w}{\partial x} + \zeta_y\frac{\partial w}{\partial y} + \zeta_z\frac{\partial w}{\partial z} = H + Z + T + S \qquad (27)$$

where H is the horizontal advection of ζ_z (terms 1 and 2 on the RHS) and Z is the vertical advection of ζ_z (term 3 on the RHS). T is the tilting term (terms 4 and 5 on the RHS), while S is the stretching term (last term on the RHS).

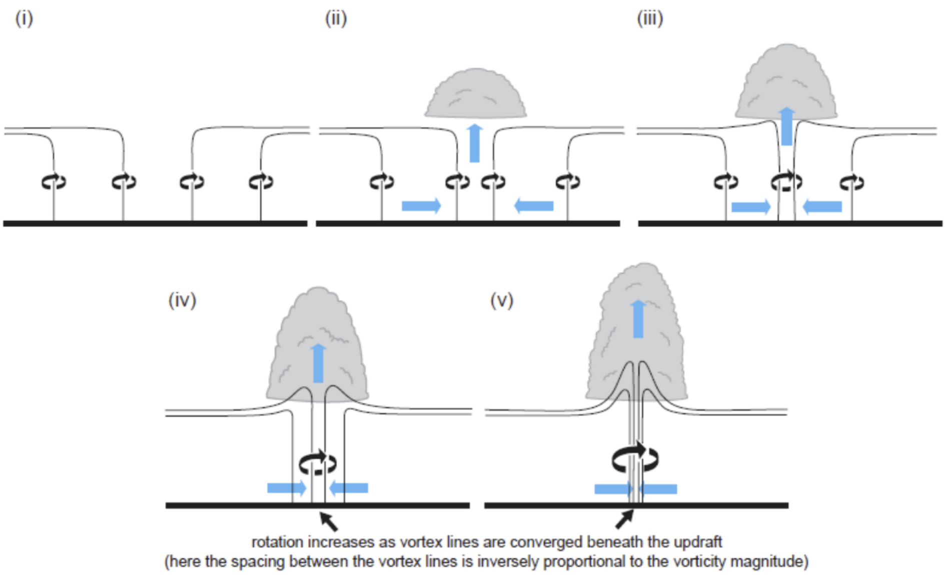

Figure 16: Simple vortex line demonstration of how waterspouts are formed due to convergence alone, in the absence of a downdraft where the black lines are horizontal convergence lines that create an updraft which is the blue arrows. [12]

ζ_z is the relative vorticity around a vertical axis and is written as:

$$\zeta_z = \frac{\partial v}{\partial x} - \frac{\partial u}{\partial y} \tag{28}$$

ζ_x is the relative vorticity around the x-axis:

$$\zeta_x = \frac{\partial w}{\partial y} - \frac{\partial v}{\partial z} \tag{29}$$

and ζ_y is the relative vorticity around the y-axis:

$$\zeta_y = \frac{\partial u}{\partial z} - \frac{\partial w}{\partial x}. \tag{30}$$

For a tornado, ζ_z has a high value that can be 3 to 4 times greater than the coriolis parameter, f. The typical value of f is $10^{-1} rad/s$ in the mid-latitudes.

In a weak vertical wind shear (figure 16), the tilt term, T, plays a minor role in generating ζ_z, as ζ_x and ζ_y have small values. In this situation, the buoyancy associated with the horizontal convergence at the surface occurs in areas with high values of ζ_z (i). Thus, the stretching term, S, plays an important role. During constant convergence, ζ_z will grow exponentially, where the final magnitude is determined by the horizontal divergence, δ, duration of buoyancy, and the initial magnitude of ζ_z (ii) to (iii). ζ_z grows fastest at the surface as δ decreases with height.

Figure 17: Landspout over land in Vendsyssel, northern Jylland. Photo: Claus Haugaard Johansen. [23]

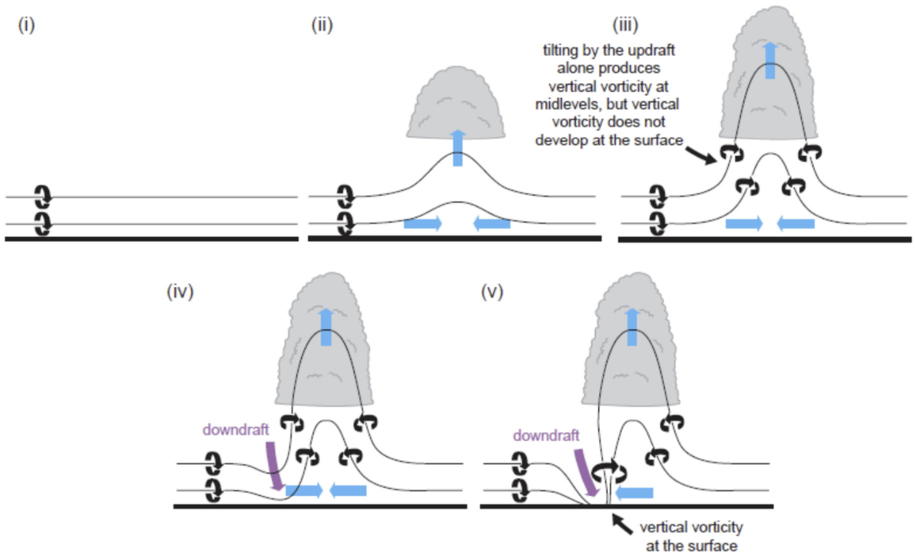

Figure 18: Simple vortex line demonstration where vertical vorticity is initially negligible at the surface and why a downdraft is needed for significant vertical vorticity to develop at the surface under the thunder cell. The black lines are convergence lines that create an updraft which is the blue arrows. The purple arrow is a downdraft. [12]

At the surface, rotation increases at the same time as the vortex lines converge during buoyancy (iv). The tornado becomes wider upwards because ζ_z decreases with height and buoyancy thus advecting ζ_z upwards (v). This situation characterises water spouts and dust vortices, which is the most common type of whirlwind in Denmark. An example of a landspout is shown in figure 17.
Figure 18 is shown a demonstration of how tornadoes can develop in a strong vertical wind shear. The formation of tornadoes requires that ζ_z occur along the ground where ζ_z is small. Thus, T in equation 27 plays a significant role, while stretching is less important. In figure 18, vertical vorticity is initially negligible (i) and there are only horizontal vorticity lines. Then, a buoyancy (ii) due to convection is assumed which will begin to tilt ζ_x and ζ_y below the vertical velocity gradient. Here, generation of ζ_z is maximal around the core of the buoyancy in EL. However, this tilt is not enough (iii) as it will only produce high values of ζ_z on the flank of the buoyancy at midlevels, while there is no ζ_z at the surface. A downdraft, see section 1.4.2, from a possible supercell will be able to evoke ζ_z to the ground (iv), while it can intensify ζ_z and form a tornado (v) during stretching.

2.4.2 Downbursts

In strong thunder cells, strong falling winds called downbursts can sometimes be formed, which cause great damage on the surface. An eyewitness report from the Gråsten cloudburst in 2007, case 3 in the analysis section, reports a downburst. In the image series in figure 19 you can see an example how a downburst has razed a garden in western Jylland.

Figure 19: The left image is before the downburst, the middle image is when the downburst is 'running', while the right image is after the downburst. Photos: Screenshots from a video by Mette Dalsgaard. [24]

Downbursts are falling winds and when water droplets in the cloud evaporate, these falling winds cool down. During evaporation, heat is taken from the air, which thus becomes colder and heavier. The force that produces downbursts is called a downdraft which also plays an important part in the formation of tornadoes (see section 2.4.1.). When the downburst hits the ground, it spreads out in all directions. The dynamics in a downburst is shown in figure 20.
The downward directed streamlines result in the downburst being associated with a relatively high pressure at the surface. The high pressure comes from the air when it reaches the surface is relatively cold, while the air also decelerates when it reaches the ground. The Bernoulli equation gives an estimate of the pressure perturbation, p' beneath the downdraft at the surface:

$$p' \approx \overline{\rho} \left(\frac{v^2}{2} + DCAPE \right) \tag{31}$$

where v is the velocity of the downdraft a few kilometers above the surface, ρ is the density of the air between the height of a given altitude where the velocity is calculated and the surface. DCAPE is the negative buoyancy in the downdraft between a given altitude and the surface. The maximum downdraft speed is given on the basis of the parcel theory:

$$w_{max} = -\sqrt{2DCAPE}. \tag{32}$$

which is very reminiscent of equation 20 for the maximum vertical velocity in an updraft. The total vertical momentum equation can be written as:

$$\frac{dw}{dt} = -\frac{1}{\rho}\frac{\partial p'_d}{\partial z} + \left(-\frac{1}{\rho}\frac{p'_b}{\partial z} + B\right) \tag{33}$$

where w is the vertical velocity, p'_d is the dynamic pressure perturbation, p'_b is the buoyancy pressure perturbation and B is the buoyancy. The first term on the RHS is the effect of the pressure perturbations on vertical motion - or the dynamic forcing. The second term on the RHS is the thermodynamic term and is the effect of buoyancy on vertical motion. In general, the main contribution to downbursts is negative buoyancy.

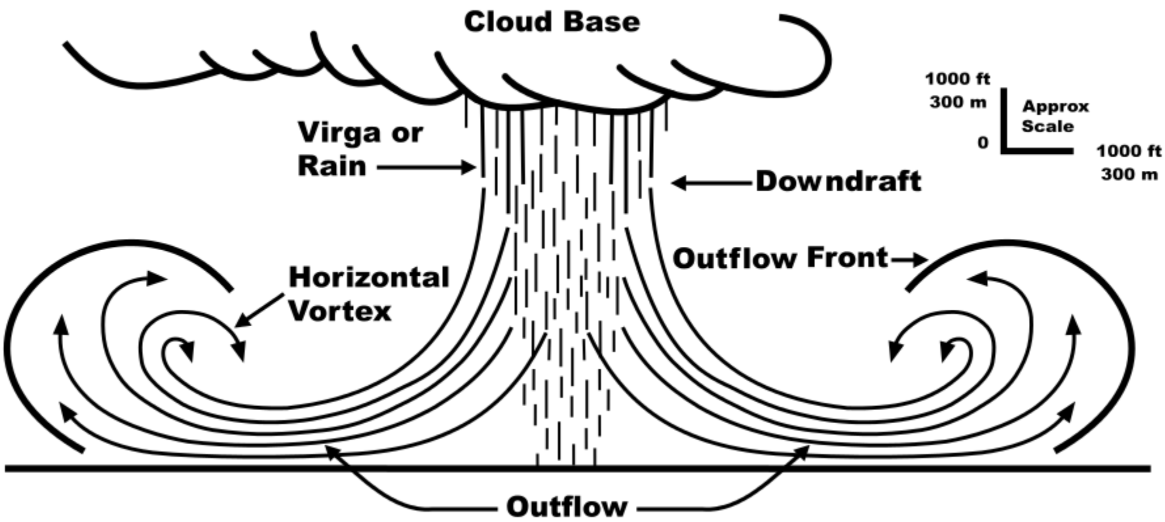

Figure 20: Fujitas model of a downburst with the outflow which create the intense ground-level wind as a vortex ring at the ground. The precipitation can be rain and hail. Tetsuya Theodore Fujita was a Japanese-American meteorologist whose primary research was severe weather. [25]

2.4.3 Floods

Floods are associated with property damage and is one of the most widespread consequences due to cloudbursts in Denmark, which is also the case in the analysis. Floods are the consequence of heavy rainfall and depending on many factors, including amount of rainfall, topography, size of the area and the stationarity of the system.

Typically, floods are seen in connection with cloudbursts that are stationary over a specific area (see figure 21), which was the cause of severe floods in Copenhagen in 2011, see case 4 in section 5 and figure 22.

This happens when the cell motion is reversed the propagation of system, which can result in the system motion becoming quasi-stationary. A warm front or a stationary front that interacts with a low-level jet can lead to backbuilding MCS, where new cells are triggered on the rear flank. If, on the other hand, the low-level wind shear is perpendicular to a front and the mid-level wind shear is parallel to the front, this can also lead to the formation of new cells over the same area. In general, an MCS with a large stratiform precipitation area will give more accumulated precipitation than an MCS with a small stratiform precipitation area. The total accumulation of precipitation in a given rainfall is given by the following expression:

$$P = \overline{R}D \tag{34}$$

where $\overline{R}$ is the average rainfall and D is the duration of the rainfall. A slow system motion will result in increase of D.

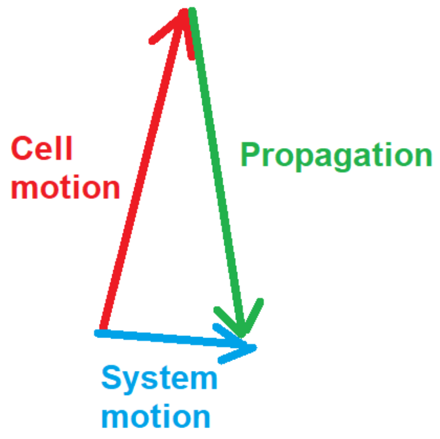

Figure 21: Cancellation between cell motion (red vector arrow) and propagtion (green vector arrow. The system motion (blue vector arrow) is slowed down.

Not all of the water vapor falls out as precipitation from the cloud. The actual rain fall depends on the precipitation efficiency, which is the ratio of the measured precipitation rate at the ground to the water vapor flux through the cloud base. The current rainfall rate, R can be expressed as:

$$R = Ewr_v \tag{35}$$

where E is the precipitation efficiency wr_v is the upward vertical moisture flux expressed with the vertical velocity, w and the water vapor mixing ratio of the rising air, r_v. For heavy rainfall, rising air must have a high content of water vapor and a rapid ascent rate. Increase of R can be a result of large low-level water vapor concentrations, which increase wr_v. It could also be large relative humidity in the environments, which increase E and thus the rainfall rate, R. In the following section, the data base for the analysis of the 7 cases will be described.

Figure 22: The Amager highway near Copenhagen is still flooded two days after the cloudburst in 2011. Photo: Keld Navntoft. [26]

3 Data

3.1 Radar Data

This thesis uses radar data from DMI. DMI has 5 radars located on Stevns, Rømø, Sindal, Bornholm and in Virring in eastern Jylland, see figure 23. All five radars are dual-pole C-band with Doppler effect and operate at wavelengths of 5 cm. Echoes can be measured at a distance of 240 km.

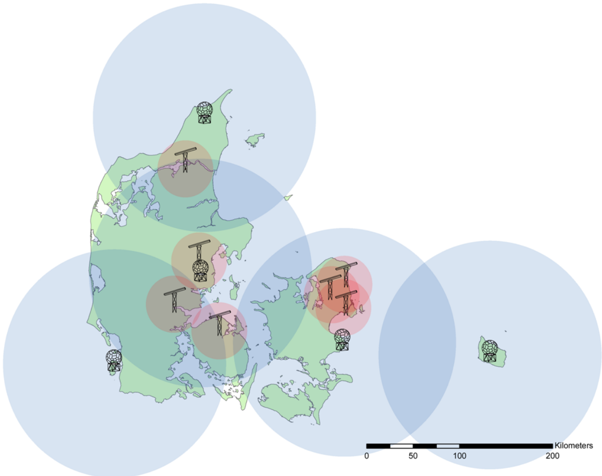

Figure 23: The location of the 5 DMI radars. The red circles are radars which is not in use. [27]

A radar works by emitting electromagnetic pulses into the atmosphere and subsequently measuring how much of the emitted radiation is returning (see figure 24). The returned energy, P_r, measured by the radar is given by the radar equation [28]:

$$P_r = \frac{P_t G^2 \lambda^2}{(4\pi)^3 r^4} \sum \sigma \tag{36}$$

where P_t is the transmitted power, G is the gain of the antenna, λ is the wavelength of the radar beam and σ is the cross section of the scatter. Equation 36 is the radar equation for isolated scattered. The emitted radiation is scattering back by precipitation particles and other meteorological targets, but also irrelevant elements to the measurement. The total radar cross section, $\sum \sigma$ for the scatters can be written as a product of the radar reflectivity, ν and the volume V, $\sum \sigma = V\eta$. This can be used in equation 36:

$$P_r = \frac{P_t G^2 \lambda^2}{(4\pi)^3 r^4} V\eta \tag{37}$$

The volume in the radar equation (37) is defined as:

$$V = r^2 \frac{c\tau}{2} \frac{\pi\theta^2}{8ln(2)} \tag{38}$$

where $\frac{c\tau}{2}$ is a normalization constant and θ is the width in radians of the one-way power. Equation 38 can be used in equation 37:

$$P_r = \frac{P_t G^2 \lambda^2 \theta^2 c\tau}{1024 ln(2) \pi^2 r^2} \eta \tag{39}$$

The distribution of the radar reflectivity, η, depends on the raindrop distribution and is given by:

$$\eta = \int_{D_{min}}^{D_{max}} \sigma(D) N(D) dD \tag{40}$$

where D is the diameter of the raindrops, N is the number of raindrops and σ is the radar cross section expressed by $\sigma = \frac{\pi^5}{\lambda^4}|K|^2 D^6$. K is a dielectric constant and depends on the condition of the particles, as it is different how much ice and water reflect [29]. Substituting σ in equation 40 yields:

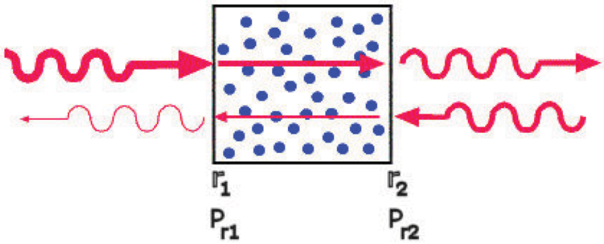

Figure 24: The square shows a volume of air consisting of gasses or precipitation particles. The radar beam changes as it passes through this volume of air in both directions due to scattering, absorption and reflection. r_1 and r_2 are the distances to the radar, while P_{r1} and P_{r2} are the energy levels at the specified distances. [29]

$$\eta = \frac{\pi^5}{\lambda^4}|K|^2 \int_{D_{min}}^{D_{max}} D^6 N(D) dD = \frac{\pi^5}{\lambda^4}|K|^2 Z \tag{41}$$

The integral on the RHS is defined as the radar reflectivity factor, Z, that is a measure of the reflected energy. Subsituting equation 41 in equation 39 gives the final radar equation expressed as:

$$P_r = \frac{P_t G^2 \pi^3 \theta^2 c\tau |K|^2 Z}{1024 ln(2) \lambda^2 r^2} \tag{42}$$

The radar equation is thus related to the transmitted energy from the radar, the reflective elements in the atmosphere, atmospheric conditions and the weakening of the transmitted energy.

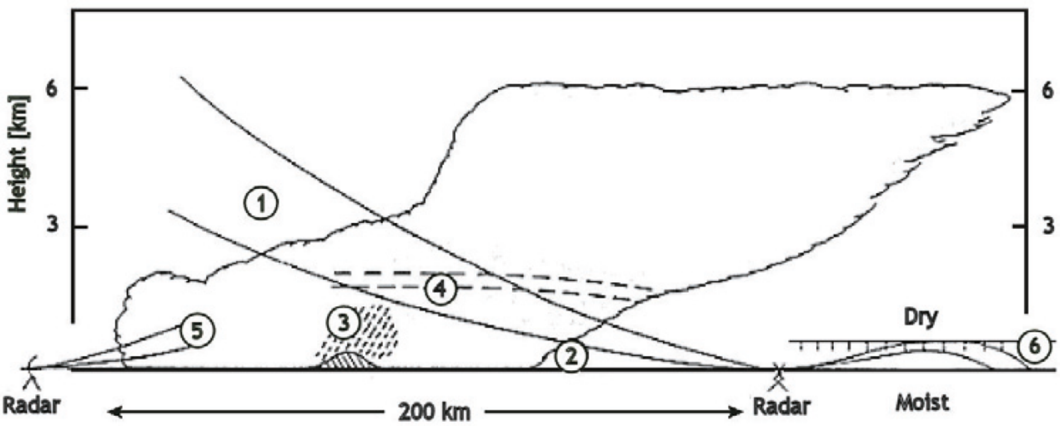

Figure 25: (1) Precipitation can be underestimated if it is below the radar beam, (2) evaporation of precipitation particles under the radar beam, (3) precipitation is amplified under the radar beam due to orographic conditions, (4) bright-band the effect, which is the effect where the beam hits a layer of melting ice crystals and thus has a too high reflection value, (5) the absence of large droplets in drizzle can give an underestimation and (6) strong deflection of the radar beam, e.g. in relation with an inversion layer. [30]

Radars are an important part of the meteorological work, for example following precipitation. However, radars also contain errors that can be linked to both atmospheric condition, objects in the atmosphere such as birds but also the radar itself. On the radar side, errors can occur due to uncertainty in antenna conditions, energy loss in the radar system and bias on the elevation. The last one means that radar measurements at a great distance are less representative, because the radar radiation is deflected. Then radar measurements are taken higher up in the atmosphere further away from the radar. This means that precipitation is missed close to the surface. The atmospheric errors related to radars are shown in figure 25.

3.2 Satellite Data

This thesis uses satellite images from the European Organization for the Exploitation of Meteorological Satellites (EUMETSAT) [31]. There are 3 types of satellite images: visible, infrared and water vapor. The first two will mainly be used in the analysis from 2 different satellite series have been used.
Visible images are only usable during the day, as clouds reflect the sun light that the satellites receive. In these types of images, clouds are usually white, the ground is gray and water is dark. Infrared images can show both clouds during the day and night. Instead of sunlight, the satellite sensors measure heat radiating from the clouds. Clouds are colder than the earth's surface, which means that cloud tops will have white contrasts due to higher reflection of sunlight. Strong convection typically results in very cold cloud peaks that are easy to identify on infrared images. Water vapor images will be used briefly. They indicate how much water vapor is in the upper troposphere. Water vapor images can identify areas where the possibility of heavy rain is present.
Meteosat First Generation (MFG) is a global system of geostationary satellites to observe the atmospheric circulation. The image data from MFG is categorized as high rate transmission with 3 different spectral channels. The time resolution is 30 minute intervals and the satellite series covers throughout Europe. Visible images, channel 0.6 μm, are used from this serie.
The second one is Meteosat Second Generation (MSG). There are 4 programs that range from Meteosat-8 to Meteosat-11, and it is Meteosat-11 that operates with a 0 degree service. The major improvements for MSG is 12 imaging channels (3 imaging with MFG), images every 15 minutes (30 minutes resolution with MFG) and improved spatial resolution [32].
It is MSG's primary instrument, the Spinning Enhanced Visible and InfraRed Imager (SEVIRI) from which the images originate. The SEVIRI instrument, see figure 26, is a satellite from 36,000 km altitude. The resolution from this altitude is 1 km for visible channels and 3 km for infrared channels. The spectral range is 0.4 to 1.6 μm for 4 visible and 3.9 to 13.4 μm for 8 infrared channels.
The SEVIRI instrument has the ability to transmit data as high rate transmission in 12 different spectral channels, see table 1. This table shows the spectral characteristics of the SEVIRI channels. VIS0.6, VIS0.8, IR1.6, IR3.9, IR10.8 and IR12.0 correspond to the six AVHRR-3

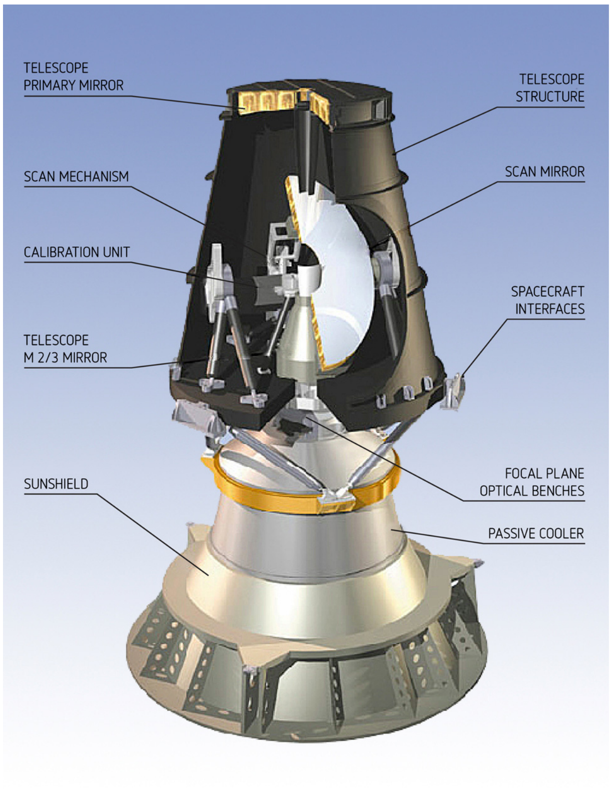

Figure 26: The SEVIRI instrument [32]

channels and the channels HRV, WV6.2, IR10.8 and IR12.0 correspond to VIS, WV and IR channels from the MFG. The visible spectrum, VIS0.6 and VIS0.8, will provide cloud and land surface during the day. This thesis uses visible images from channel 0.6 μm (VIS0.6). The infrared channels can be used for various things. IR1.6 is used to distinguish low-level clouds from snow surfaces, the IR 3.9 channel can be used to detect fog and low-level clouds at night and to discriminate between water clouds and ice surfaces during daytime. They are both supporting other infrared channels. The thesis uses the infrared channel 10.8 μm (IR10.8) which is a channel in the atmospheric window and is used together with IR3.9. The two channels in the water-vapor absorption band, WV6.2 and WV7.3, provides the water-vapor distribution in the troposphere. On one occasion, the water vapor channel 6.2 μm (WV6.2) has been used in the analysis.

3.3 Surface Synoptic Observation Data

Surface Synoptic Observation (SYNOP) data is downloaded from DMI's Free data API system. It is raw observation data from DMI's stations placed in various locations in Denmark, where mainly the local data will be used in the analysis. Raw data means that these are not quality assured. Therefore, errors must be present in this data, i.e. from the instrument itself due to wear or general exposure to weather and wind. The measurements are based on World Meteorological Organization (WMO) standards, which include that the temperature is measured at a height of 2 m and the wind is measured 10 m above open terrain.

A disadvantage of SYNOP stations is that they measure in points. The point value is very accurate but says nothing about the surface like a radar does. Interpolating the precipitation based on the point precipitation in regions to raingauges, would assume that the precipitation is evenly distributed, which it rarely is when the precipitation is convective. Convective showers can easily slip through even a dense network of raingauges.

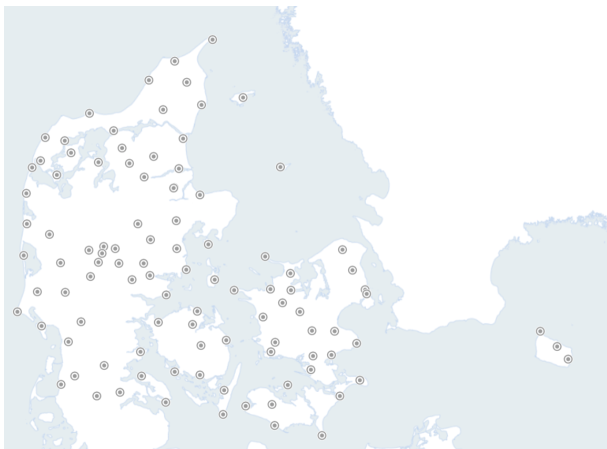

Figure 27: The current network of DMI stations that measure precipitation. Some have been set up within the last 20 years, so all of them are not involved in the individual cases. Thunder cells can also often bypass a station, so their data can be unreliable. The map is from DMI.

Therefore, a lot of data can be lost when assessing which cloudburst events have been the most powerful or with the highest intensity. Figure 27 shows a distribution of DMI's official raingauges, which are unevenly distributed, as there are some places where many are gathered, while there are also some places where raingauges are missing and where showers are possible to slip past without any problems. A somewhat denser network of raingauges around larger cities is available at SVK, see figure 28. This arises the problem that Copenhagen in particular has a predominance of stations, and therefore it is perhaps especially in Copenhagen that the heaviest precipitation events are often measured opposite the west coast where there are virtually no raingauges to be found.

The spectral characteristics of the SEVIRI channels			
Channel	Absorption Band Channel Type	Nom. Centre Wavelength (μm)	Spectral Bandwidth (μm)
HRV	Visible High Resolution	nom. 0.75	0.6 to 0.9
VIS 0.6	VNIR Core Imager	0.635	0.56 to 0.71
VIS 0.8	VNIR Core Imager	0.81	0.74 to 0.88
IR 1.6	VNIR Core Imager	1.64	1.50 to 1.78
IR 3.9	IR / Window Core Imager	3.92	3.48 to 4.36
WV 6.2	Water Vapour Core Imager	6.25	5.35 to 7.15
WV 7.3	Water Vapour Pseudo-Sounding	7.35	6.85 to 7.85
IR 8.7	IR / Window Core Imager	8.70	8.30 to 9.10
IR 9.7	IR / Ozone Pseudo-Sounding	9.66	9.38 to 9.94
IR 10.8	IR / Window Core Imager	10.80	9.80 to 11.80
IR 12.0	IR / Window Core Imager	12.00	11.00 to 13.00
IR 13.4	IR / Carbon Diox. Pseudo-Sounding	13.40	12.40 to 14.40

Table 1: The spectral channels. [32]

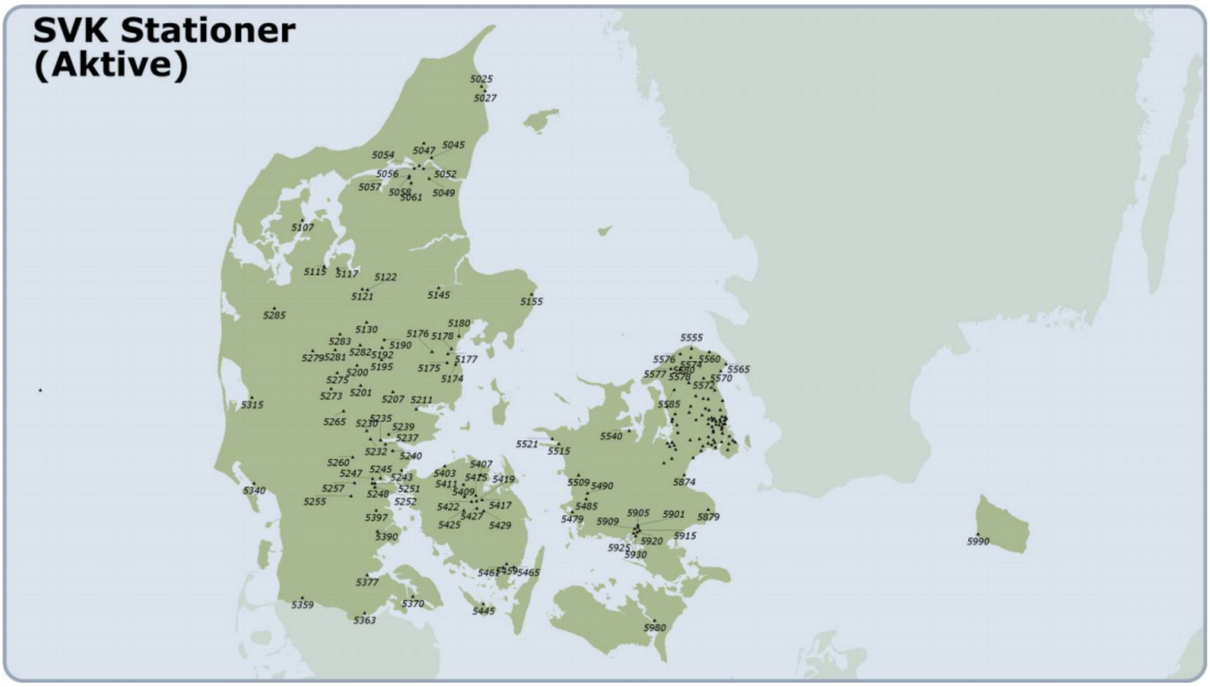

Figure 28: The network of SVK raingauges. [33]

3.4 Analysis Charts

A number of analysis maps have been used from different weather models, both global and regional. The main model in the analysis is the numerical model, Global Forecast System (GFS), where analysis maps from wetter3 [34] (freely available) are used for the synoptic analysis. GFS is a global computer model run by the US National Weather Service (NWS). GFS is a spectral model with a horizontal resolution of 13 km. Vertically, the model is part of 127 layers up to the mesopause. The analysis maps are usable in 6 hour intervals, 00UTC[4], 06UTC, 12UTC and 18UTC.

Precipitable Water (PW) maps are used from National Oceanic and Atmospheric Administration (NOAA) and their Physical Sciences Laboratory homepage [35]. Here maps or composites of variables from the joint product can be plotted from the National Centers for Environmental Prediction (NCEP) and the National Center for Atmospheric Research (NCAR) reanalysis dataset. Data is available from January 1948 to the present. The data is available 4 times daily, 00UTC, 06UTC, 12UTC and 18UTC.

Some of the figures originate from the DMI-Harmonie model, which has a hourly resolution and is a 2-day short range probabilistic weather model for northern and western Europe. Horizontally, the model has a 2.5 km resolution. Harmonie is a non-hydrostatic mesoscale system developed by the High Resolution Limited Area Model (HIRLAM).

No more maps have been used from DMI-Harmonie because of the lach of availability. It has simply been too costly to get archive raw data from this model. Some of the maps are from earlier analysis from the Danish journal 'Vejret' - all analysis by Niels Woetmann Nielsen.

A reanalysis model is also used for the precipitation map in case 1. The reanalysis data has been provided by Meteomatic. The model data has been constructed from ECMWF's reanalysis model ERA5. ERA5 provides hourly data sets and cover the Earth on a 30 km grid using 137 levels from the surface up to a height of 80 km. The ERA5 data goes back to 1979 but ERA5 dataset are available from 1950 to 1978 at the Climate data store. These maps are plotted with the software QGIS.

3.5 Soundings

The last data used is from a number of atmospheric soundings in or around Denmark. Soundings are measurement methods which typically use a radiosonde to measure atmospheric parameters up through the troposphere. Typically launches are twice a day, 00UTC and 12UTC.

Figure 29: Radiosonde balloon

Unfortunately, there are not many soundings left in Denmark, as they are gradually being phased out. Vertical profile measurements of the troposphere are invaluable for understanding the basic mechanisms behind cloudbursts. For case 1 and case 2, it has been possible to use soundings from Jægersborg in the northern part of Copenhagen with launches at 00UTC and 12UTC. However, already from 2007 onwards this has been phased out and thus in Denmark there has only been an opportunity for a sounding from

[4] French: Temps Universel Coordonné (UTC), in English: universal time

Karup in Central Jylland, which is only launched once a day around 03UTC and Ekofisk in the North Sea. Alternative solutions have therefore been used. For case 3 and case 7 from Sønderjylland, a sounding from Schleswig has been used with launches at 00UTC and 12UTC. For the remaining cases, which have primarily taken place in Copenhagen, soundings from Greifswald in the northern Germany have been used with launches at 00UTC and 12UTC as well as soundings from Visby on the Swedish island of Gotland, also with launches 00UTC and 12UTC.

The purpose of these soundings is to describe the possible air mass that has prevailed in the individual cases. All sounding has been generated freely through the database at University of Wyoming [36], which has a worldwide archive of soundings. Before we will analyze the soundings, as well as all the other mentioned data, we will review the method of this thesis in the following section.

4 Method

The general method used in the analysis is based on the funnel technique, where the analysis starts from a synoptic perspective and describe the overall weather situation in the individual cases with a focus on air masses, fronts, stability and the background flow. Analysis maps for the upper and lower troposphere will be examined as well as satellite images, which can provide important information for the frontal analysis and for how the cell structure degenerates.

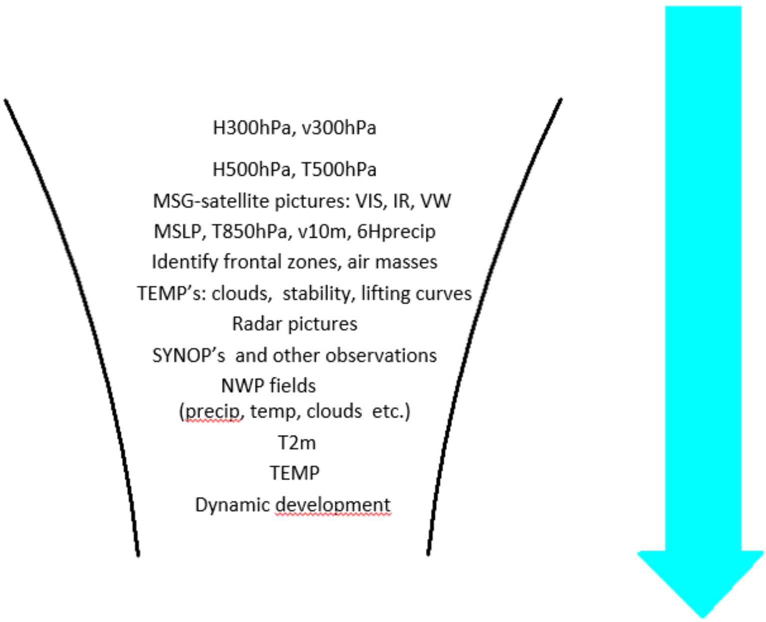

Figure 30: The funnel technique.

Then, there will be zoomed in for mesoscale analysis for the individual local areas and nearby soundings, satellite, radar and model data will be used to describe the dynamic development of MCS. Figure 30 shows the concept of the funnel method. The use of the funnel technique means that we can both gain an understanding of each individual cloudburst case at synoptic level, but also of the local circumstances behind the cloudburst triggers. At the same time, the funnel technique uses many types of data that can provide an overall picture of each case, and this means that we can assess when several different types of data support the same picture of how cloudbursts are formed. It is thus easier to see with the method, due to all the data, if for example the quality of the satellite images provides misleading information, but all other data from a case implies something else. The majority of the analysis will be on a mesoscale.

4.1 Cloudburst Indicators

Niels Woetmann Nielsen et. al. [37] has worked with an index for describing cloudbursts in numerical weather prediction, from which selected indicators will be used during this analysis so that different properties in the troposphere can be described through to the generating background for cloudbursts. The index consists of eight indicators, each indicator represent a property of the troposphere which has an effect on the development of cloudbursts.
First of all, the cloudburst index consists of a parameter that describes vertically integrated water vapor which is an important parameter in a cloudburst index as it affects other parame-

ters, where increasing values of vertically integrated water vapor result in decreasing CIN and CAPE values. In the analysis, water vapor is considered, but the main focus is on satellite images, including water vapor images in a single case.
The next parameter used is the steering level wind, which is an important indicator of how the individual thunder cells are moving. In this report, the main focus will be on the wind shear and how this changes up through the troposphere, as this is a general way in which thunder cells organizes itself.
Parameters four and five are CIN and CAPE, which is also analyzed in relation to soundings that with lifting curves can give clear indications of how unstable the troposphere is and how a cloudburst or heavy rainfall has occurred. In the overall cloudburst index the pressure difference between LFC and EL in the troposphere has been used.
The last two indicators are based on two thunderstorms indices. One is the K-index which will be used in this report and is described in section 4.2. The other is thus named Thunder-storm index. This will not be used, but other indexes will be used to give a sense of the state of the troposphere. These indices will be described in the next section, along with the K-index.
Overall, the cloudburst index gives a good sense of what parameters are important to keep an eye on. Only selected parameters from the index will be used to support the phases of the analysis. In addition, important tools such as radar images, satellite images and soundings will be used to describe the vertical profile of the troposphere in the individual cases, which is an important way of understanding cloudbursts.

4.2 Stability Indices

Different stability indices will be used to determine convection in a given atmosphere. According to Bluestein [11], the most commonly used stability indicators are the lifted index, the total-totals index, the Showalter index and the K-index.
The lifted index (LIFT) is based on an air parcel that is lifted from the surface pressure level to the LCL and then lifted moist-adiabatically to the 500 *mb* surface. The parcel temperature is then subtracted from the environmental 500 *mb* temperature, T:

$$LIFT = T_{500mb} - T_{p,500mb} \tag{43}$$

A positive index shows that the atmosphere is stable because the parcel is colder than the surroundings. A negative index shows that the atmosphere is unstable, where a lifted index less than -6 indicates the possibility of very intense convection. A zero index indicates a neutral atmosphere.

LIFT	Thunderstorm probability
> 0	Stable, only weak convection
-1 to -3	Marginally unstable, thunderstorms possible with a lifting mechanism
-4 to -5	Moderately unstable, thunderstorms likely
-6 to -7	Very unstable, strong/severe thunderstorms likely. Tornadoes possible
< -9	Extremely unstable, severe thunderstorms. Tornadoes possible

The total totals index (TOTL) consists of the sum of the lapse rate between 850 and 500 mb and the difference between the dewpoint at 850 mb and the 500 mb temperature, T:

$$TOTL = (T_{850mb} - T_{500mb}) + (T_{d,850mb} - T_{500mb}) \quad (44)$$

TOTL	Thunderstorm probability
45 to 50	Scattered thunderstorms
50 to 55	Thunderstorms more likely. Few scattered severe and isolated tornadoes
55 to 60	Severe thunderstorms most likely. Scattered tornadoes

The showalter index (SHOW) is similar the LIFT, but the parcel is lifted from the 850 mb to the LCL and then moist adiabatically to 500 mb. The resulting index parameter is given by the temperature of the parcel subtracted from the actual 500 hPa temperature:

$$SHOW = T_{500mb} - T_{parcel} \quad (45)$$

SHOW	Thunderstorm probability
> 4	Stable
1 to 3	Marginally unstable, thunderstorms possible with a lifting mechanism
0 to -2	Moderately unstable, thunderstorms likely
-2 to -3	High potential for thunderstorms
-4 to -5	Very unstable, strong/severe thunderstorms likely. Tornadoes possible
-6 to -10	Extremely unstable, severe thunderstorms. Tornadoes possible

The last index is the K-index (KINX) or Georges index. This index is derived by:

$$KINX = (T_{850mb} - T_{500mb}) + T_{d,850mb} - (T_{700mb} - T_{d,700mb}) \quad (46)$$

where T is the temperature at altitudes of 850 mb, 700 mb and 500 mb and T_d is the dewpoint temperature at 850 mb and 700 mb. This gives the following interpretation:

KINX	Thunderstorm probability
< 20	No thunderstorms
20 to 25	Isolated thunderstorms
26 to 30	Widely scattered thunderstorms
31 to 35	Scattered thunderstorms
35 to 40	Numerous thunderstorms
Above 40	Guaranteed for thunderstorms

In the tables for LIFT, TOTL, SHOW and KINX, tornadoes are indicated at different values of the individual indices. This must be assumed to be based on experience, because in the background equations used to calculate the index values there are no indicators that can give a clue as to whether tornadoes can form or not. They only provide ideas about how unstable the troposphere may be supposed to be. All indices can be calculated based on soundings.

The overall method is to get an overview of the 7 cases through many kinds of data, as it provides a better basis for comparison between the cloudbursts, instead of perhaps making one very detailed analysis of a single cloudburst. At the same time, an analysis could be done with more cloudbursts, but that would have cost precision.
Now that we have looked at the method, as well as the theory and use of data in the thesis, it is time to use this information to analyze the 7 cloudburst cases. This will hopefully end up providing a kind of overview and understanding of cloudbursts in Denmark.

5 Analysis and Discussion of Cloudburst and Extreme Rain Event in Denmark

In this section, 7 different cases with cloudbursts in Denmark over the last 25 years will be analysed with a focus on understanding the underlying mechanisms responsible. The common denominator for the cases is that they are DMC events.

The different cases are chosen based on their severity. This means that it is not a goal to go through the cases that have given the most precipitation or the highest intensity. In contrast, the cases are selected by how they have been experienced by the population. For example, tornadoes in Denmark are a unique sights that only happens rarely. The cloudburst in Copenhagen in 2011, which caused large amounts of precipitation, which put the Danish capital under water.

Table 2 contains the total cloudburst statistics from DMI and SVK in the period 2011-2019. According to DMI, the definition of a cloudburst is more than 15 *mm* of precipitation in 30 minutes. In comparison, the highest measured precipitation intensity in Denmark is 31.2 *mm* in 10 minutes from 2nd of July 2011 in Copenhagen (case 4). The second highest is a cloudburst in the midsummer 2016 on Ærø south of Fyn, where 29.2 *mm* of rain fell in 10 minutes, while the third highest precipitation intensity in Denmark is from 20th of July 2017 in southern Fyn with 27.9 *mm* in 10 minutes [38]. Here it should be mentioned that in connection with a cloudburst at Gråsten in 2007 (case 3), extreme 53 *mm* of rain was calculated in 10 minutes. However, this value is based on radar measurements and not precipitation measurements and therefore there is some uncertainty associated with this measurement.

Criterions for cloudburst	Precipitation in 30 min	2011	2012	2013	2014	2015	2016	2017	2018	2019	Means
Number of stations	>30 *mm*	29	2	2	14	2	5	3	4	6	7.4
	>25 *mm*	42	8	5	25	9	8	7	8	19	14.6
	>20 *mm*	60	22	10	64	20	25	25	20	52	33.1
	>15 *mm*	122	64	40	133	66	98	111	67	152	94.8
Number of days	>30 *mm*	6	2	2	6	1	4	3	4	6	3.8
	>25 *mm*	10	7	4	8	5	5	7	6	8	6.7
	>20 *mm*	17	12	9	14	9	11	10	8	15	11.7
	>15 *mm*	27	20	18	33	20	18	20	18	34	23.1
Raingauges in Denmark	Number	220	250	260	260	260	260	270	285	285	

Table 2: Cloudbursts registered in Denmark 2011-2019 by DMI's raingauges and the SVK system. [1]

Table 2 has been prepared by climatologist Mikael Scharling from DMI. SVK's cloudburst statistics go back to the 1980s from i.a. heating plants and treatment plants and has the same cloudburst definition as DMI. DMI's cloudburst statistics started in 2011, when DMI got a nationwide network of raingauges that could measure precipitation intensity. It started in 2010 when DMI made a number of major changes within their raingauge network. One change was that they switched from manual raingauges with measurements every 24h at 06UTC to automated raingauges, which also have the ability to measure precipitation intensity. Thus, it was only after 2010 that DMI could measure whether something was a cloudburst and thus keep statistics on this.

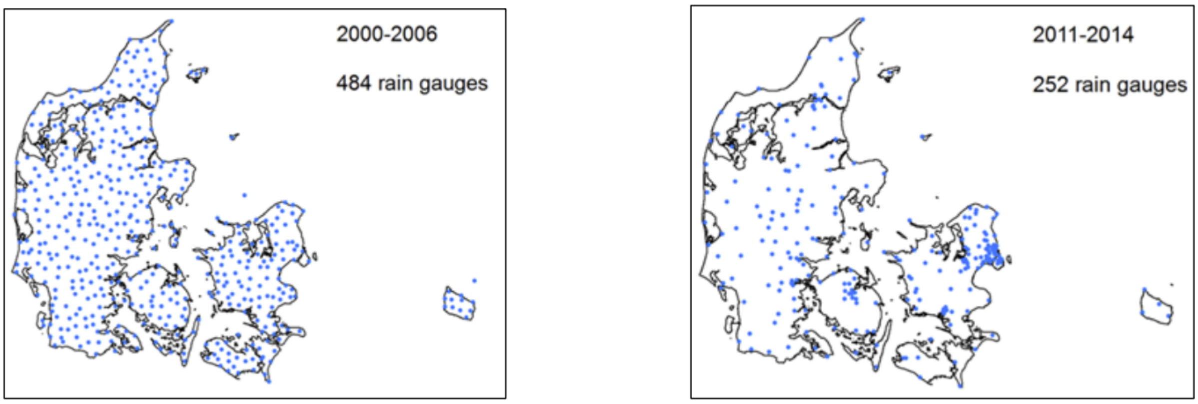

Figure 31: DMIs raingauges before 2010 (left) and after 2010 (right). [39]

The other major change was that they reduce the number of raingauges (see figure 31) by over 200 raingauges. A sharp drop in the amount of raingauges, which quite obsessively makes it more difficult to measure convective precipitation, including cloudbursts, as cloudbursts here are easier to slip past a raingauge. One problem is also the location of raingauges. SVK's raingauges are centered around the large cities as shown in figure 28. Thus, it is not possible to measure cloudbursts in sparsely populated areas and the number of cloudbursts in Copenhagen may feel higher than elsewhere in the country. Cloudbursts must therefore be expected to be missed in both SVK's and DMI's network of raingauges.
If you look at table 2, it is noted that the higher the intensity, the fewer events there are. At the same time, it should be noted that for some of the events, there are often more stations that measure a given intensity than there are number of days. 2011 is for example very significant, which can be attributed to the cloudburst over Copenhagen on 2nd of July. It was a fairly widespread rain area that gave high intensities to large parts of Copenhagen and by extension many raingauges. In relation to the station network, there are quite a few raingauges in the capital region. Therefore, it is very obvious that there were actually a number of stations that measured more than 30 mm, while the number of days is somewhat lower. In the relatively short period the table contains, there are large variations in the number of cloudbursts per. year, where 2019 is the year with most cloudbursts.
There are no years without cloudbursts - even if you only look at heavy cloudbursts. Figure 32 shows that the vast majority of cloudbursts occur in the summer months with a predominance to August. May and September also follow, while the rest of the month are more sporadic and contains only quite a few cases of cloudbursts, if any. Despite the fact that it is a very short period for the cloudburst statistic, a picture is already emerging that cloudbursts are a summer phenomenon in Denmark.
All values are the daily maximum, which is a log of sum and intensity for the individual stations. When you check for cloudbursts, you log the daily maximum of e.g. 10 minutes intensity, which will often be the cloudburst that day.
The means column in table 2 shows that there is a difference whether it is stations or days with a given intensity. At precipitation intensities above 25 mm there is a difference of approx. 50

%, while the lower the intensity the more stations have measured it. During the period, the number of raingauges increased by 65. This means that the further you go back in time, the more difficult it becomes to be able to compare the years.

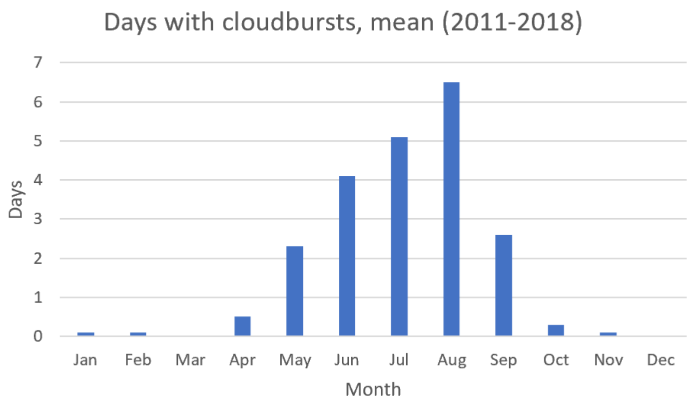

Figure 32: Distribution of cloudbursts all year round in Denmark where the statistic apply for the period 2011-2018. Data: DMI [40]

From a 9-year period, it is difficult to talk trends, but in table 3 in appendix C a total list of the 43 highest 10-minute intensities is written down from the SVK network. It is worth noting that 34 of the intensities in this table were measured in the period 2005-2019. As many as 8 of these measurements from 2nd of July 2011 are in the area of Copenhagen. This provides fertile ground for believing that Denmark is more exposed to cloudbursts.

As previously mentioned, it is too extensive to dive into every single cloudburst that has been in Denmark. Some may have only hit quite locally and have been on the border between micro and mesoscale. Therefore, the cases are primarily selected due to the largely similar to each other with quasi-geostrophic forcing as their primary source. Also orography forcing in relation to land-sea distribution comes into play and then there are a couple of cases, especially case 6, that fall a lot out of category, as forcing in extratropical cyclogenesis probably plays a role.

With the exception of case 1, where there is a lack of data but no lack of eyewitnesses to how bad it was, and case 7, which was extraordinary with a regular tornado, the cases are included on SVK's lists of most powerful cloudbursts for the individual years. During the analysis, known and unknown locations are mentioned. In appendix D a map of all locations can be found.

5.1 Case 1: 30th of June 1997, the Cloudburst in Copenhagen, 17.30UTC

In the Danish newspaper Politiken, the cloudbursts which hit the Danish capital Copenhagen on 30th of June 1997, are described as a storm of tropical dimensions with fallen trees in the flooded streets [41].

A low during deepening, moved this summer day in a northwestern lane from the northwest coast of the Netherlands to the British west coast. In figure 33 the geopotential is shown at 500 *hPa* altitude where a trough is represented over the British Isles and in the western part of the North Sea. In addition, the location of the low can be followed from 12UTC to 00UTC. A high is represented southeast of Finland which places the jet axis just across or a little bit west of Denmark.

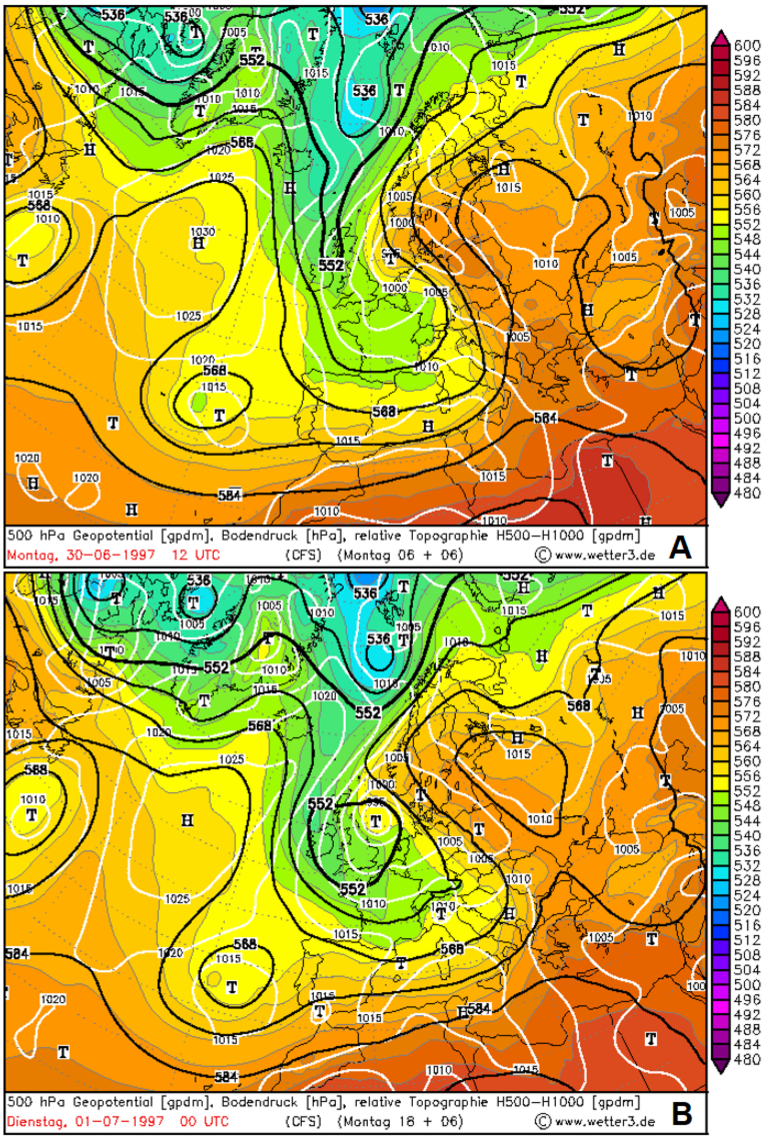

Figure 33: GFS 500 *hPa* geopotential, black curves [*gpdam*] and surface pressure, white curves [*hPa*]. H is high pressure and T is low pressure. 12UTC, 30th of June 1997 (A) and 00UTC, 1st of July 1997 (B). [34]

Due to frontogenesis, a frontal zone emerges in figure 34 A to C, which shows the change in the equivalent potential temperature from cold to warm. In the zone between the cool air flow from southwest and the warmer air flow from southeast, a confluence zone is formed, which is indicated by the divergence of the wind in figure 38 (p. 43) and is described in section 2.1.1. Figure 34 shows that Copenhagen at 12UTC is in the warm air (figure 34A) and 12 hours later is in the cold air on the other side of the frontal zone (figure 34C). At 18UTC Copenhagen is in the confluence zone (figure 34B), the same time period when the storm reached its maximum intensity from 17.15UTC to 17.45UTC, which is later supported by satellite images and observations.

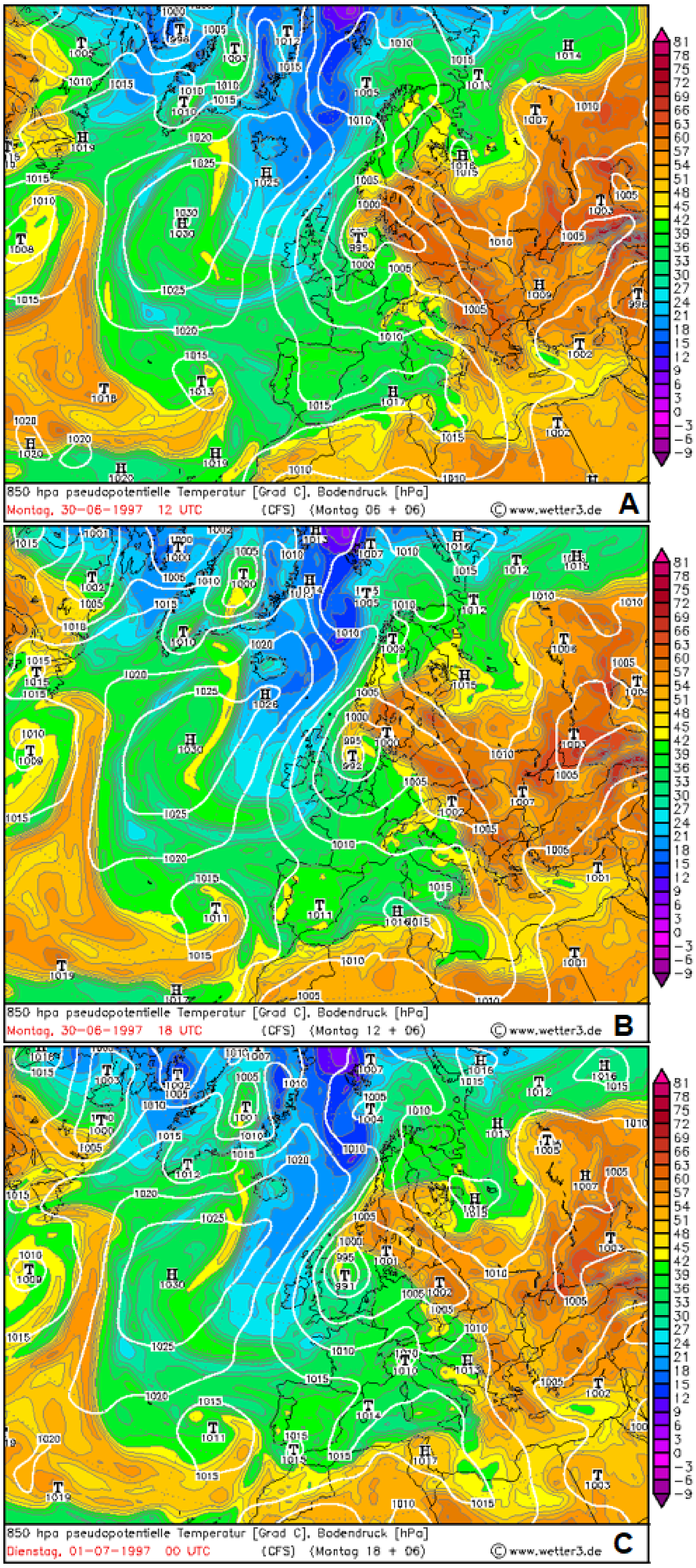

Figure 34: GFS 850 hPa pseudopotential temperature [°C] and surface pressure, white curves [hPa]. H is high pressure and T is low pressure. 12UTC, 30th of June 1997 (A), 18UTC, 30th of June 1997 (B) and 00UTC, 1st of July 1997 (C). [34]

Unfortunately, there are no radar data from this June evening, which otherwise would have been a good support for the analysis. The best way to estimate the precipitation is through the model output from Meteomatic in figure 35. In this figure there are indications that the heaviest precipitation over Copenhagen occurred from 17UTC to 18UTC. Furthermore in figure 37 (p. 43) a NCEP/NCAR reanalysis for PW is shown from NOAA. The figure indicates the amount of moisture above a fixed point as a composite mean for 18UTC. It can be observed that there is relatively high moisture content along the frontal zone and generally in the warm air mass, which favors the formation of severe storms as described in section 2.2.3.

The temporal development of the system is shown in the satellite images in figure 36 (p. 42) from the period 13UTC to 18UTC with hourly intervals. The satellite images are represented by the visible 0.6 μm channel from MFG geostationary satellite data (see details in section 3.2). The full temporal resolution of the satellite data is 30 minutes. Copenhagen is indicated with a yellow arrow, while the cold front is marked by the blue line. The satellite images shows that the thunder cells have occurred along the cold front in the confluence zone in a line that stretches from southern Sweden and to the southeastern part of Europe. The cloud belt even runs parallel to the upper tropospheric jet associated with the cold front zone (see figure 38, p. 43, for the tropospheric jet). In the entire

cloud band along the cold front zone, it is possible to register several thunder cells which are under development. The cold front is almost stationary, but has a weak component to the east-northeast direction. The weak component means that the system of thunder cells almost runs along the frontal zone in a north-western direction.
The orange ring in figure 36 marks the area that leads to the powerful cloudburst in Copenhagen. The image 18UTC is just after maximum intensity. A comparison with the model output for the precipitation in figure 35 shows that starting at 16UTC, the heavy precipitation is located over northwestern Germany in the area north of Greifswald (green arrow) and the Baltic Sea. Throughout the period, the system moves to the northwest. At 17UTC, the cells begin to develop in Skåne and move into the region of Øresund and hit Copenhagen. At 18UTC the thunder cells are located in northern Sjælland and in the evening the thunder cells are in Kattegat, which is represented by both precipitation and satellite in figure 35 and figure 36.

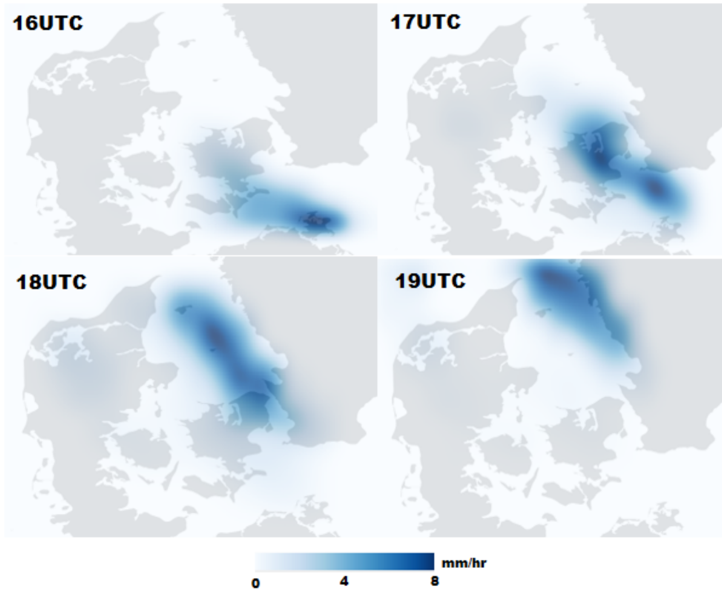

Figure 35: Hourly precipitation, model data from Meteomatic, 16UTC to 19UTC. Largest intensity represented by dark colours. The first indications of strong intensity are seen over the northwestern Germany at Greifswald, 16UTC. The system moves to the northwest and hits Copenhagen between 17UTC and 18UTC before moving further across Kattegat.

The atmosphere during the incident is described with two soundings from Jægersborg north of Copenhagen for 30th of June 1997, 12UTC and 1st of July 1997, 00UTC. The sounding from 12UTC at Jægersborg (figure 39A, p. 44) shows the conditions in the warm air before the cold front passage.
The lifting curve shows the LFC[5] in 586.7 hPa. At this altitude, an air parcel will be subjected to an upward buoyancy of up to about 360.6 hPa where it reaches EL. The presence of moisture at the bottom will cause the formation of convective showers with a cloud base in LCL in 883.4 hPa and a cloud top in 180 hPa.
A strong wind shear in the lower 4 km at 24 m/s [6] tell us that powerful thunder cells have the opportunity to develop in the atmosphere at this time. At 6 km, winds have decreased to 15 m/s, which could still indicate that we are in a spectrum that counts both multicells and possible supercells according to figure 7.
All four indexes, LIFT, SHOW, KINX and TOTL from the method section 4.2 have values that prove that in Copenhagen there is a high risk of numerous cloudbursts in a moderately unstable atmosphere. The TOTL is even on the verge of the possibility of scattered tornadoes being present.

[5]Sounding parameters are defined in section 2.2.3
[6]The measured wind shear is from the background data for the different soundings [36]

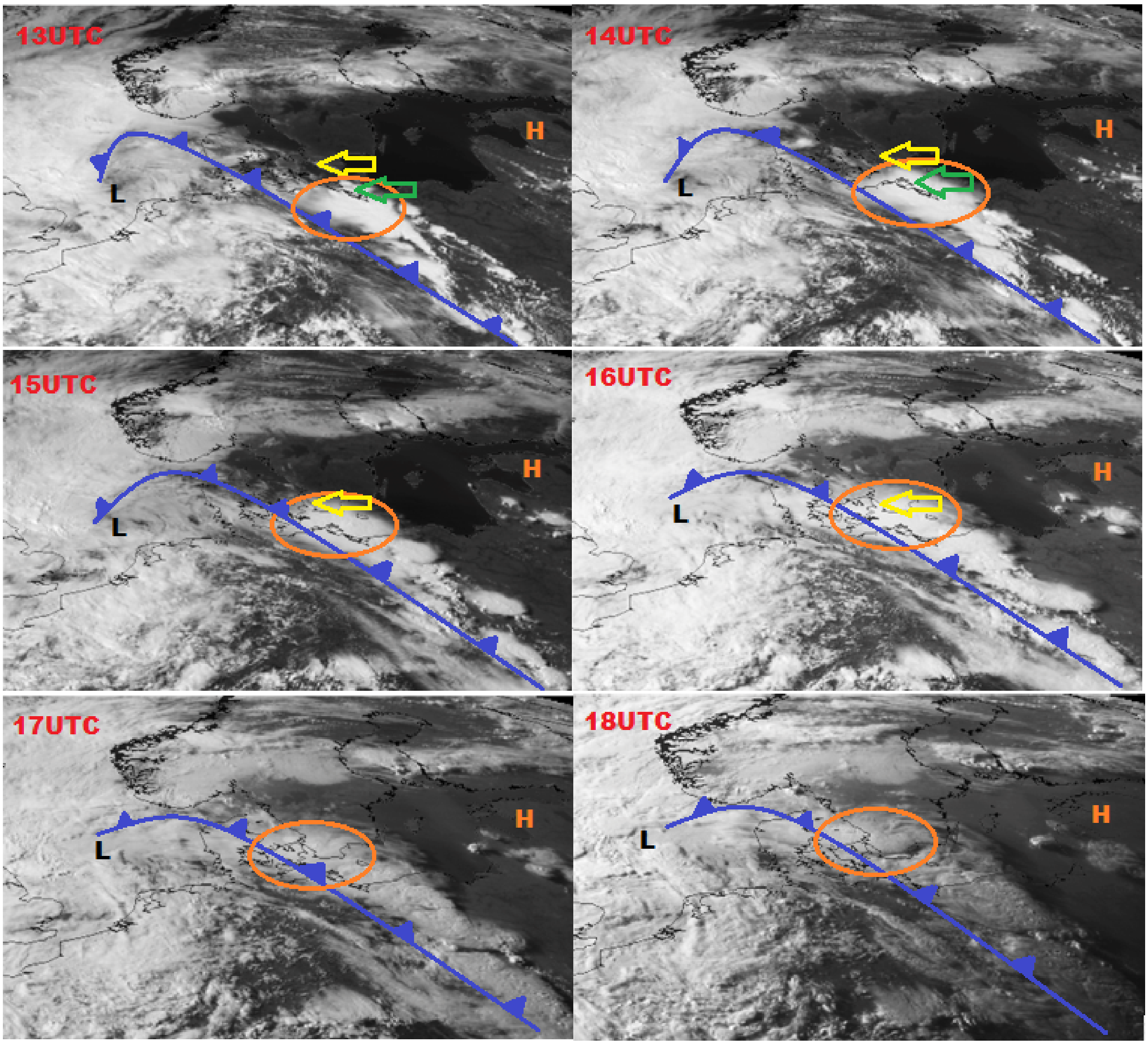

Figure 36: HRI Level 1.5 Image Data - MFG - 0 degree, EUMETSAT [31]. Visible, channel 0.6 μm. 30th of June 1997, 13UTC to 18UTC. The analysis is based on 30 minute intervals - in the figure the intervals are hourly. The orange ring marks the thunder cells which are strengthend until they reach Copenhagen. The low center is marked by the "L". The blue line represents the cold front. Yellow arrows shows the location of Copenhagen and green arrows the location of Greifswald.

It is worth noting that the CAPE value is not very high in Copenhagen at 12UTC, taking the later situation into account. A CAPE value of 231.9 Jkg^{-1} is typically associated with single cells (section 2.3.2) and is not alarming. Soundings farther inside the warm air (see figure 108 in appendix E) show higher values than at Jægersborg, which must mean that a positive value of CAPE is not a sufficient condition for cell formation. In a troposphere with a positive CAPE, dynamic forcing is often required to trigger thunder activity according to section 2.2.1.
Figure 39B shows the sounding after the passage of the cold front where a significant cooling has taken place in the lower troposphere between the surface and 700 hPa. This cooling is due to the confluence zone moving towards the northeast. At the same time, the specific humidity has not changed much. Furthermore, a dry intrusion can be observed from about 600 hPa to 500 hPa which is dry air from the lower stratosphere that help to weakening the frontal zone in the middle troposphere. No CAPE is observed, which emphasizes that CAPE decreases from the warm air mass and becomes zero in the confluent flow.

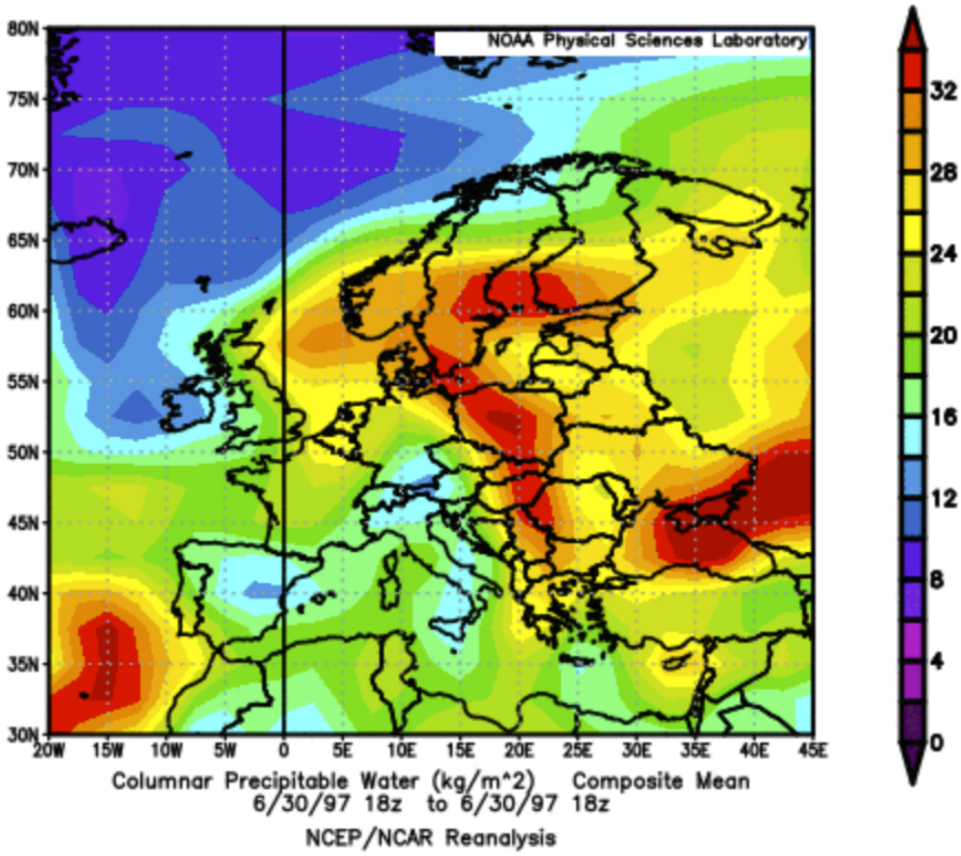

Figure 37: Columnar precipitable water, composite mean in the units of kg/m^2. [35]

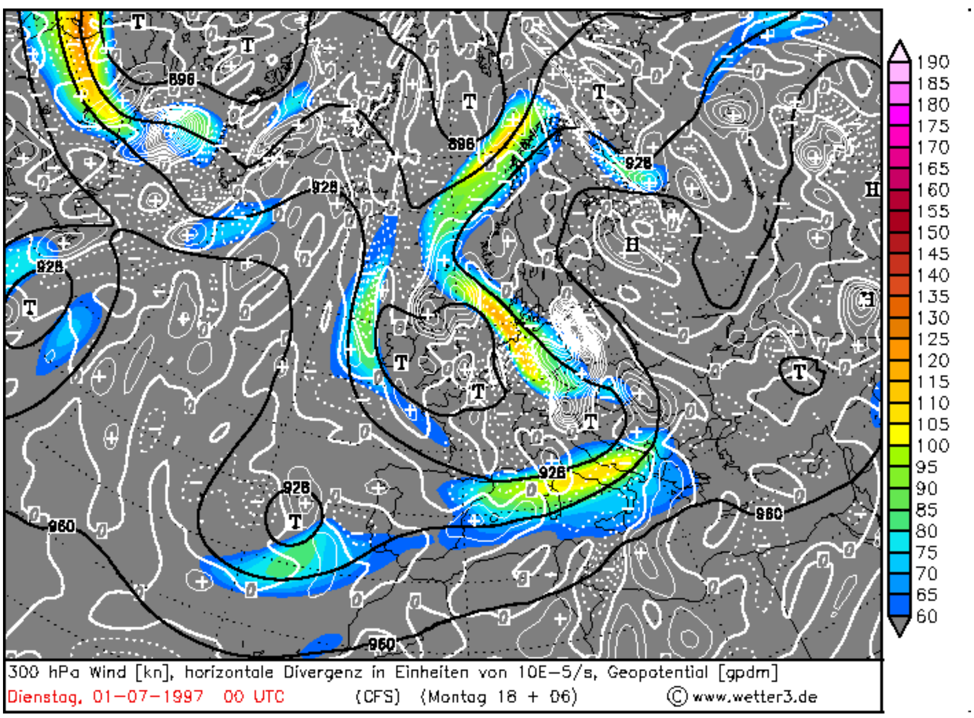

Figure 38: GFS 300 hPa wind [kn], horizontal divergence [$10^{-5}s^{-1}$] and geopotential, black curves [$gpdm$]. H is high pressure and T is low pressure. 00UTC, 1st of July 1997. Displays the flow of the jet stream. [34]

A sounding from Greifswald, Germany (green arrow in the satellite image) shows a troposphere with a higher potential for thunder cells than Copenhagen with a CAPE value of 671.9 Jkg^{-1} and indices that all show a moderately unstable troposphere with a risk of scattered thunder cells (figure 40). With a wind shear of 19 m/s, Greifswald is on the verge of developing a supercell as indicated by the spectrum in figure 7. The drop in temperature at the surface may be due to precipitation from a heavy shower which is producing a cold pool (see section 2.3.3). The sounding from Greifswald are included because this is in the initial stage of the thunder cells (see satellite images, 13UTC and 14UTC, figure 36).

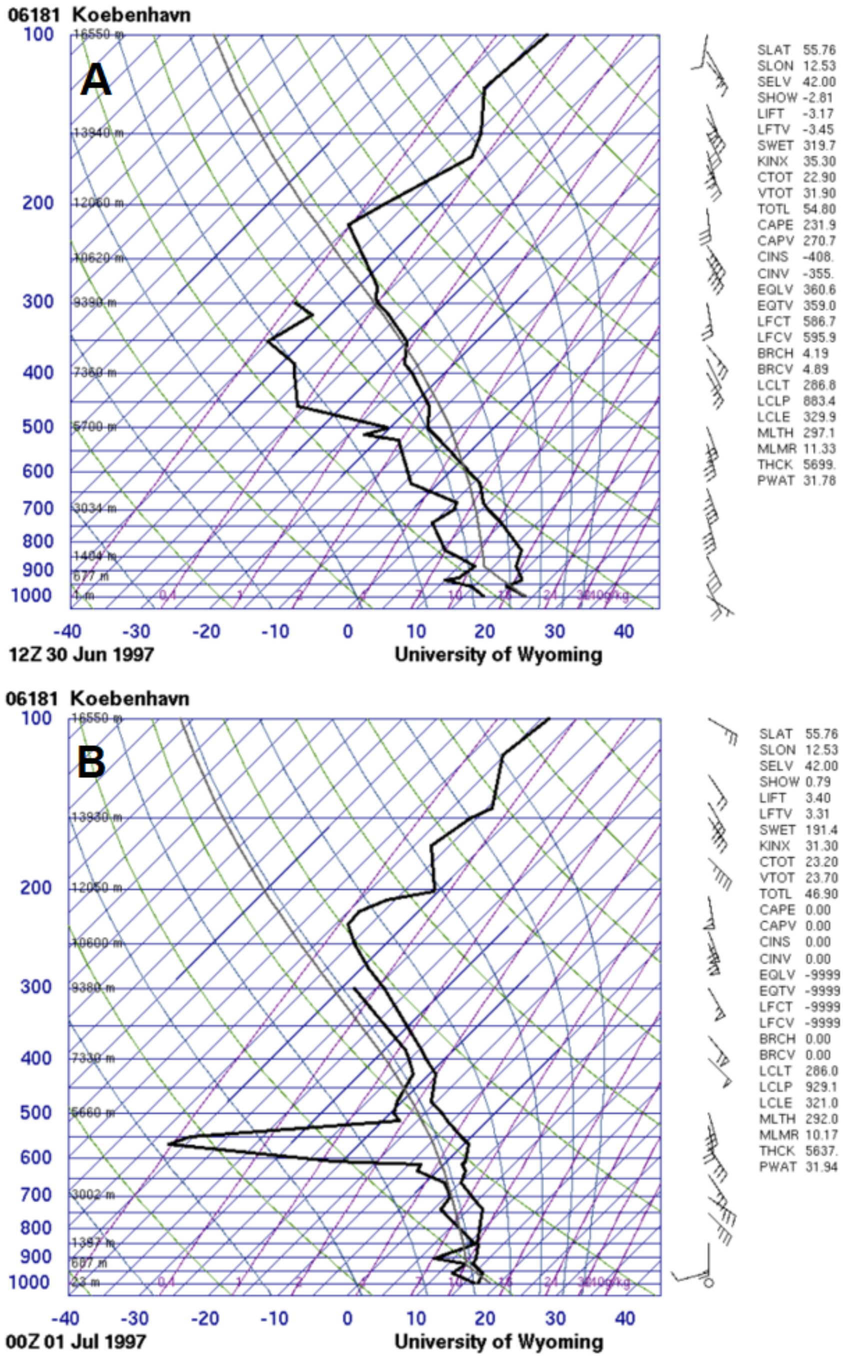

Figure 39: Sounding from Jægersborg, 12UTC, 30th of June 1997 (A) and 00UTC 1st of July 1997 (B). The black curves is the dew point temperature (left) and the air temperature (right). In addition, the change in the wind is with height is displayed to the right of the diagram. Green curves are the dry adiabatic lapse rate, blue sloping lines are isotherms, blue horizontal lines are isobars, purple lines are saturation mixing ratio and blue curved lines are the moist adiabatic lapse rate. [36]

The intrusion of dry air in the sounding for Copenhagen (figure 39B) may be due to the upper tropospheric jet streak. Figure 38 shows the wind speed in 300 hPa for 00UTC, 1st of July 1997. It can be observed that there is a jet streak on the jet stream axis southwest of Denmark with very high wind speeds (up to 50 m/s). Based on quasi-geostrophic arguments, the left entrance of this jet streak may be the source of the dry intrusion. In appendix F, the theory behind jet streaks can be found.

It has been previously observed that the band of thunder cells (figure 36) are parallel to the jet stream axis. With a strong jet, the upper level forcing will also be stronger.
The jet streak in the upper troposphere is an important trigger of thunder cells due to the rise of air below the jet stream in the right entrance of the jet streak. Therefore, it is not inconceivable that a jet streak may play a part in the formation of new thunder cells.

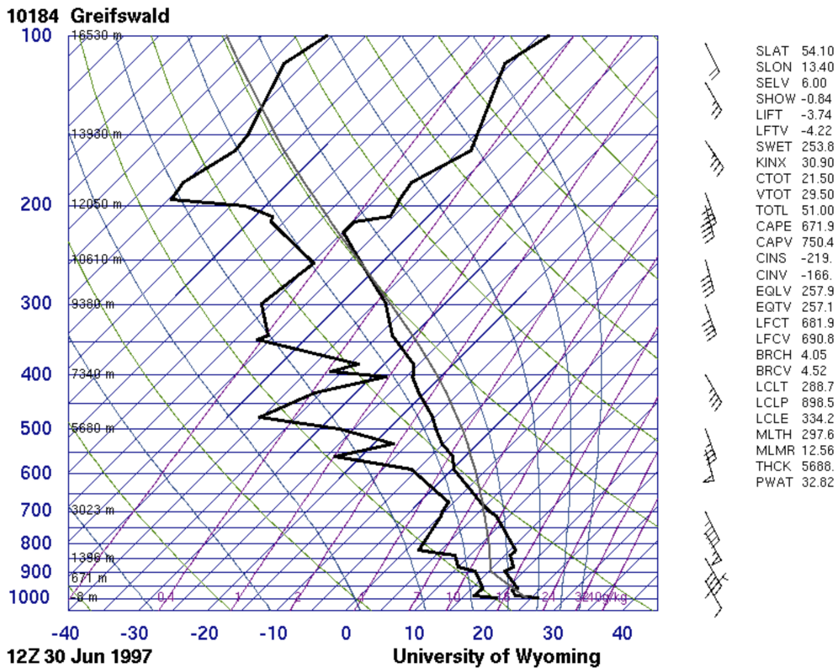

Figure 40: Sounding from Greifswald, Germany, 12UTC, 30th of June 1997. Same description as figure 39. [36]

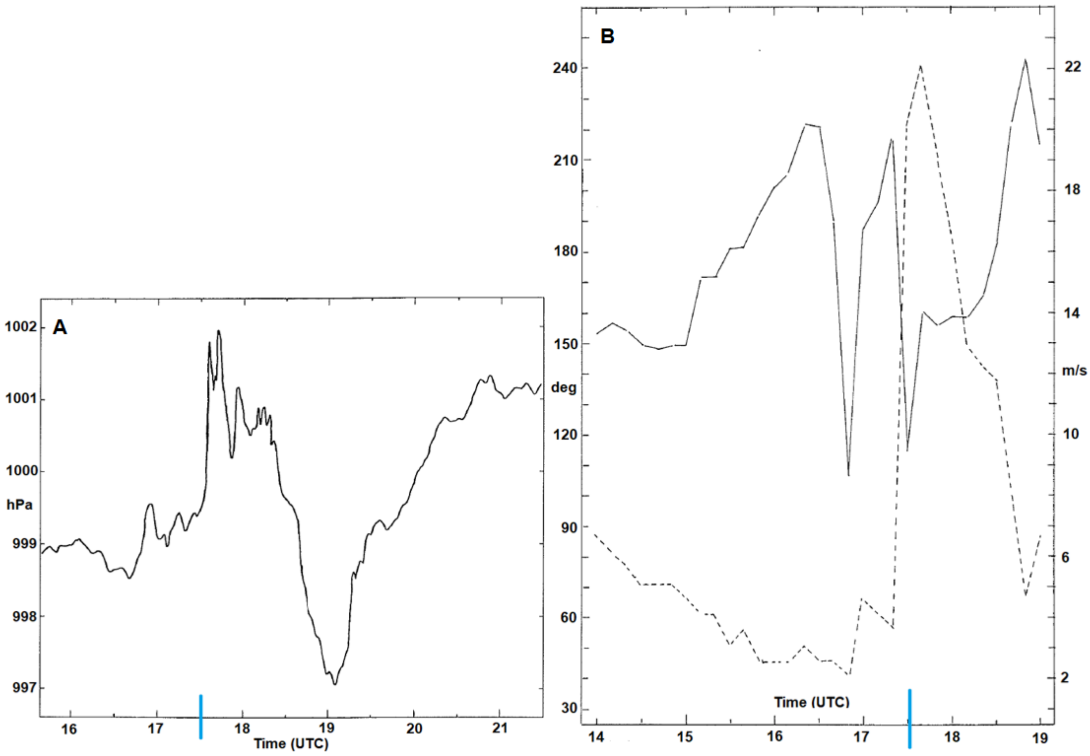

Figure 41: Pressure measurements [hPa] (A) from DMI with a temporal resolution of one minute. Wind measurements (B) from the Gladsaxe mast (200 m altitude). The scale on the left is wind directions (degree) and the scale on the right is the wind speed (m/s). In both cases the blue line marks the passage of the gust front, while times are UTC. [41]

From DMI's free archive there are no very good SYNOP data at this time, but from an article by Niels Woetmann Nielsen et. al. [41] there are pressure observations from DMI in a very good temporal resolution, see figure 41A. The pressure observations from DMI show the pressure fluctuations with a frequency of one minute and show the passage of the cloudburst. At 17.30UTC a pressure increase of 2.5 hPa within a short time is shown. The increase in pressure is the passage of the gust front of the storm (see section 2.3.3 for gust fronts), where the passage time of the gust front is marked with a vertical blue line.

Wind measurements (figure 41B) from a mast in Gladsaxe (200 m altitude) show a sharp increase in wind speed during the same period that the pressure rises, from 4 m/s to around 22 m/s (dashed line). The wind further turns from southwest to southeast which is the same wind direction in 300 hPa (drawn line).

Just after the passage of the gust front, the pressure drops by about 1 hPa with relatively large oscillations before a pressure drop of about 2 hPa to a minimum around at 19UTC.

Figure 42 shows lightning strikes in the period 05UTC 30th of June 1997 to 05UTC 1st of July 1997 and confirms the extent of the entire system as both the model of precipitation in figure 35 and the satellite images in figure 36 are shown. The lightning strikes indicate that the thunder cells follows the cold front in a north western direction. The system is intensified over the Baltic Sea reaching before maximum intensity over the region of Øresund. As it moves across Kattegat, the storm weakens and dies out in the northern part of Jylland. A comparison with the precipitation model in figure 35 shows that the system moves in a northwestern line and the width of the entire band is about 90 km.

Based on wind shear, structure and observations, it must be assumed that the cloudburst over Copenhagen was generated by a MCS - a cluster of thunder cells in very moisture air and with a horizontal extent from Øresund and a long distance into the southeastern part of Europe. Furthermore, based on characteristics, it can be assumed to be a squall line (see section 2.3.5 for elaboration of squall lines) with a significant wind shear and a relatively dry layer in the middle part of the troposphere (figure 39).

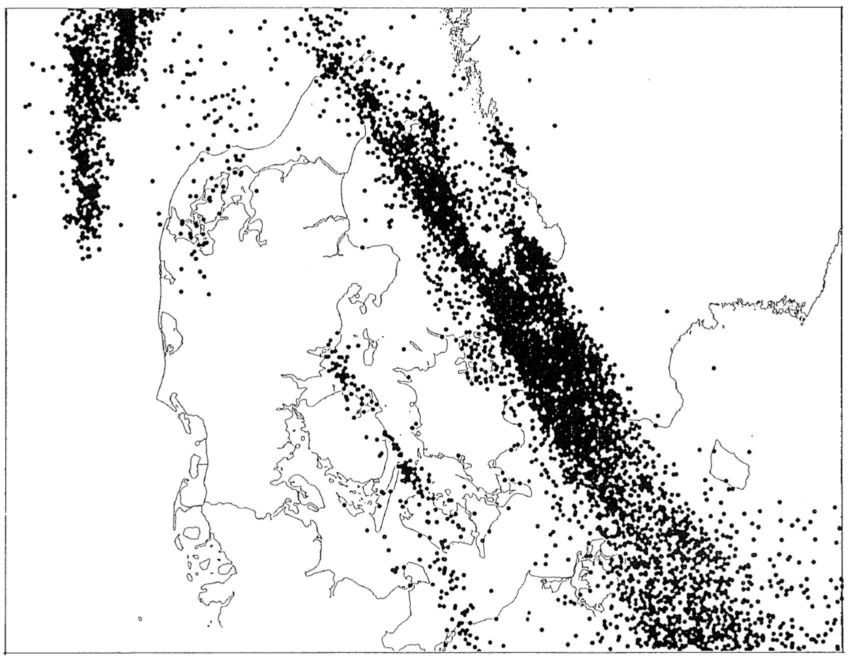

Figure 42: The registration of lightning in the period 05UTC, 30th of June 1997 to 05UTC, 1st of July 1997. [41]

For a squall line, the ratio between the transverse and the longitudinal dimensions must be less than one. The pressure observations in figure 41A show the pressure maximum as the gust front passage which in a squall line indicates the mesohigh. The corresponding pressure minimum 90 minutes later shows the opposite pole to the mesohigh, the wake low (see figure 15).

The length of a squall line is measured from the pressure maximum to the pressure minimum, in this case about 125 *km* and thus it satisfies the dimensions of a squall line. The length is estimated from the measurement that the thunderstorm had a movement of about 23 m/s [41] as well as the time interval from the mesohigh to the wake low.
In the sounding from Jægersborg at 12UTC (figure 39) in the warm air, the wind direction does not change a lot with the altitude, so might be an ordinary squall line that hit Copenhagen. In Greifswald there was a fairly high wind shear, but since supercells according to the theory do not occur in ordinary squall lines, it must be assumed that it was a powerful multicell system, where new cells appeared on the gust front, according to section 2.3.3.
The analysis of the thunderstorm over Copenhagen in 1997 shows a squall line system that developed in the confluence zone of a cold front in the lower part of the troposphere. The system occurred in relation with cyclogenesis over the North Sea. The squall line originated in the area around Greifswald and moved northwestward along the cold front across the region of Øresund and further up through Kattegat to the northern part of Jylland with maximum intensity around Øresund. Measurements from DMI amount to be 15 to 20 *mm* of precipitation in 30 minutes, but it cannot be ruled out that there have been locally higher intensities [41].

5.2 Case 2: 23rd of June 2003, the Stormy Midsommer in the Southern Part of Denmark, 16UTC to 20UTC

The midsummer of 2003 was the culmination of a period of erratic weather [42]. The storm this summer day was linked to a low, which during moderate deepening moved over the southern part of Denmark in the afternoon and evening hours. It reached maximum intensity around 18UTC over Fyn and later over Sjælland with many lightning strikes and strong wind gusts as a result. The lightning registration is represented in figure 43.

Figure 43 shows the entire process from 00UTC, 23rd of June until 00UTC, 24th of June. It starts with two areas with lightning activities above the North Sea and Benelux. Lightning activity dies out in the North Sea around 06UTC, while between 06UTC and 12UTC new lightning activity occurs over the Netherlands. The lightning activity over the Netherlands moves east-northeast and reaches the southwestern Denmark between 14UTC and 16UTC. Maximum is achieved between 16UTC and 18UTC in the area around Fyn and Langeland. The lightning activity over Benelux has the same direction of movement. In the period from 18UTC to 20UTC, lightning registration forms an almost coherent belt from the eastern part of Jylland over Sjælland to northern Germany and Poland. Bornholm is first hit in the period from 20UTC to 22UTC. In figure 45A (p. 50) PW from NOAA is shown for 18UTC. Here it is clear that high values of PW can be linked to lightning activity, as the highest values of PW are in the same band as the lightning activity in figure 43.

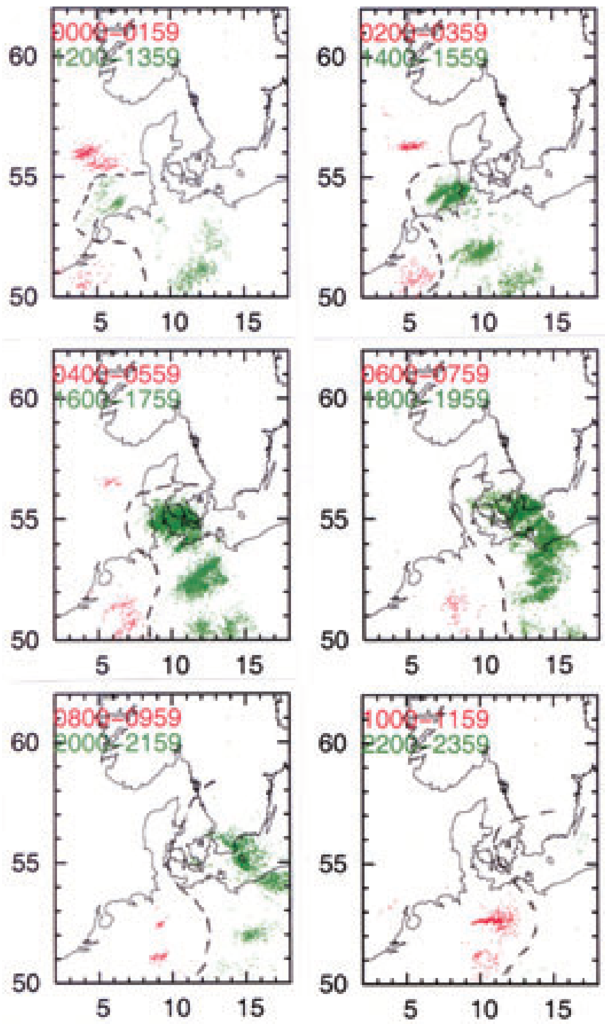

Figure 43: Lightning registration in two-hour intervals generated by B. Amstrup. Each sub figure shows two 2-hour intervals where red lightning are in the period 00UTC to 11.59UTC and green lightning are in the period 12UTC to 23.59UTC, separated by a dashed curve. [42]

The weather situation in the midsummer 2003 is dominated by a ridge in 500 *hPa* with relatively large amplitude in the upper troposphere over the northern part of Europe and southern Scandinavia, with a high to the right of the ridge axis over Sweden and Finland, and a primary low to the west of the ridge axis, northwest of Scotland which is shown in figure 44. Over Ireland there is a secondary low. Represented by figure 44B, 24 hours later than figure 44A, we can see that the secondary low moves faster than the primary low and thus is the low which gives thunder cells over Denmark. The whole system moves to the east and northeast corresponding to the movement of lightning activity from figure 43.

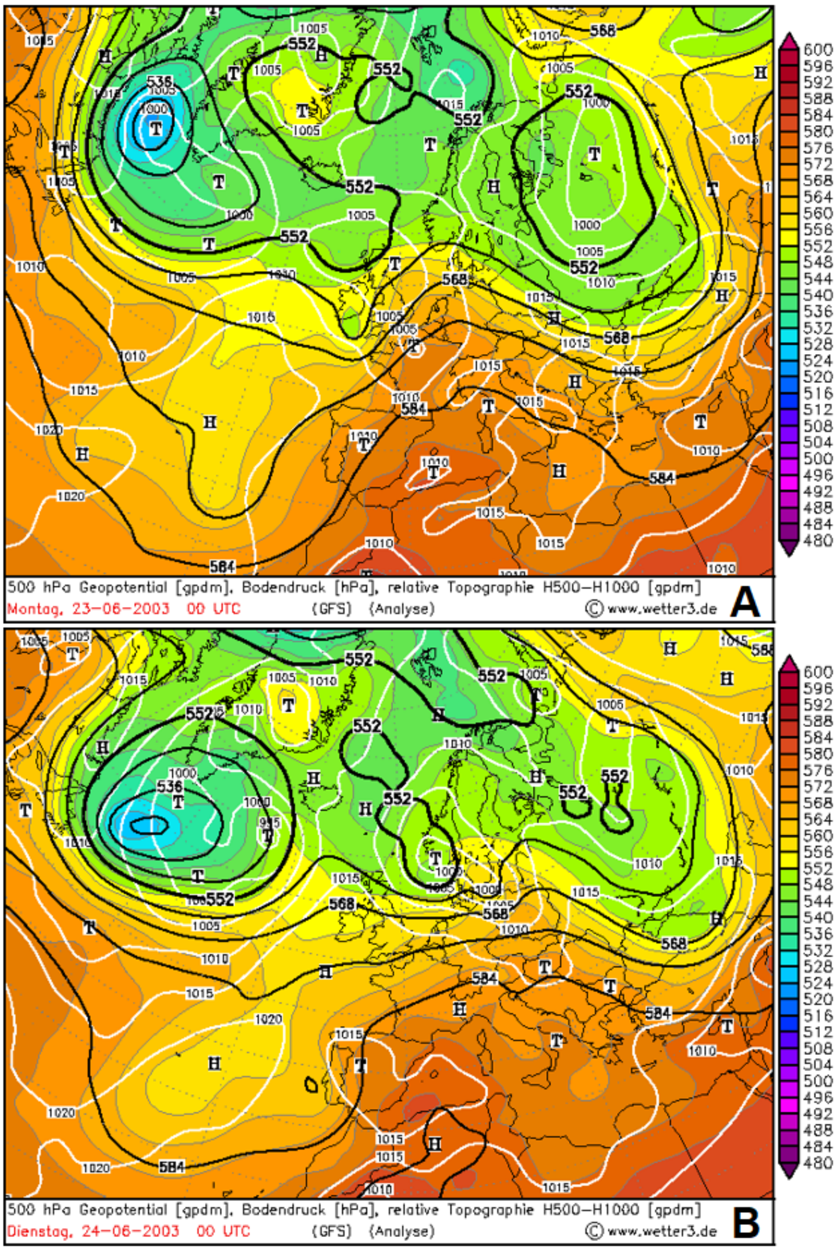

Figure 44: GFS 500 hPa geopotential, black curves [$gpdam$] and surface pressure, white curves [hPa]. H is high pressure and T is low pressure. 00UTC, 23rd of June 2003 (A) and 00UTC, 24th of June 2003 (B). [34]

Based on the maps, the secondary low over Ireland, has a greater tendency for deepening due to a greater upstream slope than the northern low over Scotland. For a cold frontal zone, the average slope is 1 in 70 [43], that means it rises 1 km in vertical distance for every 70 km of horizontal distance. For more active fronts there is a steeper slope and then greater likelihood of the development of thunder cells according to the theory in section 2.1.1.

The development of the low over Ireland follows the pattern of a secondary low development, where the low in the beginning is on the anticyclonic shear side of the jet axis (figure 44A and 45B). During evolution, it moves across the jet axis and ends up on the cyclonic shear side of the jet axis in the most intense phase, 6 hours before figure 44B.

The lightning activity takes place on the anticyclonic shear side of the jet and if we compare figure 43 (18UTC) with the equivalent potential temperature (figure 46A, p. 51) and the absolute vorticity advection (figure 46B, p. 51), we can see there are favorable conditions for the development of thunder cells due to the quasi-geostrophic omega equation (equation 14), where the potential temperature is high and at the same time there is PVA (see section 2.2.3). In this case, there will be a lift of air parcels into the atmosphere due to positive vertical velocities.

The satellite images in figure 47 show the temporal development of the system in the period from 12UTC to 18.30UTC with hourly intervals, which is presented by the visible 0.6 μm channel from MFG geostationary satellite data. The full resolution of these satellite data is 30 minute intervals (see section 3.2 for details).

The secondary low is over the North Sea at 12UTC with a characteristic cloud head just north of the entire low system consisting the cold front (blue line) and the warm front (red line). During this period, lightning is recorded off the north coast of the Netherlands. These lightnings are associated with the low evolution and high values of PVA at 300 hPa and weak temperature advection at 850 hPa (figure not shown). The high values of PVA in the upper troposphere have probably forced the air upward from a potentially unstable[7] air in the Warm Conveyor Belt[8] (WCB) air in the lower troposphere, thus triggering lightning activity and showers in the warm air. The WCB is shown in figure 47, 15UTC as a red arrow along the cold front. The WCB extends all the way up to Emden in northern Germany and then turns off at Denmark and follows the warm front. This means that thunder cells along the fronts can be associated with the air mass in the WCB. This area will become vital for the development of the cloudbursts over Denmark. The yellow ring in 13UTC marks the first cell developments over Germany which later became a coherent cloud band with cells over Denmark.

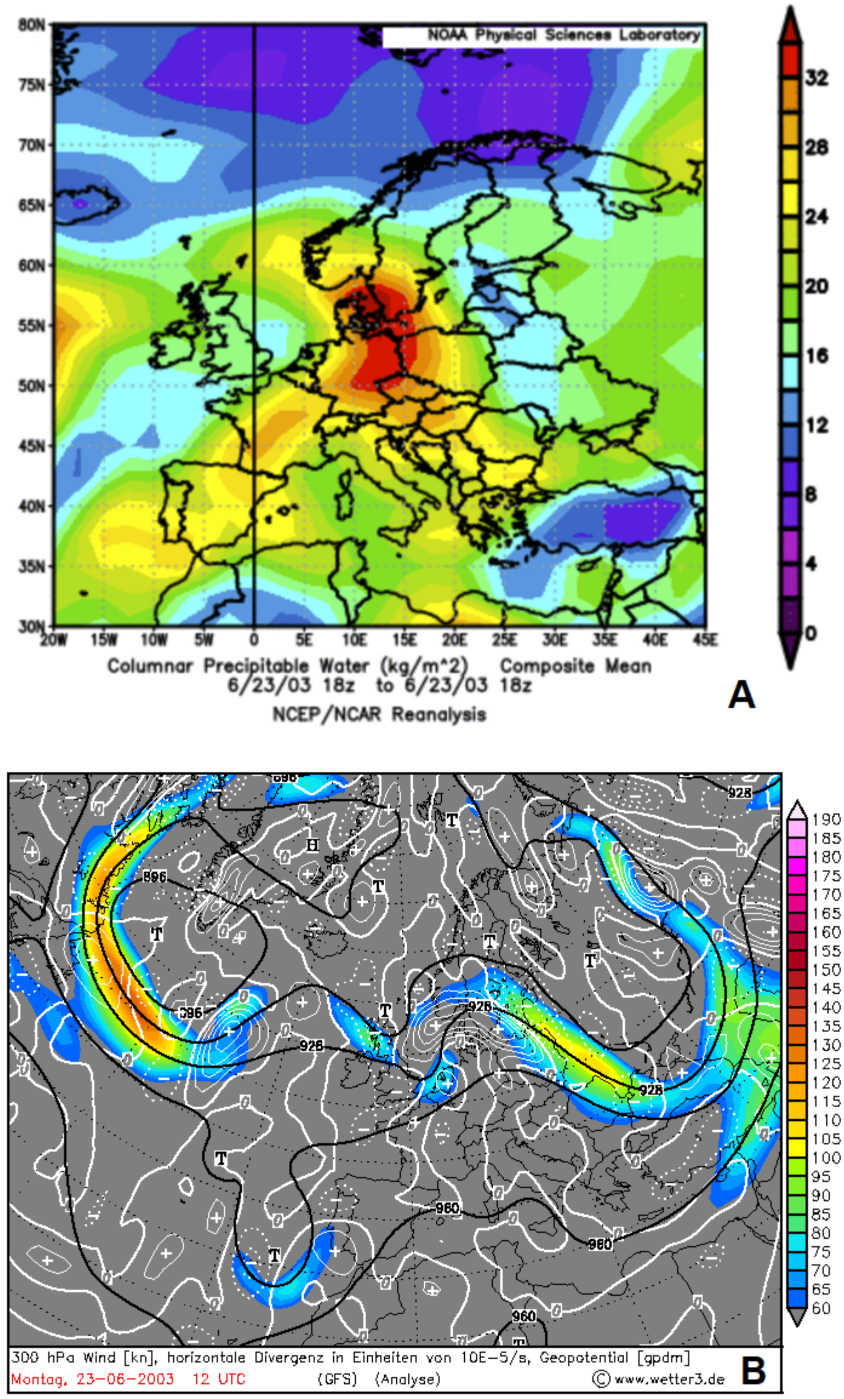

Figure 45: Columnar precipitable water, composite mean in the units of kg/m^2 (A) [35] and GFS 300 hPa wind [kn], horizontal divergence [$10^{-5}s^{-1}$]. H is high pressure and T is low pressure. 12UTC, 23rd of June 2003. Displays the flow of the jet stream (B). [34]

[7] See section 2.2.3 for a description of potentially instability

[8] The Warm Conveyor Belt is a warm and moist airstream in the boundary layer of an extratropical cyclone's warm sector

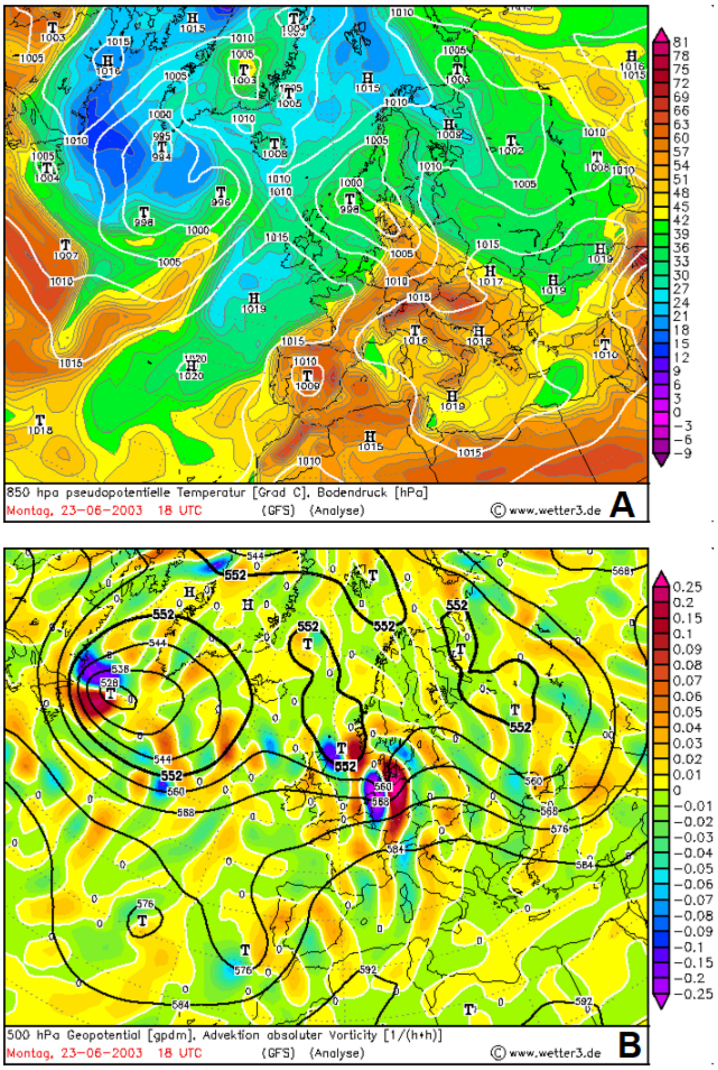

Figure 46: GFS 850 hPa pseudopotential temperature [°C] and surface pressure, white curves [hPa], 18 UTC, 23rd of June 2003 (A) and 500 hPa geopotential, black curves [$gpdam$] and absolute vorticity advection, 18UTC, 24th of June 2003 (B). H is high pressure and T is low pressure. [34]

In figure 47, 14UTC, new cell developments are underway, resp. southwest of Denmark over Emden (left yellow ring) and between Hamburg and Hannover (middle yellow ring), both marked in the 14UTC image. In total, there are 3 powerful CB's under development one close to Denmark, one in extension of the cold front and one southeast of the middle in the warm air - all three are marked with orange rings in the 14UTC image. In the following hours, these cells stengthen to maximum intensity - according to the lightning detection for Denmark between 16UTC and 20UTC for Fyn and Sjælland in figure 43. During this period, the cell has reached its full stage of development and is maintained. In the evening as the cell moves to the northeast does it reaches the decaing stage and therefore register less lightning are registered over Bornholm than over Fyn and Sjælland. In addition, a cloud hook is created over Denmark in the evening hours, which shows a low that has reached the saturation stage and thus a low that has reached maximum intensity and then begins decaying. The high values of PW in figure 45A roughly follow the front system, where the highest values are present in the warm air with a clear demarcation along the cold front. The whole system with the secondary low to the south and the primary low to the north is called an extratropical cyclone, for an explanation of extratropical cyclones, see appendix G.

A comparison of the satellite images in figure 47 and figure 46 shows a clear correlation between high values of potential temperature, PVA and development of the thunder cells. At the same time, it is known that there is a warm advection of 850 hPa in the same area. The connection between PVA and warm advection is positive vertical velocity (see section 2.2.3 for vertical velocity) with a lift, which in the range of high positive potential temperature, i.e. an area with an unstable air mass, provides favorable conditions for the marked thunder cells on the satellite to strengthen/maintain their size.

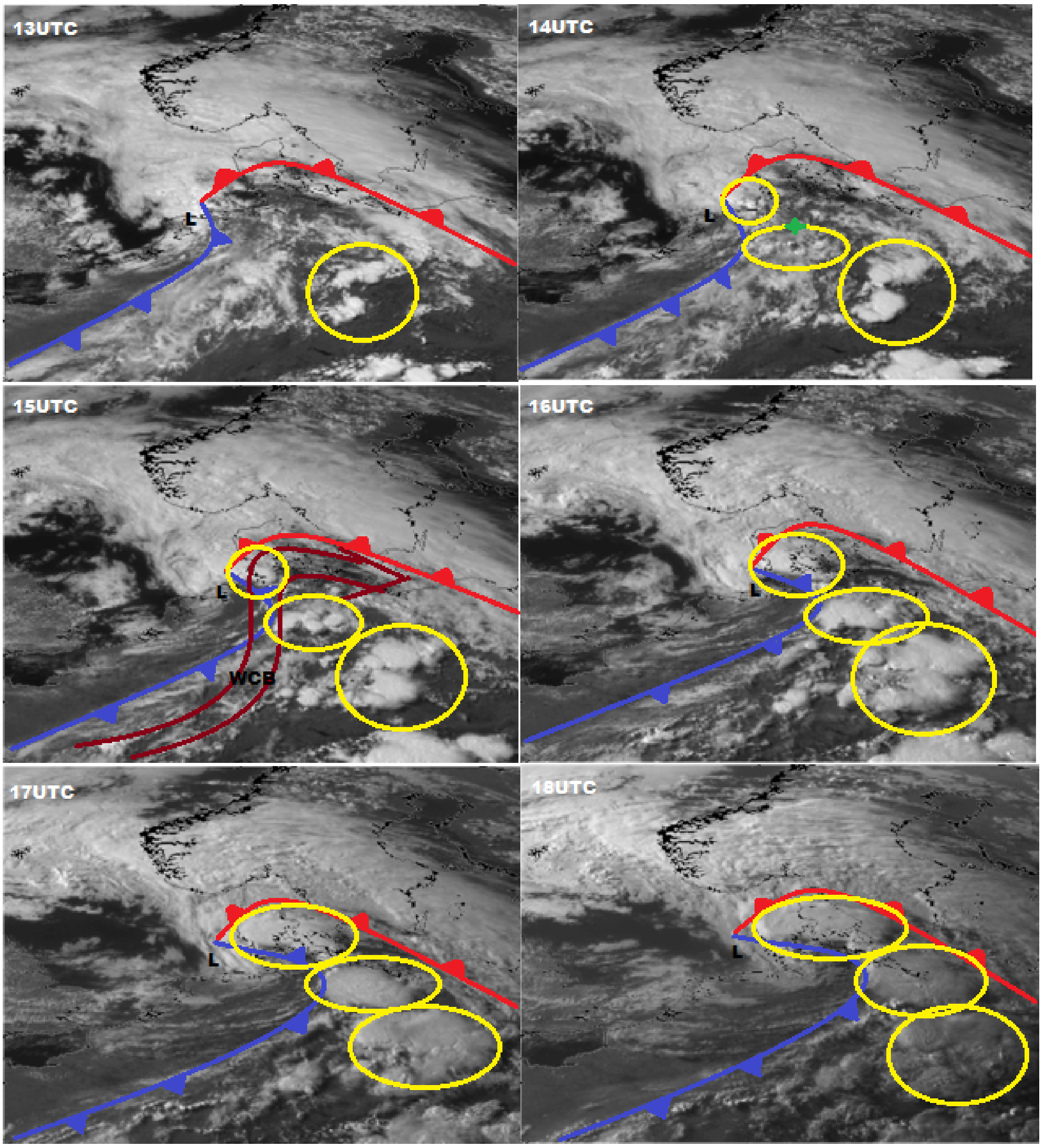

Figure 47: HRI Level 1.5 Image Data - MFG - 0 degree, EUMETSAT [31]. Visible, channel 0.6 μm. 23rd of June 2003, 13UTC to 18UTC. The analysis is based on 30 minute intervals - in the figure the intervals are hourly. Yellow rings marks thunder cells described in the text. The low center is marked by the "L". The blue line is the cold front and the red line is the warm front. The green point is the location of Bergen, Germany and the red arrow is the WCB.

SYNOP data is selected to describe the details. Figure 48 shows precipitation, pressure, 2m air temperature and wind direction from Årslev, Midtfyn. Årslev was one of the stations located in the middle of the storm during the passage of the thunder cells. From figure 48 it is clear that there has been a passage of a low during the period. It appears i.a. of the marked pressure drop in figure 48B with a little bump due to the front passage. The wind direction in figure 48D changes rapidly from southeast to northwest at the same time as the passage of the front according to the theory in section 2.1.1. Furthermore, it also appears that the temperature in figure 48C drops from around 15UTC and onwards - the same time period when lightning development began and the cold front passes.

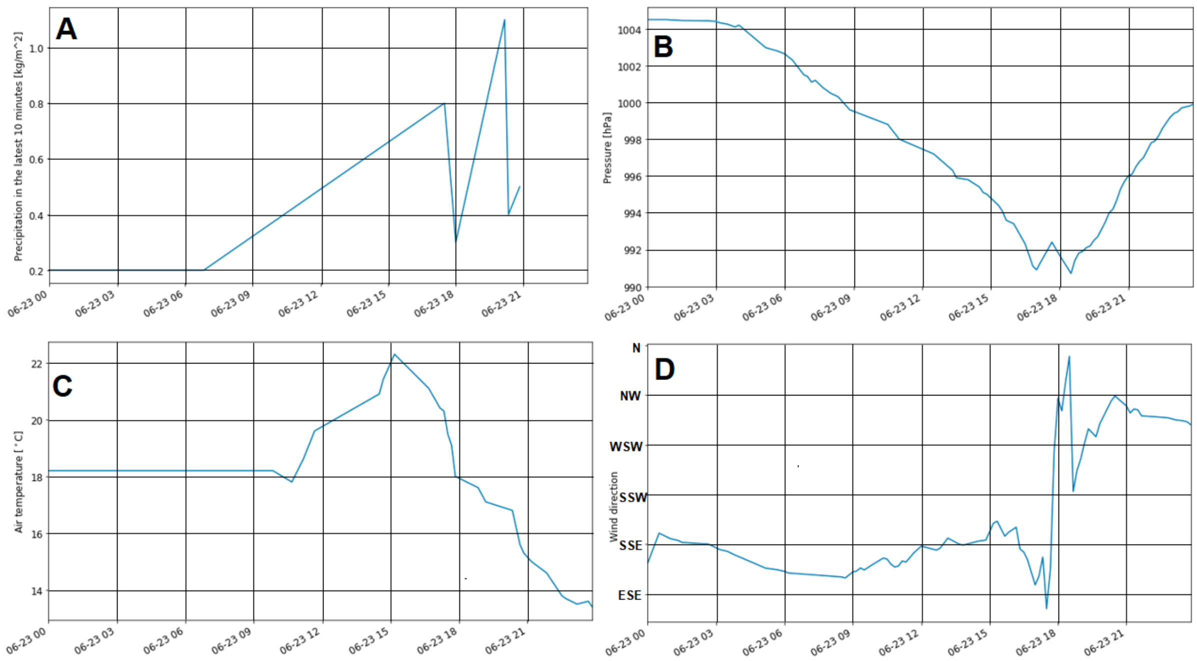

Figure 48: SYNOP data from Årslev (no. 06126), Midtfyn. Precipitation [mm] (A), pressure hPa (B), 2m air temperature [°C] (C) and wind direction (D). The x-axis is time (UTC).

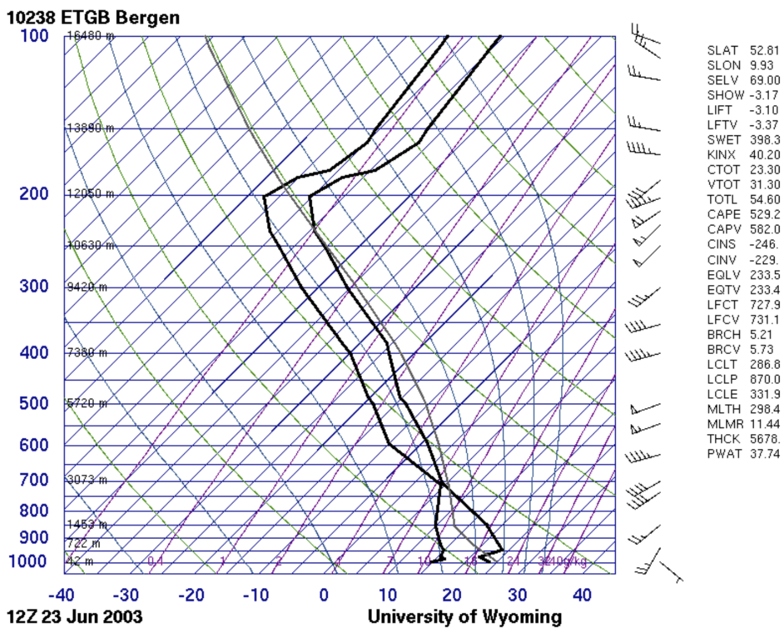

Figure 49: Sounding from Bergen, Germany, 12UTC, 23rd of June 2003. Same desciption as figure 39. [36]

A number of soundings help to describe the state of the atmosphere this summer day.

The first sounding in figure 49 is from Bergen, Germany, 12UTC, which shows the conditions for the middle cluster (figure 47) of thunder cells. From figure 43, it can be seen that there is a development of lightening in the area around Bergen, 12UTC, which is the WCB of the southern low with warm and moist air. The diagram shows the dew point (left curve) and the temperature (right curve) as a function of the air pressure - this gives an indication of dry and warm air at the surface layer with a temperature of approximately 24 °C at 950 hPa height, corresponding to the top of the surface layer. At the surface, the air is relatively cold compared to the inversion layer, which can be described by eventual outflow of air from a thunder cell (see section 2.3.3 for this). At 700 hPa the air is saturated.

A conditional unstable layer[9] can be identified from 700 hPa to 500 hPa, as the vertical temper-

[9] In section 2.2.3 are the theory described for potentially and conditional instability

ature gradient is larger than the moisture adiabatic curve but smaller than the dry adiabatic. Furthermore, the air is potentially unstable from 700 hPa to 600 hPa, because θ_e decreases up through the layer from $328.1°K$ at 700 hPa to $322.3°K$ at 600 hPa. I.e. in this case we have an unstable troposphere with favorable conditions for the development of thunder cells. The parcel method reveals that air parcels reach their LFC at an altitude of 727.9 hPa and thus become warmer than the surroundings all the way up to the tropopause at 200 hPa altitude, which in this case gives a CAPE value of 529.2 J/kg. All four indexes, LIFT, SHOW, KINX and TOTL have values that prove that in Bergen there is a high risk of scattered or severe thunder cells at this time.

The cells over Denmark originates in the northwestern part of Germany. The best sounding to describe the initial state of these cells is Emden, shown in figure 50. This sounding shows how potential instability in the WCB has the opportunity to develop in cyclogenesis. The sounding shows really dry air (dry intrusion) above 600 hPa which displaces the warm and humid air in the WCB due to the sinking of dry air, upstream of the low. Upon displacement, the WCB air mass is forced upward and the conditions are set for heavy convection. Figure 43 shows that eastern Denmark, including Copenhagen, also experienced the powerful thunder cells.

A sounding from Jægersborg, figure 51, north of Copenhagen, 12UTC, shows the state of the atmosphere before the arrival of thunder cells. The sounding has some characteristics reminiscent of the sounding from Bergen, figure 49, with an inversion layer. In the layer from 750 hPa to 600 hPa is the air more or less saturated and with a potentially unstable layer from 600 hPa to 500 hPa. Despite the fact that CAPE is zero at this point, the indices indicate the chance of thunder cells. A later sounding from Jægersborg, 00UTC 24th of June (not shown), shows the dry intrusion as from the Emden sounding.

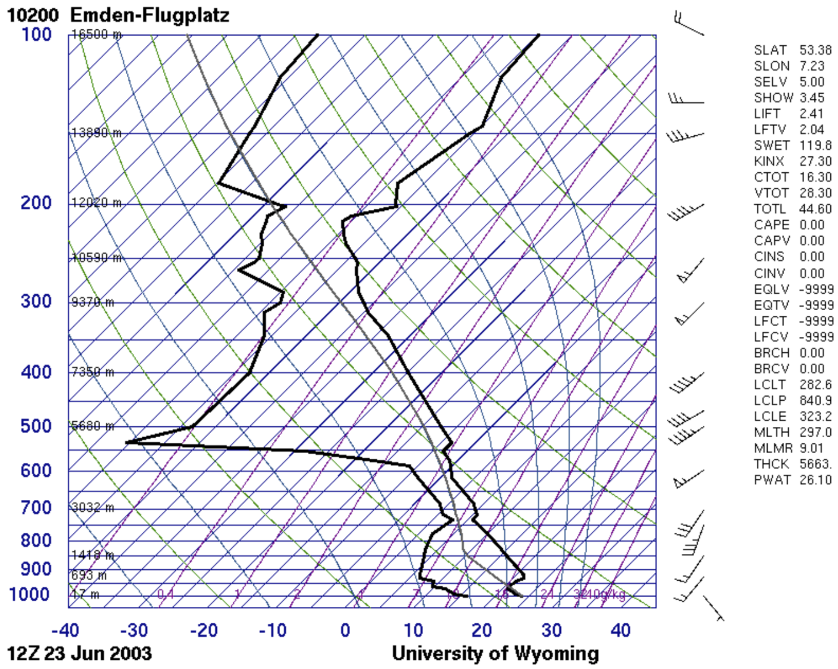

Figure 50: Sounding from Emden, Germany, 12UTC, 23rd of June 2003. Same description as figure 39 [36]

A significant vertical wind shear, 0-6 km, is registered with 20 m/s in Jægersborg 12UTC, which is in the boundary between multicells and supercells. However, the wind shear at Emden, the initiate area for the thunder cells, is 14 m/s, which indicates that the cells are developing as multicells. With a wind shear of 19 m/s near Bergen, it can be concluded that the cells develop as powerful multicells compared to figure 7. In the satellite image in figure 47, 17UTC, two cells can be sensed which also indicate a multicell system. The satellite sequence shows that the system is moving in an eastern

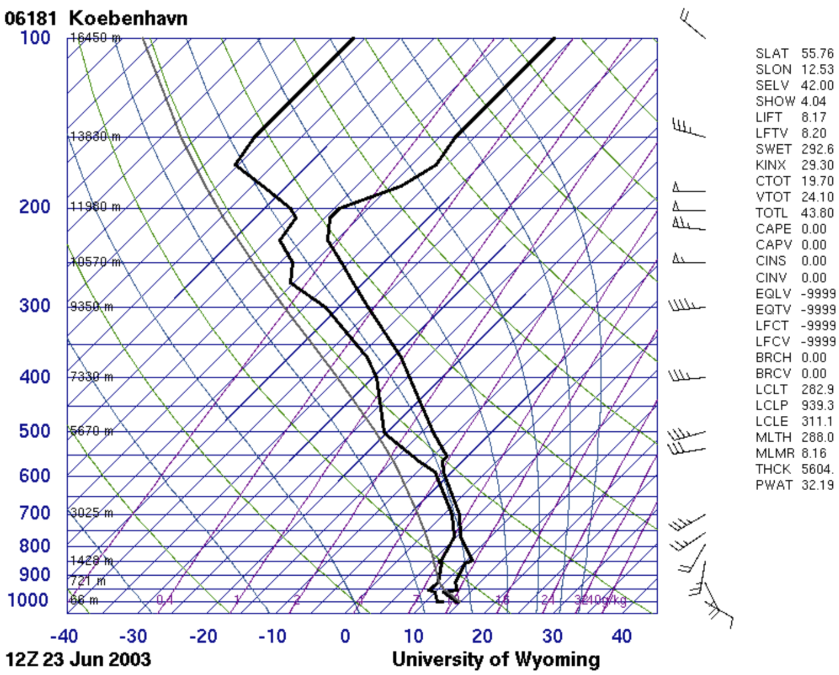

Figure 51: Sounding from Jægersborg, 12UTC, 23rd of June 2003. Same description as figure 39. [36]

direction, while new cells are emerging on the western flank of the system where the gust front is located, according to the theory in section 2.3.3. This indicate a reverse wind shear (figure 8), which make this thunderstorm very powerful.

The storm this summer evening was associated with a low on a small scale that during moderate deepening moved across the southern part of Denmark and resulted in a multicell system. Maximum intensity was reached over Fyn and Sjælland in the period 18UTC to 20UTC. The thunder cells arose in an area of potential instability in the WCB and very high content of water vapor. The potential instability probably arose from dry air in the upper troposphere displacing the warm and humid air in the WCB.

Two intensities from this summer evening are included in a top 10 for registered intensities from SVK for 2003 [1]. It is resp. 22.67 $\mu m/s$ at Kolding Renseanlæg and 21.00 $\mu m/s$ at Odense Vandværk, which gives indications that this was the equivalent of more than a double cloudburst intensity according to Danish definitions.

5.3 Case 3: 20th of August 2007, the Multi-Cloudburst at Gråsten in Southern Jylland, 20.30UTC to 22UTC

The evening on 20th of August in Gråsten in the southeastern part of Jylland was hit by a severe storm with significant flooding ensuing, with both a railway bridge and a road being torn up. An unofficial but functional raingauge at Fiskbæk measured 142 *mm* of rain during the period, which is the fourth largest amount of precipitation measured in one day in Denmark. The weather situation this summer day was a low trough over the North Sea with a low located over The Netherlands/Belgium (figure 52A) and warm and humid air over the Baltic Sea. Associated with the low system is a cold front which reaches Denmark during the same period where the thunder cells over southeastern Jylland develop as can be seen in figure 53.

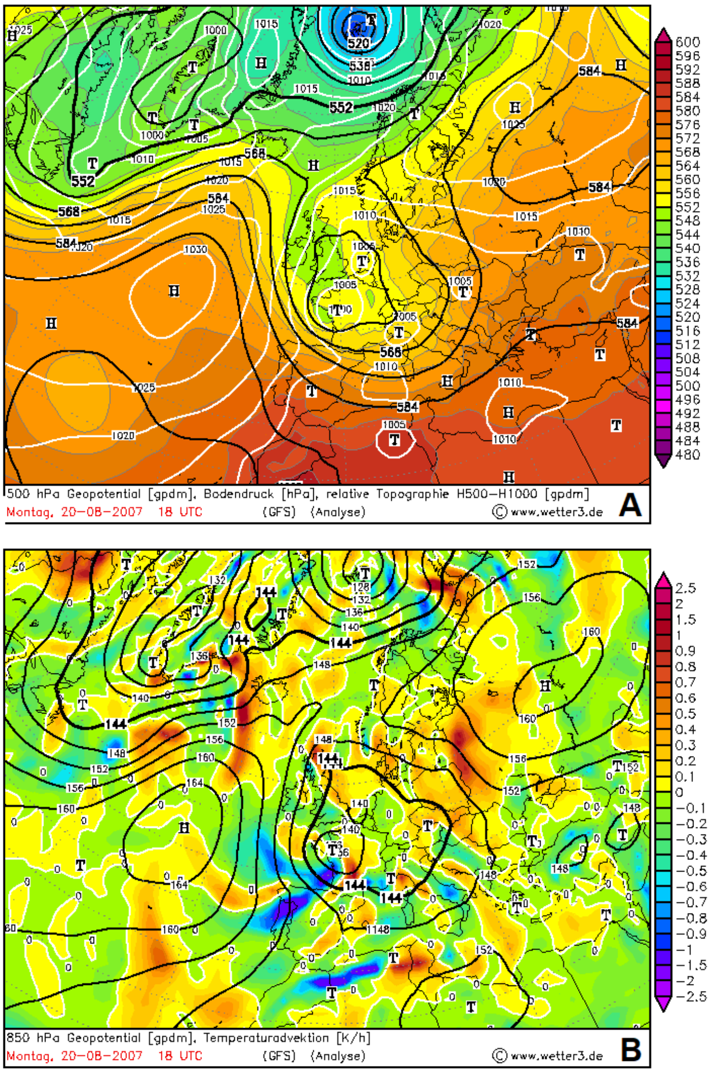

Figure 52: GFS 500 *hPa* geopotential, black curves [*gpdam*] and surface pressure, white curves [*hPa*], 18UTC, 20th of August 2007 (A) and 850 *hPa* geopotential, black curves [*gpdm*] and temperature advection, 18UTC, 20th of August 2007 (B). H is high pressure and T is low pressure. [34]

The satellite images in figure 53 show the progress this late summer evening starting from 20UTC where the first cells occur and until 22.30UTC where the last cells die out. They are displayed at 30 minute intervals with infrared 10.8 μm channel from MSG geostationary satellite data. The infrared spectrum shows white colors at cold temperatures and dark color at warmer, see section 3.2 for more details. In figure 53, the first thunder cells over Gråsten and Als are developed in the 20UTC picture. The satellite images indicate that the thunder cells occur along the cold front of the low on the border between moist and warm air and the colder and drier air in the trough (see section 2.1.1) and occur in a band from southeastern Denmark to the northwestern North Sea. The cells occur in approximately the same area around Als and Flensburg Fjord and propagate to the north, while the system moves to the northeast. In figure 54, PW for 18UTC is shown, which displays high content of moisture in the troposphere and thus favorable conditions for the formation of thunder cells according to the theory in 2.2.3. It can be seen that the high moisture values roughly follow the cloud band in the satellite images, which extends from a larger area southeast of Denmark to a narrower line of showers that extends from around Sjælland and out into the North Sea.

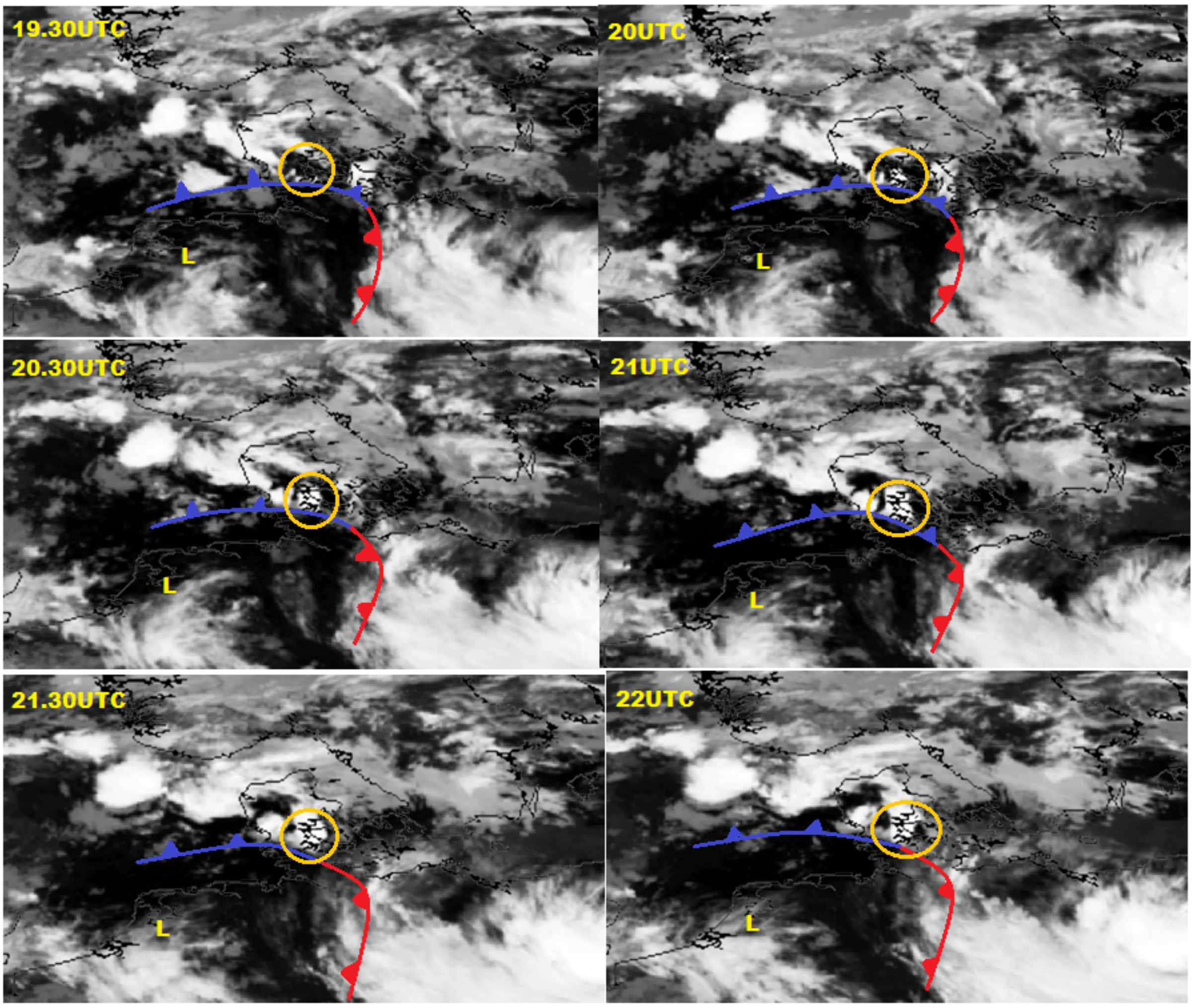

Figure 53: High Rate SEVIRI Level 1.5 Image Data - MSG - 0 degree, EUMETSAT [31]. 20th of August 2007, 19.30UTC to 22UTC. Infrared, channel 10.8 μm. White colors show cold areas (cloud tops for example), while dark areas are warm. The satellite images have a 15 minutes resolution, in the figure 30 minutes. The blue line is the cold front, the red line is the warm front and "L" is the low. The orange ring shows the area with cloudbursts at Gråsten in the southeastern Jylland.

To describe the stability conditions of the atmosphere before the cloudburst, a sounding from Schleswig, 12UTC, figure 56 (p. 59) is used. There are two primary levels in the sounding that are worth noting. From the surface to about 800 hPa, the air is conditionally unstable as the environmental temperature (right curve) drops faster than the moisture diabatic curve (left curve), also see section 2.2.3. If parcels at this level are lifted to their LCL, they will immediately become warmer than the surroundings, as they are at the same time in the LFC and achieve positive buoyancy according to the theory in section 2.2.3. In this case, LCL and LFC are at 908.2 hPa while EC is at 263.3 hPa altitude. The second level worth noting is from 800 hPa and up to the tropopause. At this level, the ambient temperature decreases more slowly than the

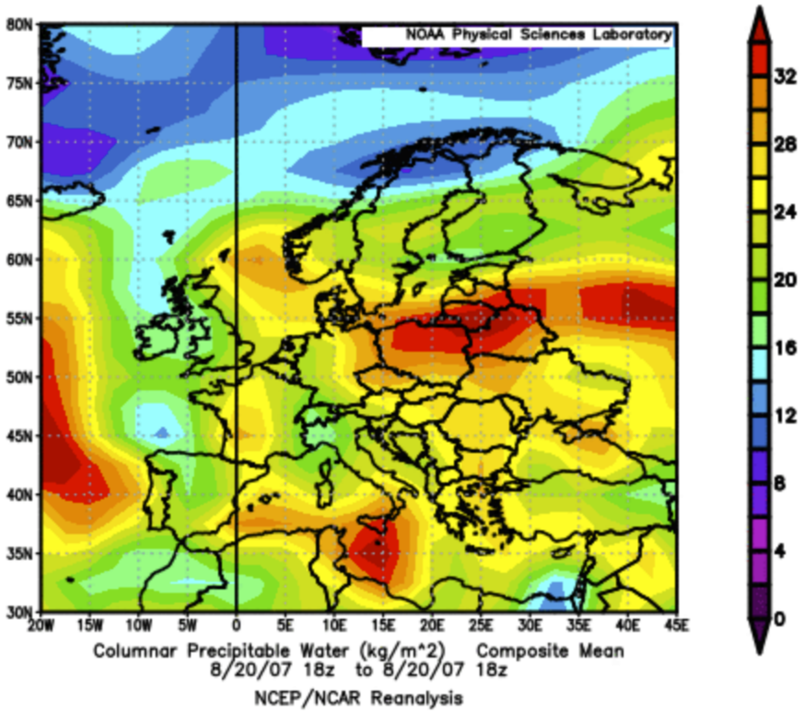

Figure 54: Columnar precipitable water, composite mean in the units of kg/m^2. [35]

moisture diabatic curve and then thunder cells cannot be formed by lifting parcels, as these will be colder than the surroundings. The four indices KINX, TOTL, LIFT and SHOW indicate exclusively widely scattered thunder cells in the area under marginally unstable conditions where a lifting mechanism is required.

Observations from the Schleswig sounding show a temperature of 21 °C at the surface and a dew point of 15 °C. Wind shear is 16 m/s. CAPE will depend on whether the temperature rises or falls, but in the sounding there is a significant CAPE as well with the thunderstorm indices there must be a high probability of heavy thunder cells in the afternoon. The necessary lifting could be initiated by turbulence in the boundary layer (see section 2.2.3).

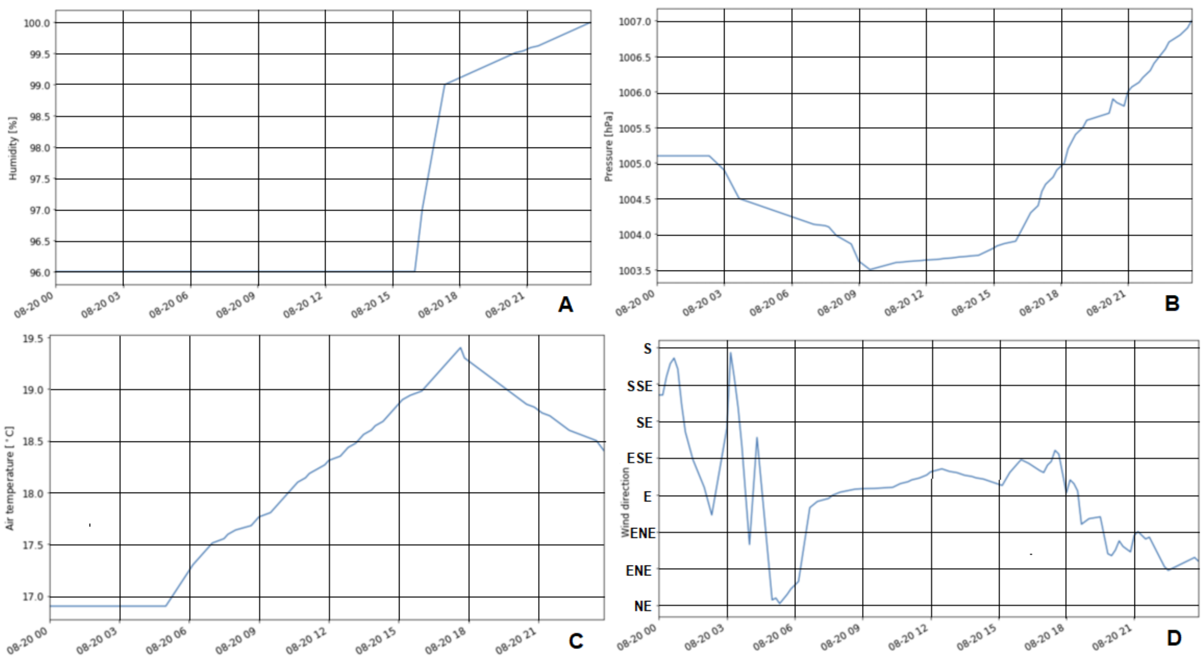

Figure 55: SYNOP data from Kegnæs (no. 06119), Als. Humidity [%] (A), pressure [hPa] (B), 2m air temperature [°C] (C) and wind direction (D).

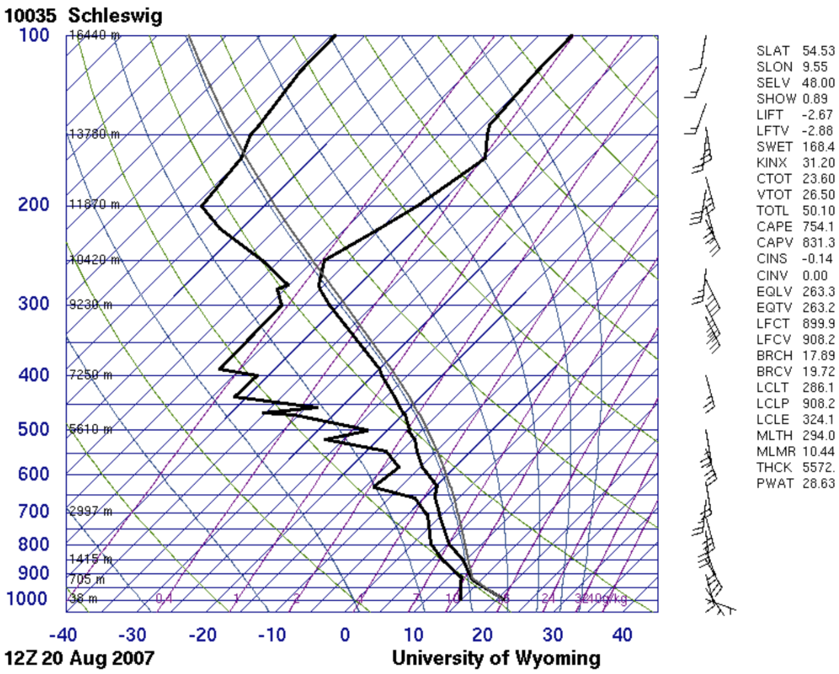

Figure 56: Sounding from Schleswig, Germany, 12UTC, 20th of August 2007. Same description as figure 39. [36]

The turbulence's ability to lift parcels is weakened in the evening, when the temperature is falling due to less sun forcing. Since the thunder cells arose in the evening, the starting point for the lifting must be different from the turbulence.

We can imagine that a sounding at Gråsten has been similar to the Schleswig sounding, because southern Jylland has been in the same air flow as Schleswig with warm and humid air from the Baltic Sea. The nearest SYNOP station at that time was Kegnæs on the island of Als, figure 55, where observations show that the temperature in the period 18UTC to 23UTC drops from 19.5 °C to 18.5 °C while the relative humidity in the same period was 100 %. While measurements from Sønderborg Airport show that the temperature from 18UTC to 22UTC fell 19.3°C to 17.2°C and a relative humidity of 100 %. Therefore, it is not unlikely that the temperature at Gråsten may have been slightly lower than at Schleswig, while the dew point has been slightly higher. Under these conditions, it does not require much to give the necessary lift, which in this case is obtained by dynamic processes as known from the quasi-geostrophic omega equation (14) that are a necessary for organizing the ascent of air. During the period of the cloudburst development, there is a jet streak over Jylland and northern Germany [44], see figure 57A. The jet streak is a local wind maximum on the jet stream axis. With the quasi-geostrophic approximations, it can be argued that there is an ascent in the right entrance area and left exit area of a jet streak, while there is a descent in the right exit area and the left entrance area. A more detailed description of jet streaks is given in appendix F. The sounding from Schleswig clearly shows that the wind rises with the altitude, which means that there is warm advection in the area as stated in the theory in section 2.3.1 and figure 9. This is supported by figure 52B. During warm advection, the ascent areas will move closer to the jet axis and therefore the cloudburst may have developed by ascending air close to the jet streak axis, which according to figure 57 is in the right entrance area. The passage of the jet streak must necessarily last long enough for this lift to bring surface air to the LFC. Figure 57 A and B show that there is warm advection as the wind is veering from 850 hPa to 300 hPa, as the red wind vane in the figure is to the right of the black wind vane during the period the jet streak passes the cloudburst area.

Figure 58 shows radar measurements of the precipitation echo from the Rømø radar. The radar images are pseudo-CAPPI images, where CAPPI stands for Constant Altitude Plan Position Indicator, which gives radar images from a constant altitude. In the images, radar reflectivity is calculated using the following equation:

$$dBZ = (DN \cdot 0.5) - 32 \tag{47}$$

where DN is 8-bit values with a range from 0 to 255. A DN value of 100 gives a reflectivity of 18 dBZ. The images have a temporal resolution of 10 minutes but in the figure is the resolution of 30 minutes in the period from 18UTC to 23.30UTC.

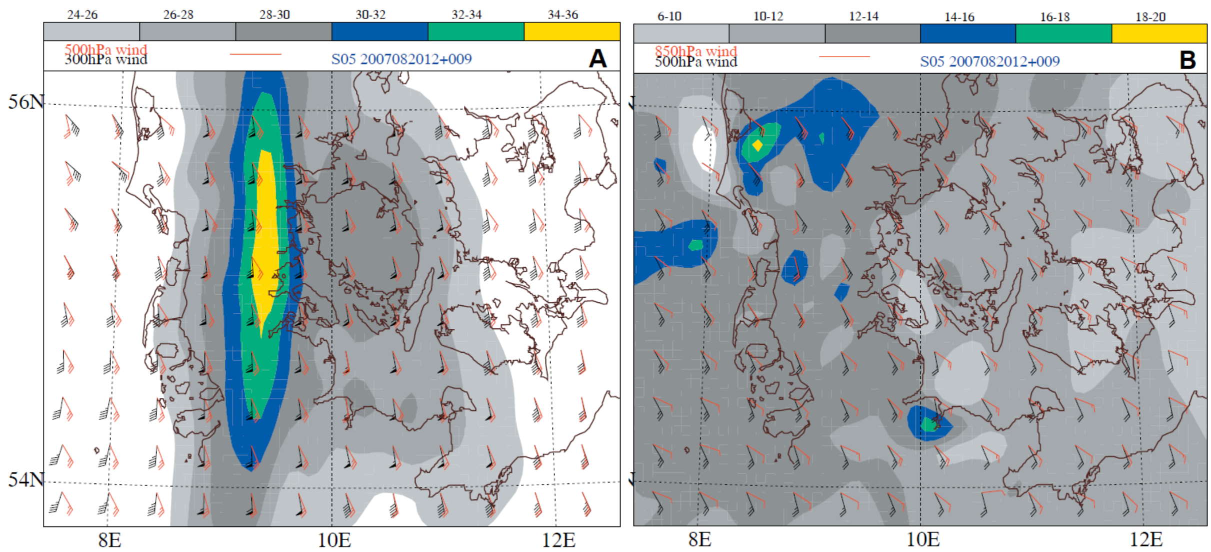

Figure 57: 9 hour forecast from DMI-HIRLAM, valid until 21UTC, 20th of August 2007 [44]. Wind speed in 300 hPa stated with color scale (m/s) as well as wind barbs in 500 hPa (red) and wind barbs in 300 hPa (black) (A). Wind speed in 500 hPa stated with color scale (m/s) as well as wind barbs in 850 hPa (red) and wind barbs in 500 hPa (black) (B).

In the radar echoes in figure 58, it is clear that the storm was coming up from the southeast. The first radar echo (cell 1 in figure 59) occurs south of Schleswig at 18UTC, hits Flensburg Fjord around 19.30UTC (green arrow at 19.40UTC and 20UTC in figure 58) and grows in intensity and area distribution and reaches maximum intensity 20.20UTC around Gråsten (yellow ring, 20.20UTC). The next radar echo (cell 2, figure 59) appears in the southeastern area of Flensburg Fjord 20.30UTC (green arrow, 20.40UTC) and reaches maximum intensity over Fiskbæk around 20.50UTC (yellow ring, 21UTC). Shortly thereafter (21.10UTC), cell 3 comes up and reaches maximum intensity around 21.20UTC (yellow ring, image 21.20UTC). Common for cell 2 and 3 is that they develop a little farther east than cell 1. The last radar echo (cell 4) occurs around 21.20UTC in the eastern part of Flensburg Fjord. This cell reaches maximum intensity around 22UTC. Common to the entire storm system is that it originates from the southeast, but intensifies over water in Flensburg Fjord.
Figure 59 is based on the radar echoes and shows the paths (lines) of the cells and location for maximum intensities (dots). As can be seen, new cells arise upstream (east) of old cells, which agrees with the fact that there is warm advection in the area (figure 52B and figure 9). All cells have a direction to the north-northwest, which corresponds to the wind direction in 500 hPa.
An eyewitness account [45] helps to emphasize that there were several cells during the thunderstorm. The eyewitness is Anders Brandt, who at the time was a meteorologist at TV 2 Vejret.

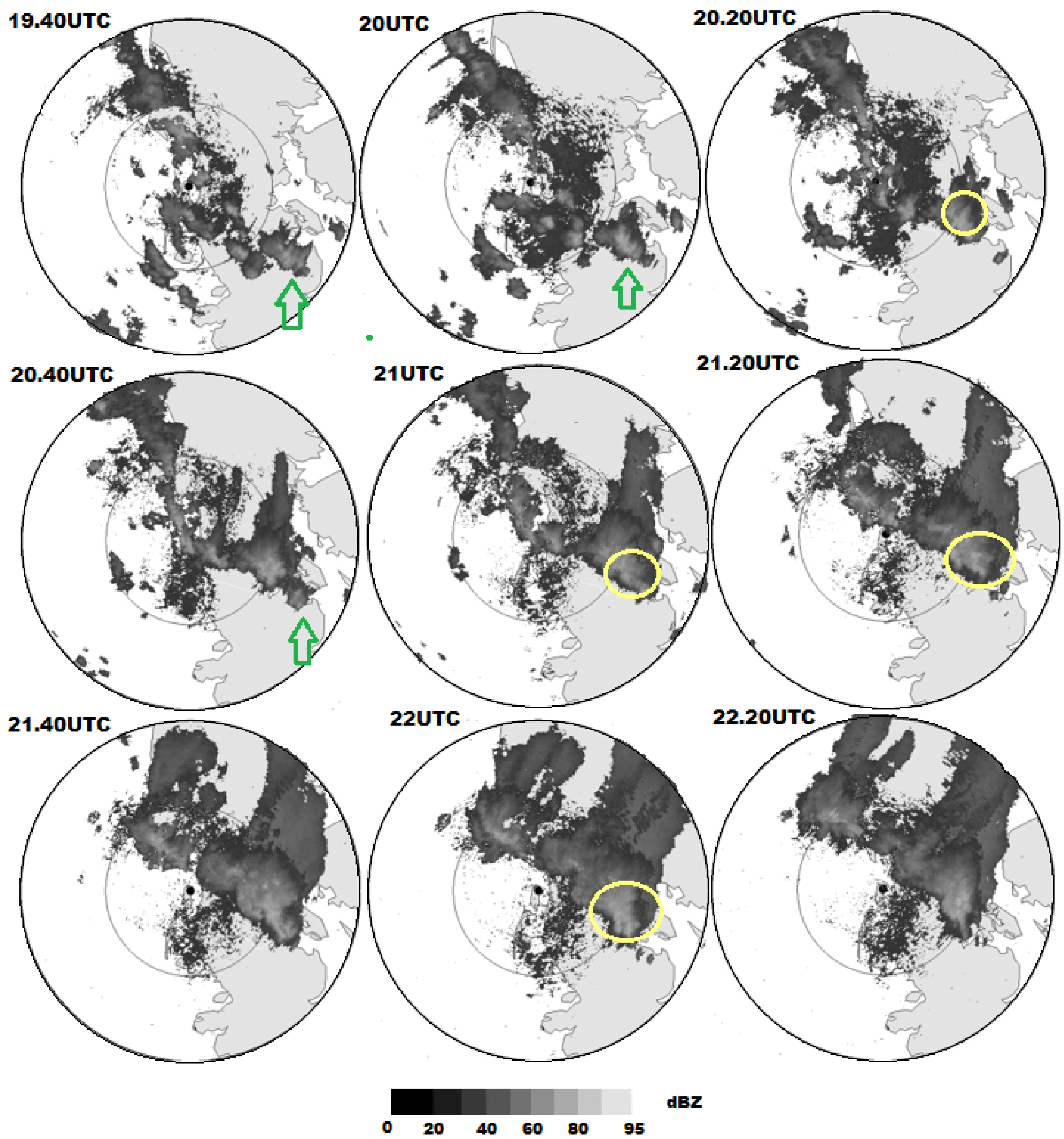

Figure 58: Pseudo-CAPPI radar images with the pixel size of 500 m from the available volume data for the Rømø radar in the period 19.40UTC, 20th of August 2007 to 22.20UTC, 20th of August 2007. The data are 8 bit values in the range from 0-255. The unit is dBZ. The green arrow point out new cell formations and the yellow ring point out maximum intensity. The radar images are generated by Thomas Bøvith, DMI.

Living by Broager, this gives a pretty good insight into how the individual cells built up during the evening. The story begins with Anders Brandt observing a large amount of lightning over Flensburg Fjord around 22UTC. At the same time, on the front of the first cell, there is a dravat over Broagerland which lies south of Broager.
According to the report, the intensity increases very suddenly around 20.15UTC - five minutes before the first cell. The intensity became so strong that a sound inferno of hail, large raindrops and severe thunder cells are reported. After 5 to 10 minutes, it is felt by Anders Brandt that the lightning intensity is northwest of Broager. The thunder cell was now driven up to Gråsten.
The next cell is registered at 20.45UTC which is described even more severe than cell 1. The

sound inferno was now primarily caused by strong wind which in the report is described as a downburst (see section 2.4.2 for the theory for downbursts). The wind at this time now came primarily from the northeast which can be explained by cell 2 having a slightly more northerly path than cell 1. Already around 21.15UTC cell 3 is registered which, with a duration of 20 minutes, had less intensity than the two previous ones. Only 3 cells were registered around Broager and Gråsten because cell 4 was registered over Aabenraa Fjord.

Figure 59: Thunder cells identified with radar echoes. Circles show the area with maximum intensity from the individual cells. Cell 1 (20.20UTC), cell 2 (20.50UTC), cell 3 (21.20UTC) and cell 4 (22UTC). The lines show the paths the individual cells have moved along. The map is Google maps.

A summary of this event is that the cell structure was a multicell system in an air mass that was conditionally unstable. A jet streak was an important factor in triggering the cloudbursts, where the rise of air during warm advection has been able to develop into thunder cells on the cold front of the low in a deep troposphere. Warm and humid air from the Baltic Sea has increased the CAPE of the air mass and promoted cloudburst formation. In addition, Flensburg Fjord has certainly played a role when the showers have come from the south and have been able to intensify across the inlet and up to the Gråsten area.
Calculations based on radar data [29] have later revealed precipitation intensities in the cloudburst that have not been seen in Denmark before. The highest 10 minute intensity recorded was 53 mm. Within half an hour 111 mm fell where the precipitation was heaviest - around 7 times cloudburst intensity. At the same time, radar data also show that up to 155.8 mm of rain has probably fallen over Aabenraa Fjord.

5.4 Case 4: 2nd of July 2011, the Cloudburst Over Copenhagen, 17.15UTC to 18.15UTC

On Saturday 2nd of July 2011, Copenhagen was hit by a historically powerful cloudburst in the afternoon with thousands of lightning strikes, severe floods and damage worth several billion Danish kroner. The largest official rainfall within 24 hours was measured in Botanical Garden with 135.4 *mm* while the highest 10 minutes intensity was measured in Ishøj southwest of Copenhagen with 31.2 *mm*.

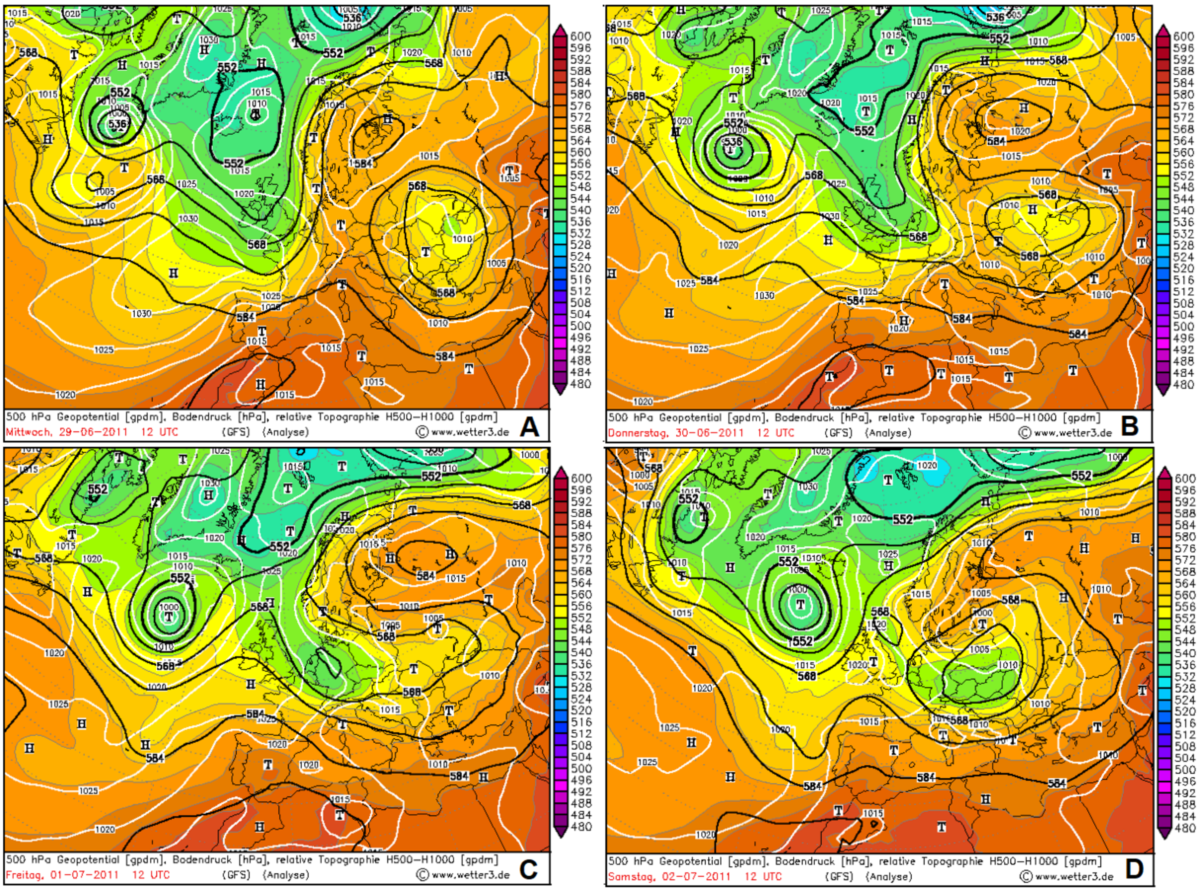

Figure 60: GFS 500 *hPa* geopotential, black curves [*gpdam*] and surface pressure, white curves [*hPa*]. H is high pressure and T is low pressure. 12UTC, 29th of June 2011 (A), 12UTC, 30th of June 2011 (B), 12UTC, 1st of July 2011 (C) and 12UTC, 2nd of July 2011 (D). [34]

The days leading up to the cloudburst were controlled by a high ridge that stretched from southern Europe to Scandinavia, see figure 60A. Both west of the high ridge and east of the high ridge are two low circulations, southeast of Iceland and over Ukraine respectively. In the following days, the two lows move towards each other, thus forming a high circulation over Finland and western Russia. The western low ensures that cool air is sent over Denmark from west in relation with a cold front passage during 29th of June and 30th of June (figure 60B).
At the same time, the eastern low sends warm and moist air from the south, up over the Gulf of Finland. Farther from here to the southwest around a low that has been formed out in the Baltic Sea (figure 60C) and farther southwest towards the southern Sweden and Denmark. At this time, there is now a warm front passage across Copenhagen on 2nd of July, figure 60D.

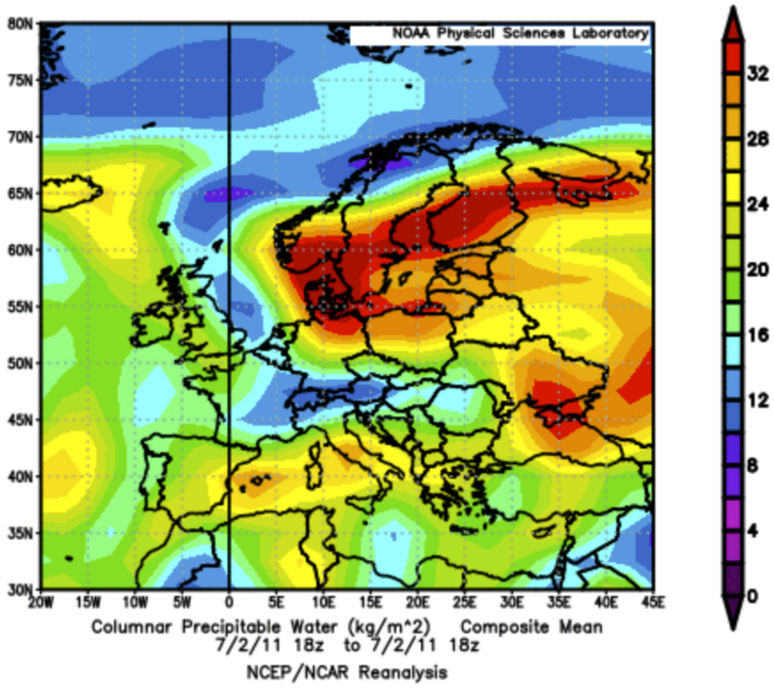

Figure 61: Columnar precipitable water, composite mean in the units of kg/m^2. [35]

The warm, humid and unstable air from the north-east has now replaced the cool air from west and it is in this air mass where a strong thunder cells develops over the southern part of Sweden and Copenhagen in the late afternoon of 2nd of July. The PW in figure 61 shows the moist air over the Baltic Sea and southern Scandinavia. In particular, the highest values of PW are roughly in the same range as the high CAPE values in figure 63 (p. 65).

There is no sounding from Copenhagen. The closest sounding that must be assumed to be representative of the atmosphere over Copenhagen is Visby on the Swedish islands of Gotland. At 12UTC, figure 62 is in the same warm air that drew over Copenhagen.

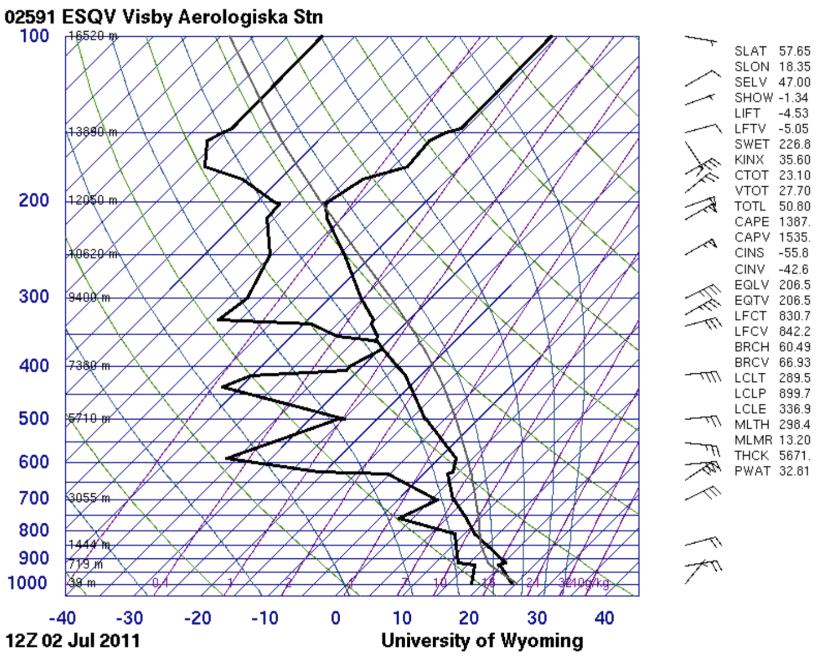

Figure 62: Sounding from Visby, Sweden, 12UTC, 2nd of July 2011. Same description as figure 39 [36]

The sounding indicates that the convective temperature[10] is 27°C at a dew point of 20°C in 1000 hPa. If the convective temperature is not reached, forces must be present for the air to receive the necessary lift to the LFC. Measurements of the 2m temperature in Copenhagen show 25 to 26°C around 16UTC, i.e. on the verge of thunder cells can occur spontaneously [46].

The lifting curve for Visby has a surface temperature of 24.4°C, where LCL is 899.7 hPa and LFC is 830.7 hPa. In this case, CIN is required to lift the air from the LCL to the LFC. A significant CAPE over 1300 Jkg^{-1} in this case can play

[10] The approximate temperature that air at the surface must reach for cloud formation without dynamical processes

a role in the formation of the thunder cells. In general, the area in the warm air over most of southern Sweden is characterized by quite high CAPE values, see figure 63. The high CAPE values indicate that the thunder cells that occur in the area can become quite powerful and achieve a cloud top at an altitude of more than 12 km. These statements agrees with the theory in section 2.2.3.

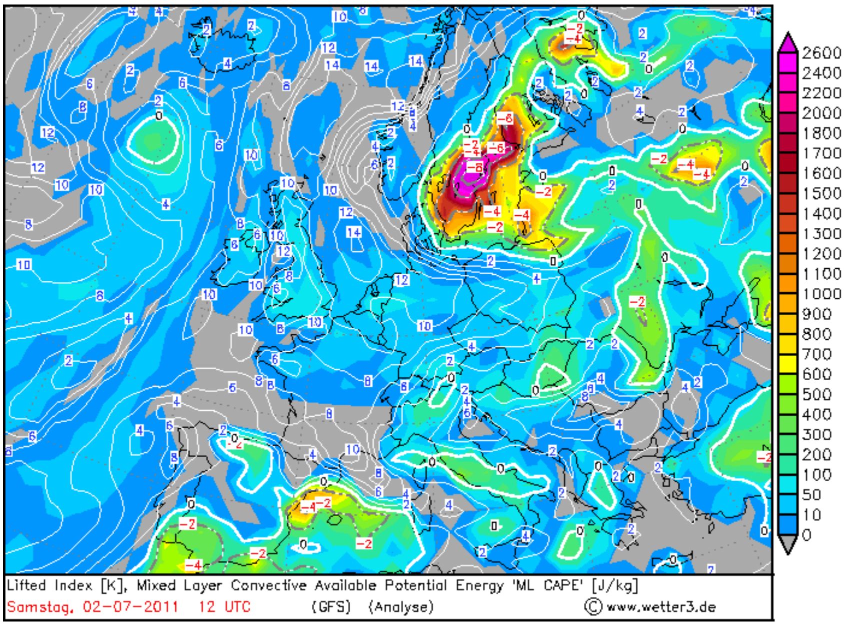

Figure 63: GFS CAPE $[J/kg]$ and lifted index, white curves [k], 12UTC, 2nd of July 2011. [36]

The lower layer of the troposphere from the surface to about 600 hPa is potentially unstable, because there is a positive difference for the equivalent potential temperature (θ_e), i.e. θ_e decreases up through this layer from 337°K at the surface to 315.5°K at 606 hPa. The larger the positive difference are in a given layer, the more potentially unstable the layer is. The underlying data from the Visby sounding shows that, the positive difference is 21.5°K which is relatively high. A potentially unstable layer is sometimes called convective instability, where dry air in the middle troposphere lies above warm and humid air in the lower troposphere, where the dry mid-level air is seen in the sounding from around 625 hPa to 400 hPa.

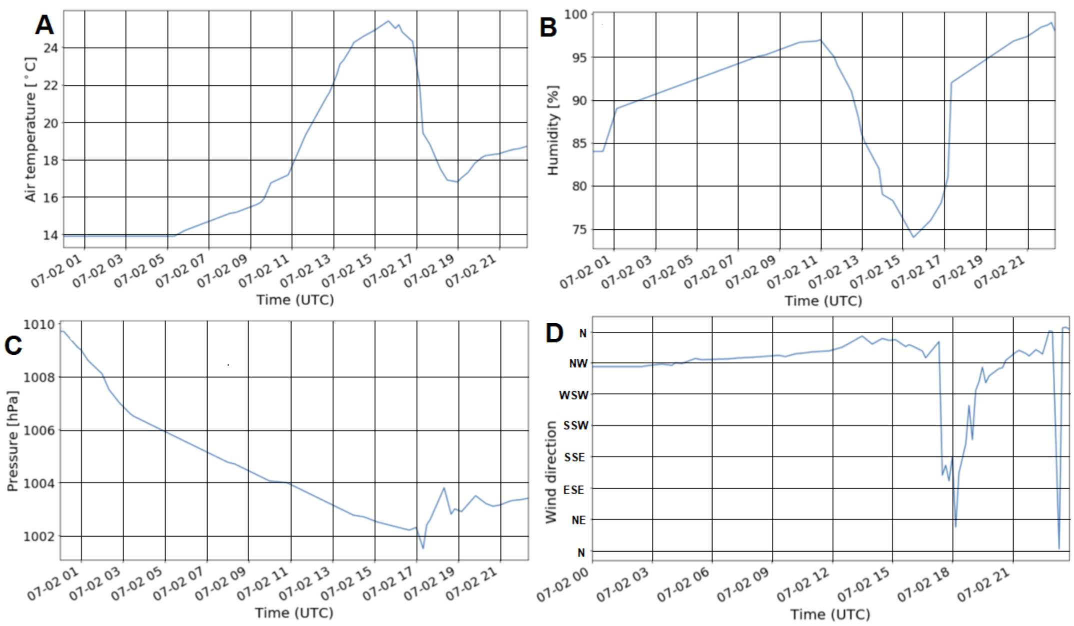

Figure 64: SYNOP data, 2m temperature [°C] (A), humidity [%] (B), pressure $[hPa]$ (C) from DMI (no. 06184) and wind direction (D) from Jægersborg (no. 06181).

A moderate wind shear from a weak wind at the surface to 15 m/s at 7 km altitude leads to the presumption that it is a multicell system as indicated in figure 7. Furthermore the wind direction from east northeast do not change notably with the height, which could be the same case for Copenhagen because Copenhagen is in the same air mass as Visby. Moreover, the value of LIFT, SHOW, KINX and TOTL indicates a moderately unstable atmosphere with the possibility of numerous thunder cells.
Figure 64 shows the synoptic data from the DMI station (A) to (C) and Jægersborg (D). The 2m temperature (figure 64A) at DMI reaches a maximum of 25.2°C around 16UTC. If the sounding from Visby is representative for Copenhagen, it means that forces are required to lift the air sufficiently for new cells to form, e.g. in relation with gust fronts as decribed in section 2.3.3. Measurements from southern Sweden show that the temperature during the day was above 27°C in the the period where new cells occured, which allows for spontaneous thunder cells to grow. The humidity (figure 64B) has a dive during the same period where the temperature reaches maximum. As the thunder cells begin to reach maximum intensity, humidity rises quite rapidly, where a sharp drop in temperature is detected due to the cold pools generated by the thunder cells (see section 2.3.3). The pressure (figure 64C) is gradually decreasing, as the low over northern Poland is directed towards Denmark. The relatively significant pressure drop around 17UTC is probably related to the first gust fronts occurring over Copenhagen. The wind direction (figure 64D) is mostly from northwest but at two points the wind direction is changed to north east, which is probably due to exhaust air from a shower.

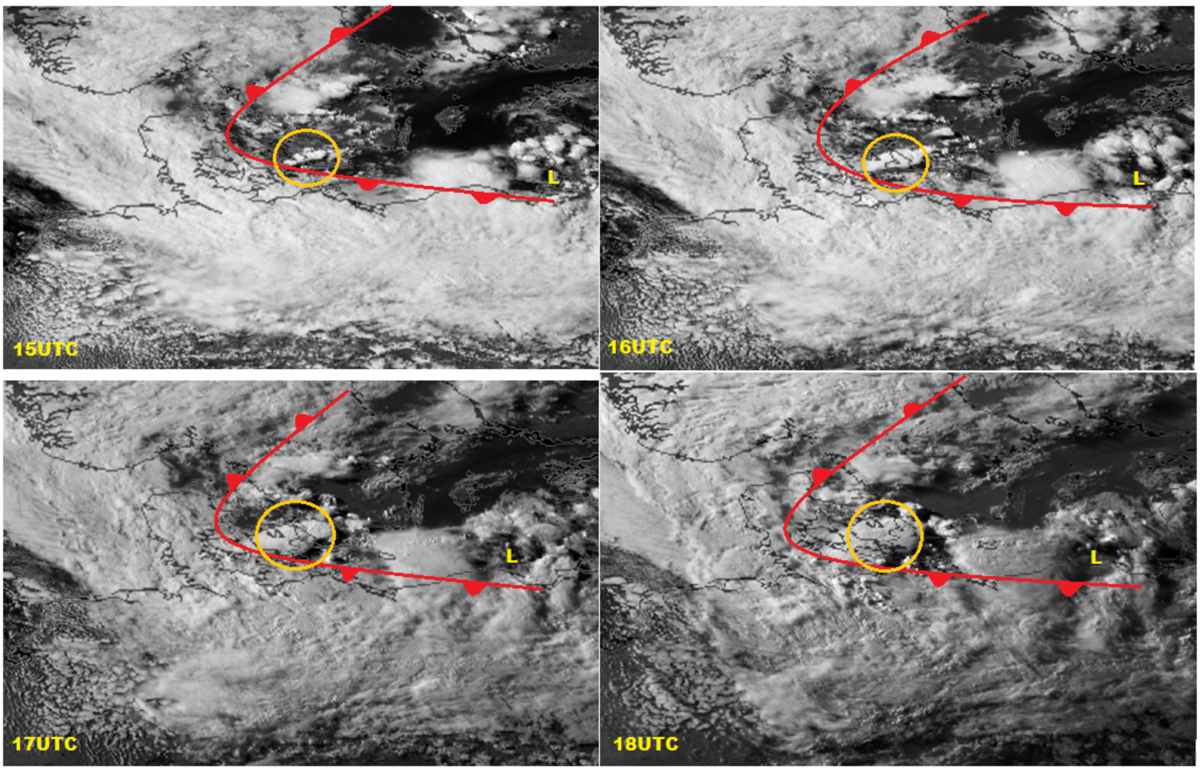

Figure 65: HRI Level 1.5 Image Data - MSG - 0 degree, EUMETSAT [31]. 2nd of July 2011, 15UTC to 18UTC. Visible, channel 0.6 μm. The analysis is based on 15 minute intervals - in the figure are the intervals hourly. The orange ring marked Copenhagen and Malmö. The low center is marked by the "L". The red line is the warm front.

The satellite images (figure 65) from EUMETSAT's MSG visible 0.6 μm shows the evolution in time steps of 30 minutes. The warm front that passed Denmark this summer day is drawn with a red line, while the showers that form over southern Sweden, which hit Copenhagen in the late afternoon, are marked with an orange ring in each picture. The low that provided the warm flow of air is located along the Polish north coast of the Baltic Sea. At the same time, convective thunder cells are seen in several places in Sweden and across the Baltic countries. It is thus in the warm and humid air at the back of the warm front that heavy thunder cells occur, where high values of CAPE (figure 63) can be detected, when the potential temperature is also high in this area. If figure 65 is compared with figure 61 it is easy to see that the moist air mass that comes with the warm front in the satellite images have high PW values because this air mass is very moist and then this is just agree with the theory where thunder cells are most likely to develop.

The first cells occur around 14UTC in southern Sweden, where they appear as a band of small convective rain clouds in both figure 65 and figure 66. Figure 66 shows radar images from the radar at Stevns that provide an insight into the development of the thunder cells. The radar images have a 10 minute resolution. Here they are selected at 30 minute intervals. The first radar image from 14.45UTC shows that the thunder cells have begun to accumulate in clumps parallel to the wind direction at 300 hPa, see figure 67A.

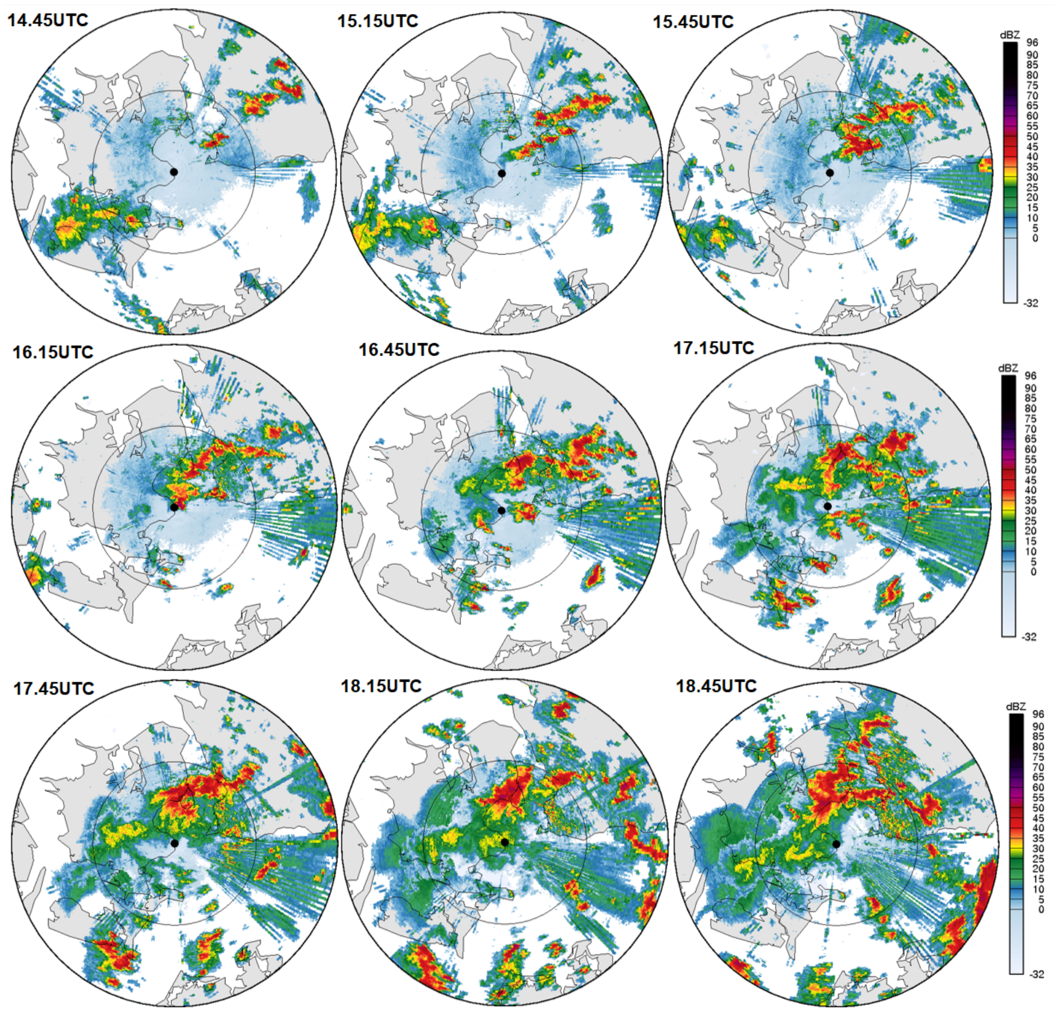

Figure 66: Reflectivity (dBZ) from the radar at Stevns in the period 14.45UTC to 18.45UTC, 2nd of July 2011. The radar images are generated by Thomas Bøvith, DMI.

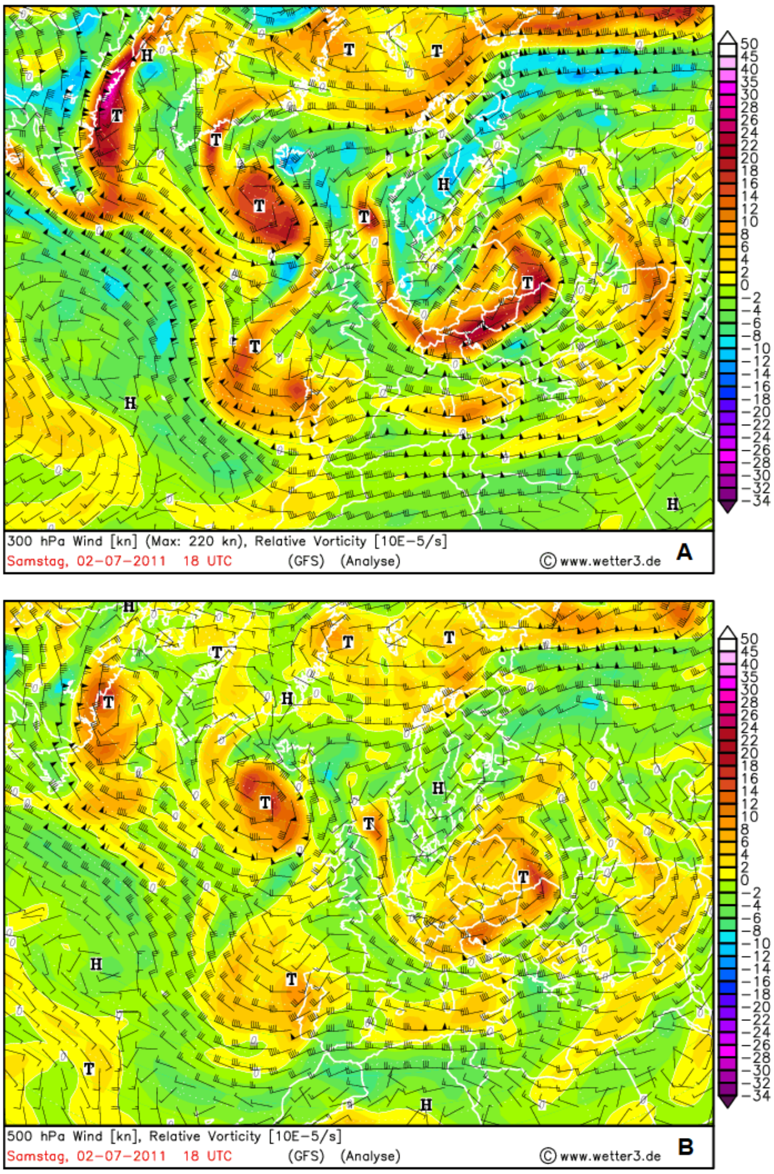

Figure 67: GFS 300 *hPa* wind (wind barbs) [kn] and relative vorticity [$10^{-5}s^{-1}$], 18 UTC, 2nd of July 2011 (A) and GFS 500 *hPa* wind and relative vorticity, 18UTC, 2nd of July 2011 (B). H is high pressure and T is low pressure. [34]

From around 15.15UTC, the precipitation pattern shifts from the relatively simple shower system, where the cells form in a neat band, probably as a multicell system, to a more complex system where new thunder cells can arise both spontaneously and along the gust front (see figure 12 for the theory for lifting by gust fronts) of old thunder cells. In the satellite images in figure 65 from 15.30UTC, it appears that the entire system gradually gathers as the thunder cells develop based on different criteria in the same area.

The radar image in figure 66 from 15.15UTC shows there are two bands of thunder cells; a band located southeast of Amager and a band located northeast of Amager. Characteristic of both bands is that the precipitation areas become an approximately contiguous precipitation area across Øresund and Copenhagen.

The first band south of Amager develops into a larger precipitation area (just before radar image 16.15UTC in figure 66) before it goes ashore at Stevns and dies out as it moves towards the southern part of Sjælland. The northeast band develops into a larger contiguous precipitation area over Copenhagen which appears in radar image at 16.45UTC and the satellite sequence from 16UTC to 17UTC.

In the period 16.45UTC to 18.25UTC, the precipitation area is almost stationary over central Copenhagen with maximum intensities between 17.35UTC and 18.25UTC. This is due to a reverse wind shear (figure 8) which makes the system almost stationary and gives strong floods in the capital (section 2.4.3 described floods). The fact that the precipitation area has been almost stationary over Copenhagen made this cloudburst particularly extreme. During the same period as the precipitation area ravages, there is a relatively sharp boundary to the north that is parallel to the wind at 500 *hPa*, figure 67B. The boundary zone moves slowly to the northwest before it dissolves around 18.35UTC. The relative vorticity advection in figure 67 is close to zero, which confirms that the first thunder cells arose spontaneously over southern Sweden.

The fact that there is no relative vorticity means that no forces, which are able to lift the air parcels sufficiently, are present at the synoptic plane. Conversely, had there been positive values of relative vorticity, then it would have resulted in divergence of the air aloft, which would produce convergence at the surface and thus an ascent of air and then potential buildup of showers. Relative vorticity is one of the terms in the quasi-geostrophic omega equation (14).
In relation with the showers over Copenhagen, there has been an outflow air from the thunder cells where wind measurements show that the flow has been perpendicular to the precipitation band. At Jægersborg (figure 64D) and Drogden Lighthous in Øresund (figure 68) shows, while there has been a thunder cell, the wind direction has been from the southeast, at other times is the flow from northwest. This means that a convergence zone (see section 2.1.2 for the theory behind convergence zones) was created along the precipitation band.
An explanation for the stationary phenomenon may be that new cells in the convergence zone have emerged at the eastern end of the precipitation band, while old cells die out at the western end. For example during a life cycle in the precipitation band, a cell will reduce CAPE, which from figure 63 explains that the CAPE values grow upstream of Copenhagen to the east-northeast.

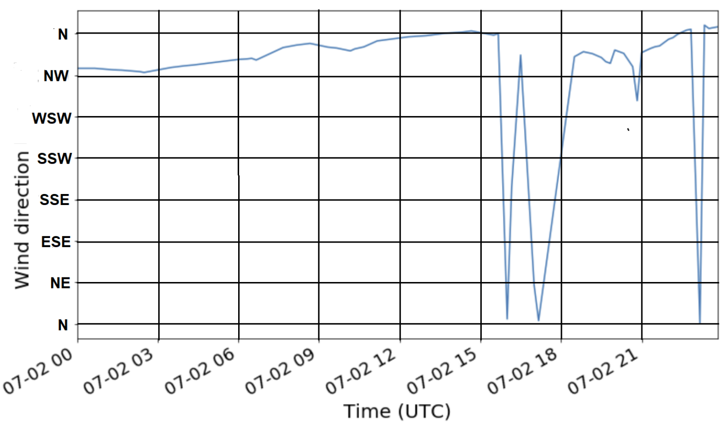

Figure 68: 10m wind direction from Drogden Lighthouse in Øresund (no. 06183).

Thus, it seems that the propagation vector has been opposite to the motion vector and has had the same velocity, see figure 21. New cells propagate to the east-northeast at the same velocity as the direction of the movement of the cells to the west-southwest, which helps making the system stationary. According to the theory in section 2.3.3, new cells appear approximately every 10 minutes. The storm was strongest over Copenhagen in the period from 17.25UTC to 18.15UTC, i.e. 50 minutes, thus five cells have moved across the Danish capital according to the hypothesis.
To summarize thunder cells arose spontaneously in southern Sweden under warm, humid and potentially unstable conditions and drifted with the upper air flow in parallel bands toward Copenhagen, where they created an almost contiguous precipitation area. New cells emerged in a convergence zone that occurred in the interaction between two air flows. The new cells probably arose upstream of the old cells, where CAPE values have been high, i.e. the horizontal gradient of CIN and CAPE has been key players in the formation of new cells.
It is concluded that it was a multicell system that gave the heavy rainfall over Copenhagen on this day in July. It was a historic cloudburst took place, where the largest official measurement was 135.4 *mm* in the Botanical Garden - the largest measured daily rainfall amount in Denmark, at that time, in 57 years. The intensities also spoke for themselves, where in some places more than 50 *mm* of rain fell in 30 minutes, resulting in a triple cloudburst intensity. In appendix C, the 43 highest precipitation intensities are registered from SVK's raingauges in the period 1984-2019, and 8 out of the 43 intensities are from this day.

5.5 Case 5: 30th of August 2014, the Multi Cloudburst Over Copenhagen and Malmö, 00UTC to 02UTC

The night between 30th of August and 31st of August 2014, Copenhagen was hit by the strongest cloudburst since the severe cloudburst in 2011 mentioned in section 5.4 [47]. Many streets in the capital were flooded and the amount of rain at DMI was registered to be 119 *mm* of rain in approximately two hours. Malmö in Sweden, on the opposite side of Øresund from Copenhagen, also experienced severe cloudbursts later this night, but the focus in this section will be on the Danish capital.

Figure 69 represents the development up to the cloudburst, where a low northwest of Ireland (A) moves during deepening in a path, towards the cloudburst development, into the North Sea southwest of Norway (B). The cloudburst over Copenhagen occurred at the eastern end of the low, where an occlusion point is registered.

The low moves into the North Sea over the warm seawater and is thus filled up, where turbulence at the surface transports water vapor and sensible heat up into the lower part of the troposphere. Cold air in the free troposphere characterizes this low and thus DMC can be maintained while the low moves over warmer surfaces. The core of the low is homogenized and favorable conditions are created for thunder cells to develop, as the atmosphere becomes saturated because the vertical profiles for temperature and dew point become almost the same.

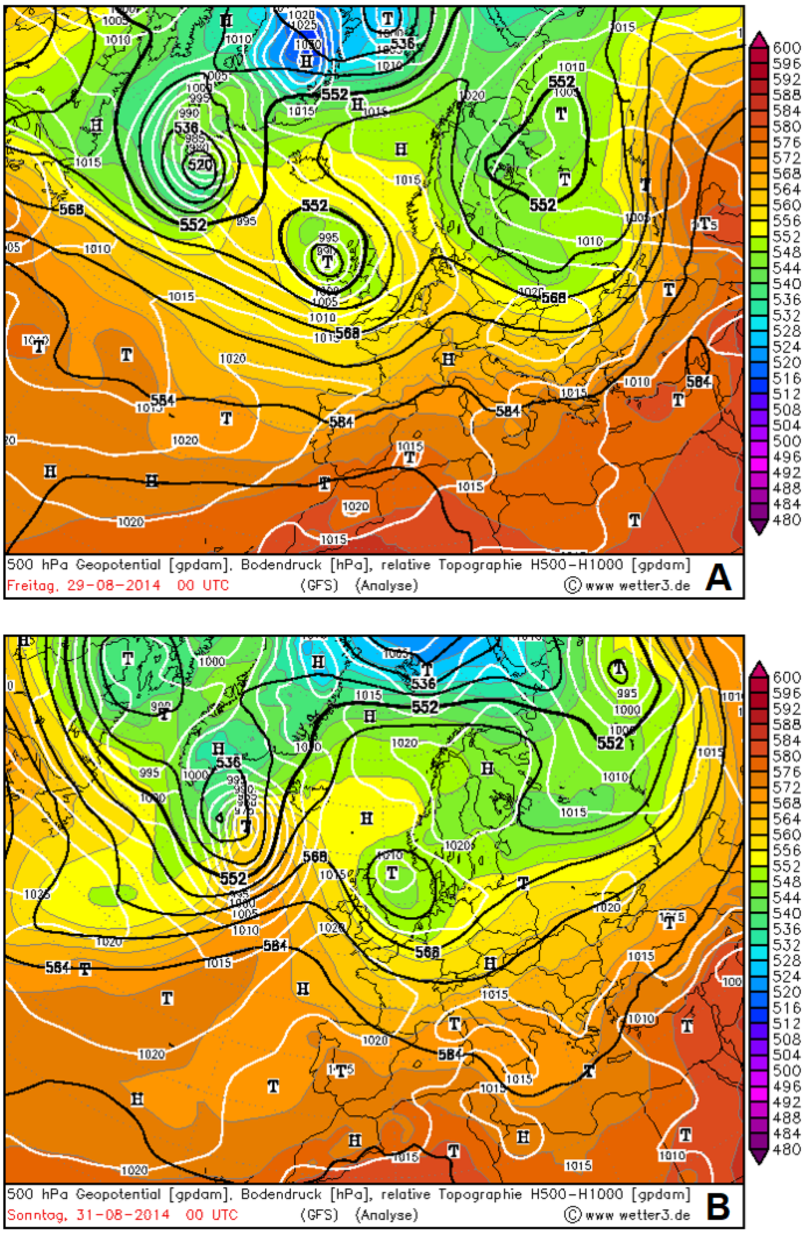

Figure 69: GFS 500 hPa geopotential, black curves [$gpdam$] and surface pressure, white curves [hPa]. H is high pressure and T is low pressure. 12UTC, 28th of August 2014 (A) and 00UTC, 31st of August 2014 (B). [34]

The satellite sequence from EUMETSAT's infrared channel 10.8 μm (figure 70) illustrates how the low moves in the evening to the southeast with a cold front located to the south and a weak warm front across the Baltic Sea. The cold front and the warm front forms an occlusion front that runs up to southern Norway. Copenhagen is located in the orange ring. The first sequence of something that could look like powerful thunder cells takes place in satellite image 00UTC.

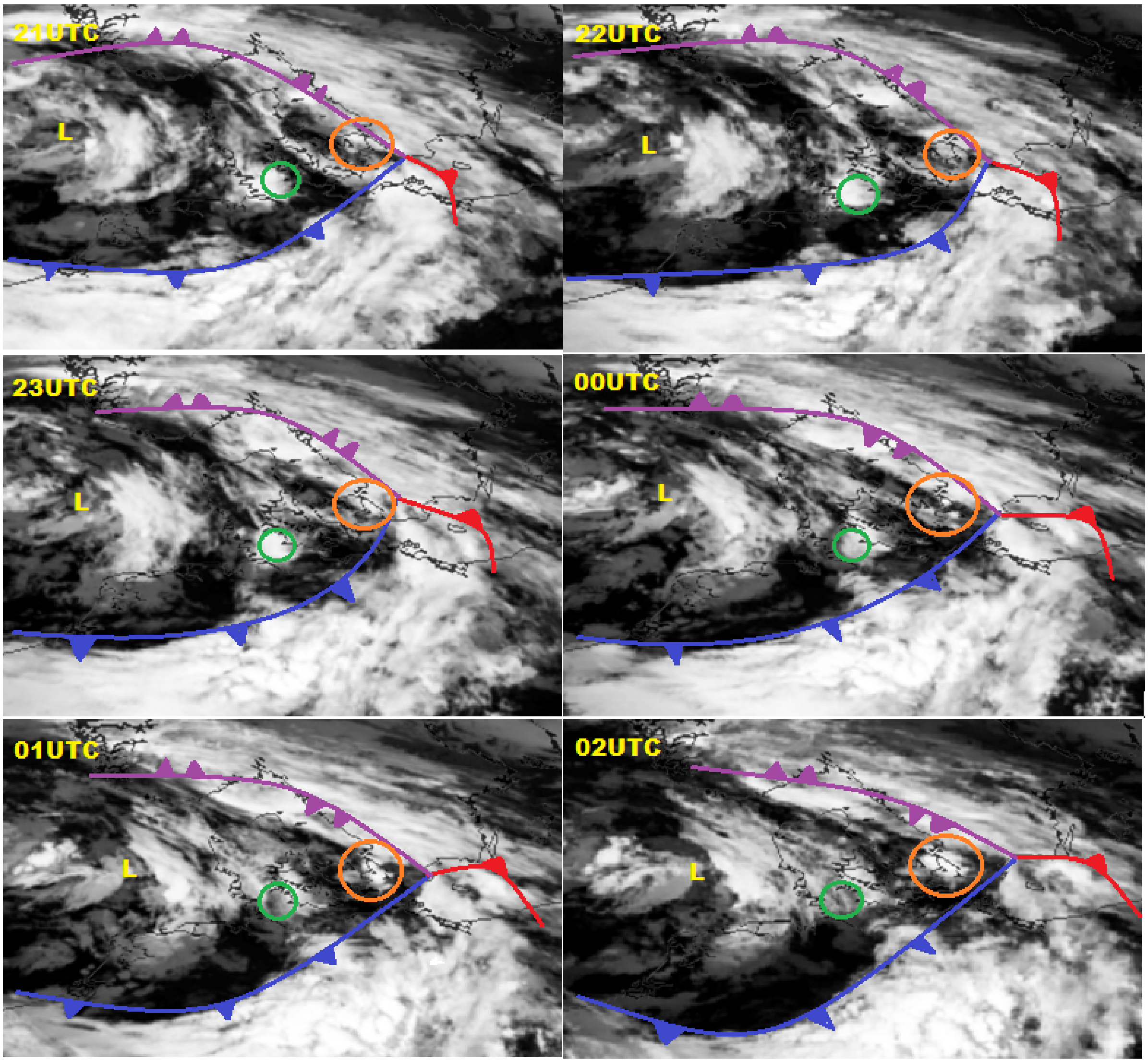

Figure 70: High Rate SEVIRI Level 1.5 Image Data - MSG - 0 degree, EUMETSAT [31]. Infrared, channel 10.8 μm. 30th of August 21UTC to 31st of August 02UTC 2014. White colors are cold areas, while dark areas are warm areas. The satellite images have a 15 minutes resolution - in the figure is the resolution hourly. The blue line is the cold front, the red line is the warm front and the purple is the occlusion. "L" is the low. The orange ring shows the area around Copenhagen and Malmö with the cloudbursts and the green ring point out the Schelswig sounding.

Prior to the cloudbursts, the frontal zone passed so that Copenhagen enters the slightly cooler air from the low in contrast to the slightly warmer air to the southeast. The radar image from 17.05UTC (figure 72, p. 72) clearly shows how the frontal zone has just passed Copenhagen. The satellite images also show that the entire system is moving east-northeast, where the cloudbursts are formed in the low air which will be analyzed using a sounding from Schleswig, marked with the green ring.

PW in this case shows a relatively humid troposphere in figure 71B, The troposphere for 31st of August, 00UTC, is also quite cool. The cool troposphere in figure 71B is more humid than the warmer troposphere that preceded the cloudburst in figure 71A. There is a maximum in PW on 31st of August, 00UTC, around the Baltic Sea and up to the Øresund region. Therefore, it is expected that the cloudburst potential is greater in the cooler troposphere that Copenhagen entered after the front passage on 30th of August in the afternoon, figure 72, due to the high content of moisture according to the theory in section 2.2.3.

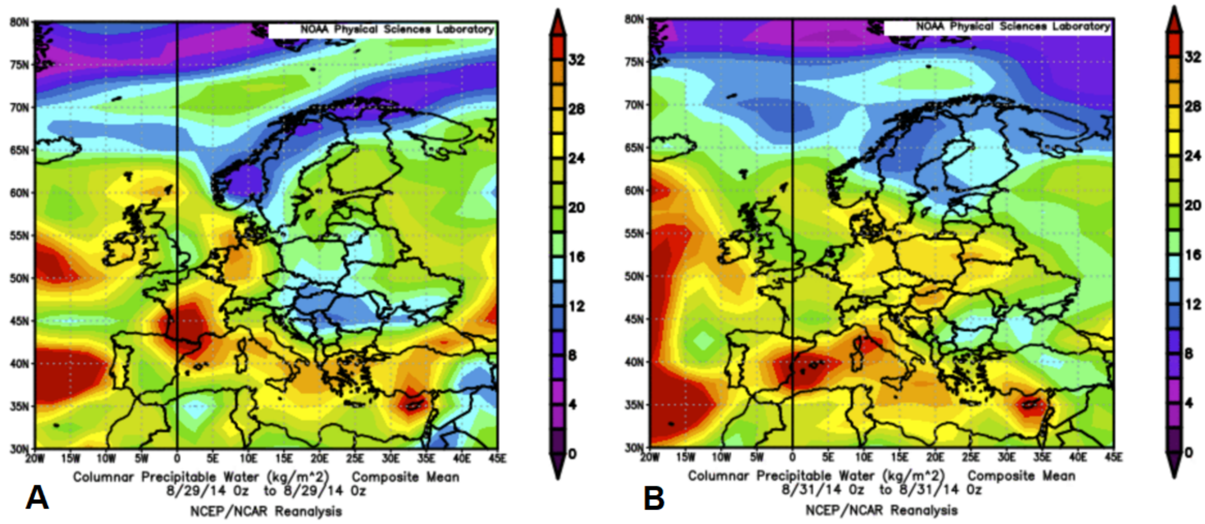

Figure 71: Columnar precipitable water, composite mean in the units of kg/m^2, 29th of August 2014, 00UTC (A) and 31st of August 2014, 00UTC (B). [35]

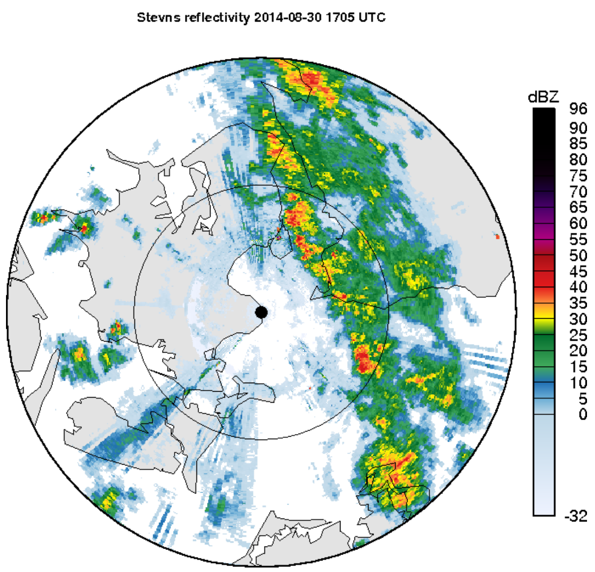

Figure 72: Reflectivity (dBZ) from the radar at Stevns 17.05UTC 30th of August 2014. The radar image are generated by Thomas Bøvith, DMI.

The radar echoes from the Stevns radar in figure 73 shows the sequense of the cloudbursts. The first echoes can be observed around 20.25UTC south-southwest of Copenhagen. These echoes drifted north-northeast, while new ones emerged upstream over Køge Bay (20.55UTC) as a multicell system (see section 2.3.3 for multicell systems). These could be detected between 21UTC and 22UTC and were a precursor for the later cloudburst event.

A new band of echoes is registered in western Copenhagen (22.25UTC). This band of echoes are moving slowly in a north-northeast direction and from 23UTC almost stationary along Øresund. Throughout this process, new cells emerged once again, upstream of the old ones over Køge Bay as a particularly active area for the initiation of the new thunder cells. Then they drifted north-northeast over Copenhagen and further up the coast where they slowly decreased in intensity.

Between 23.30UTC and 00UTC, new echoes appeared in the Baltic Sea east of Møn (south of Stevns radar). This new band of echoes gradually became longer, with new cells still being formed north of this band in Køge Bay. From around 01UTC, the two echo bands are almost one band from Helsingør in the northern part of Sjælland to Møn with the highest intensities over the stretch from Copenhagen to Møn. After the merger, the center of gravity for the strongest echo intensities drifted over to Malmö on the Swedish side of Øresund.

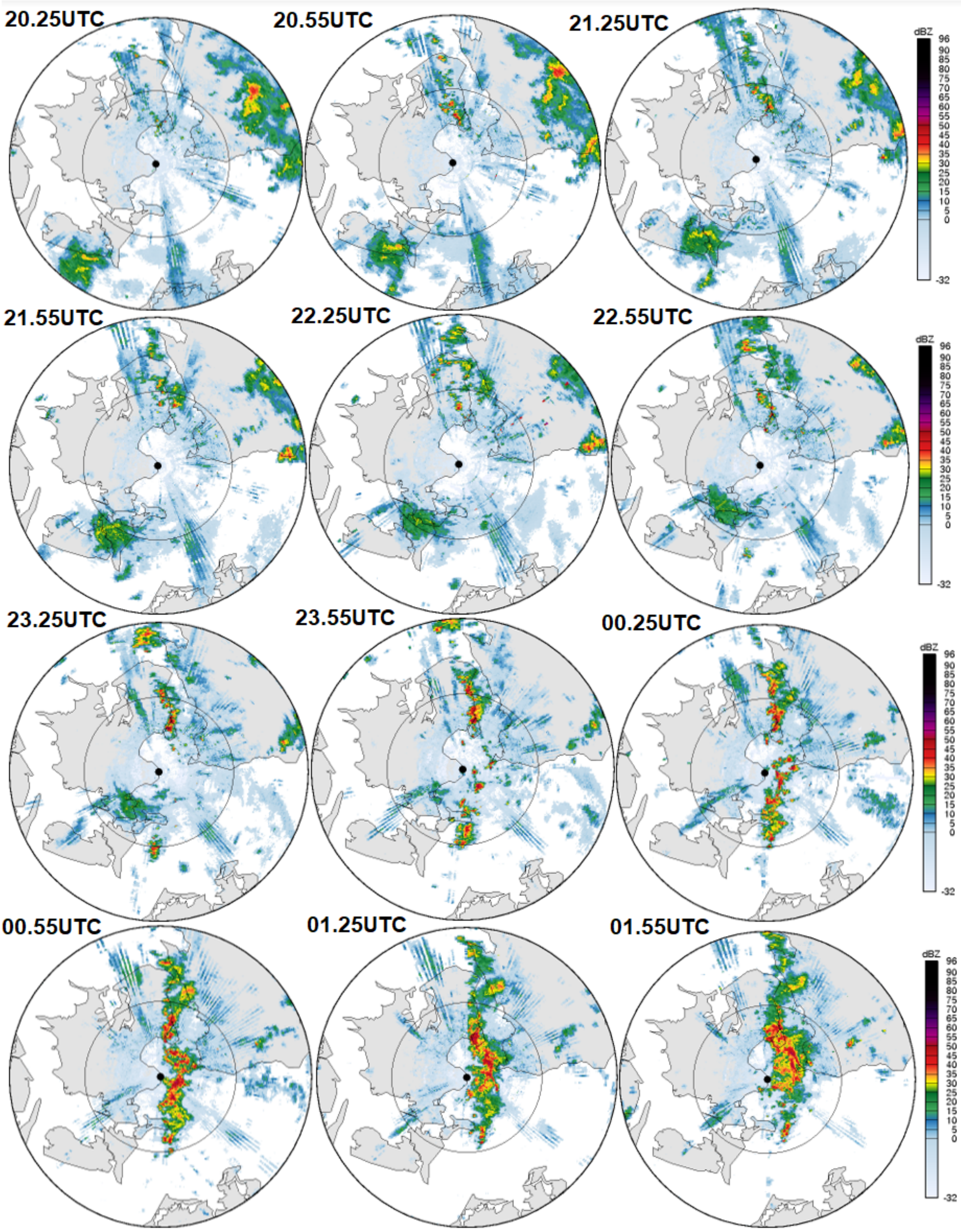

Figure 73: Reflectivity (dBZ) from the radar at Stevns in the period 20.25UTC 30th of August to 01.55UTC 31st of August. The radar images were generated by Thomas Bøvith, DMI.

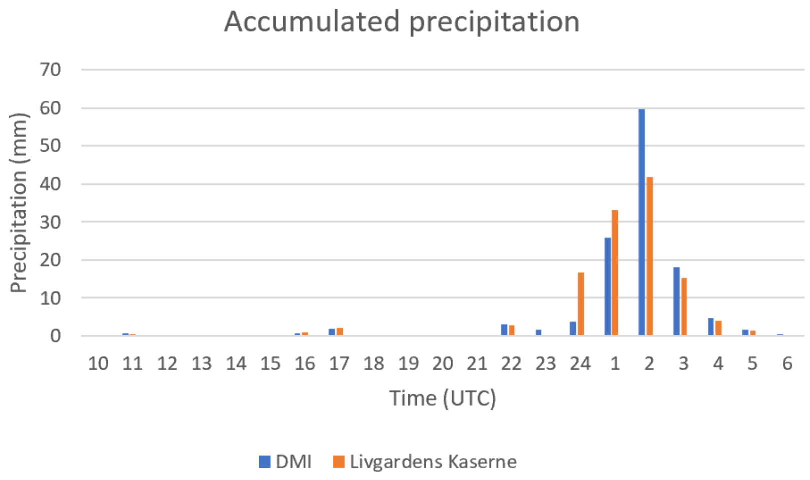

Figure 74: Accumulated precipitation (*mm*), hourly 10UTC, 30th of August 2014 to 06UTC 31st of August 2014 from Livgardens Kaserne and DMI. Front passage 15UTC to 18UTC.

There was thus a relatively narrow band of thunder cells. New cells emerged both over land and over sea, the most powerful cells being formed over the sea, probably due to warmer and more humid surface air. A significant contribution to the thunder cells becoming so powerful over Copenhagen can probably be described by the fact that many of the new cells arose upstream of the old ones overseas after the reverse wind shear concept in figure 8.

Figure 74 shows precipitation amounts for the two stations Livgardens Kaserne and DMI (4 *km* distance between these locations). The figure reflects the three precipitation events from the radar images in figure 73. The frontal zone that passes Copenhagen in the afternoon hours results in precipitation 16UTC to 17UTC. According to the radar imgaes in figure 73 the echoes passed the measuring station around 21UTC and 22UTC before the heavy rain hit around midnight.

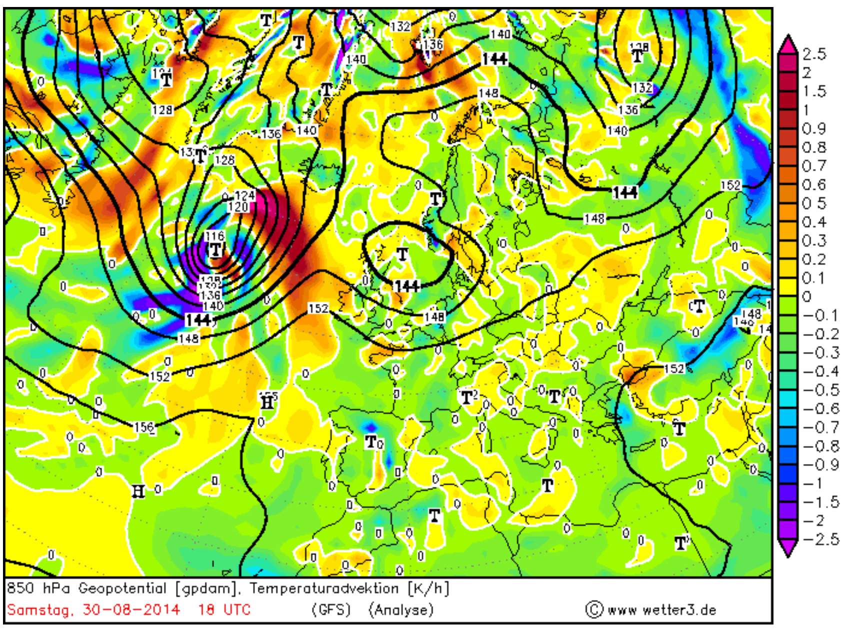

Figure 75: 850 *hPa* geopotential [*gpdam*] and temperature advection. H is high pressure and T is low pressure. 18UTC 30th of August 2014. [34]

The satellite images in figure 70 and the GFS geopotential maps in figure 69 show that Denmark in the evening is in the air mass connected to the low. The two soundings closest to Copenhagen are Schleswig and Greifswald in Germany, but since Greifswald is in the frontal zone, the most representative sounding for the low is the one located in Schleswig, see figure 76.

The first sounding from 12UTC (figure 76A) has no CIN. Therefore the showers that occur at this point will occur spontaneously. However, there is still a potential for showers to occur in the air mass. In fact, a few showers were formed in Schleswig this day. That no more showers were formed

can be attributed to a dry inversion layer around 850 hPa while the wind is reversing, which in the northern hemisphere means cold advection (figure 9), which can also be attributed the temperature advection in figure 75. This shows there is a weak cold advection in 850 hPa over Schleswig, while over Copenhagen there is a weak warm advection which is according to the omega equation (14) is an important trigger for thunder cells.
The sounding in figure 76A also shows a surface temperature of 15°C and a dew point of 14 °C, which shows an atmosphere that is almost saturated. Figure 76B shows the sounding for 00UTC - the same time when the cloudbursts were most intense over Copenhagen. Up through the entire troposphere to an altitude of about 10 km, the temperature and the dew point temperature are close to each other, respectively 13°C and 12.3°C at the surface. In addition, the temperature curve almost follows a moist adiabat, which indicates a moist air mass. The wind is quite weak and hardly changes direction - 0-6 km wind shear reaches around 8 m/s, while the maximum is 17 m/s at the tropopause. The weak wind shear may be a reason for the high rainfall amounts in Copenhagen, as precipitation intensity grows with a decreasing vertical wind shear [48]. LCL is at an altitude in 962.6 hPa where an air parcel will be saturated by adiabatic cooling. LFC is achieved at 814.2 hPa while EL is at an altitude of 525.4 hPa - relatively far from the tropopause at 275 hPa. CAPE has a value of 52.34 Jkg^{-1} on 31st of August, 00UTC, which is slightly lower than the CAPE value from 30th of August, 12UTC of 59.92 Jkg^{-1}. The indices from Schleswig indicate an atmosphere

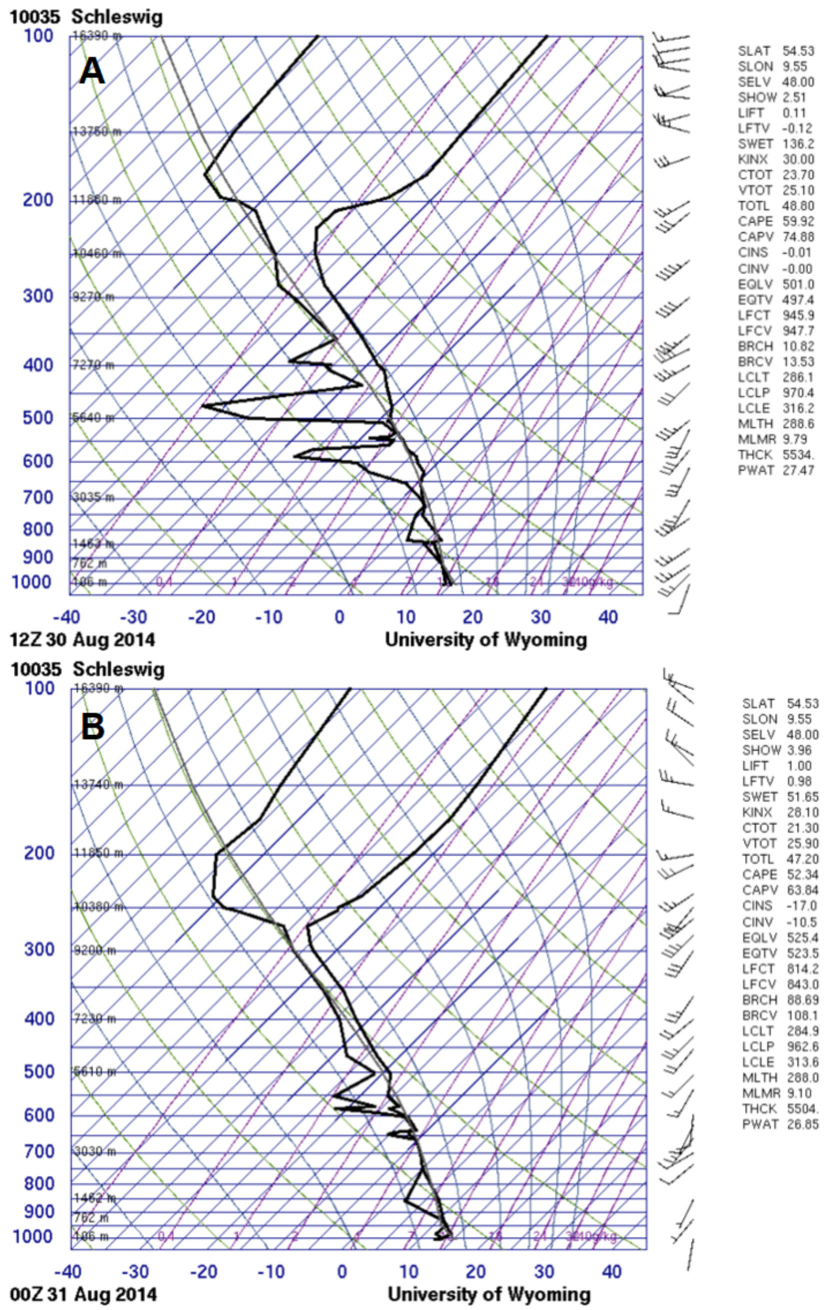

Figure 76: Sounding from Schleswig, Germany, 12UTC, 30th of August 2014 (A) and 00UTC, 31st of August 2014 (B). Same description as figure 39. [36]

in the low with only weak convection and only a small chance of scattered thunder cells.
The sounding from 00UTC is slightly more unstable than the one from 12UTC where the lower CAPE value is most likely because 00UTC is slightly colder than 12UTC.
A hypothetical sounding in Copenhagen would probably looked like the one in Schleswig - just a little warmer. At DMI, air temperature of 16°C and a dew point temperature of 15.3°C were measured. This may indicate a higher CAPE value for Copenhagen as well as a less negative value for CIN and EL closer to the tropopause. That is, a more unstable troposphere with greater probability for cloudbursts.

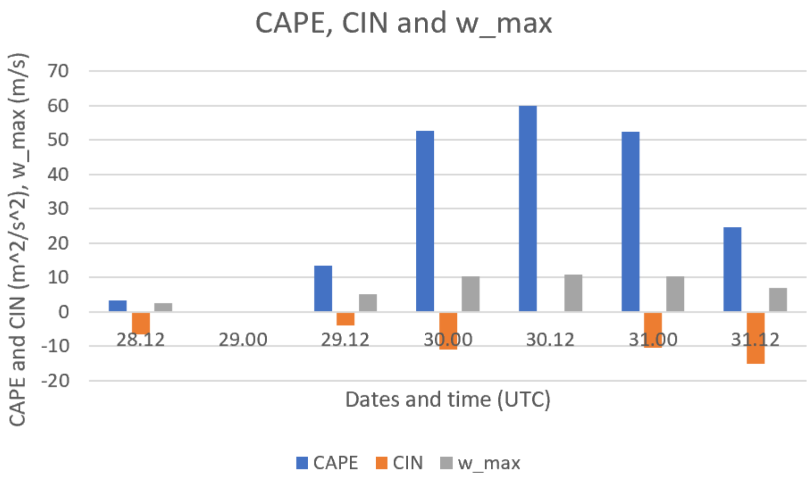

Figure 77: CAPE (blue) CIN (orange), unit: m^2/s^2 and w_{max}, unit: m/s, for the sounding from Schleswig, 12 hours intervals from 12UTC, 28th of August 2014 to 12UTC 31st of August 2014.

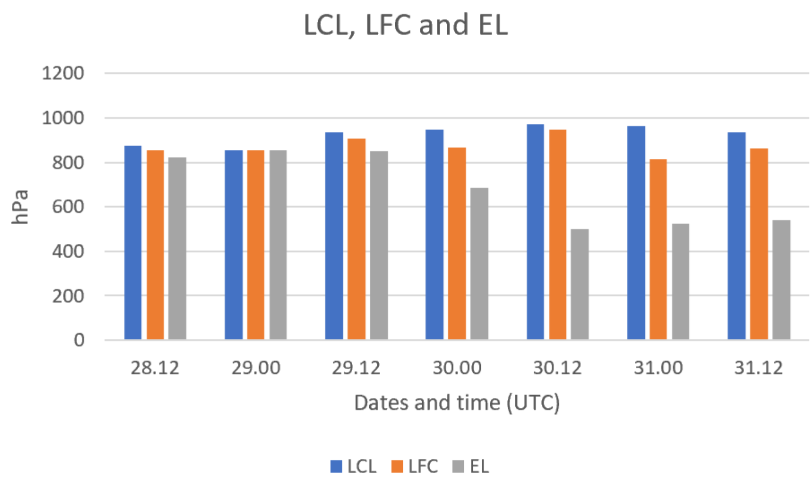

Figure 78: LCL (blue) LFC (orange) and EL (grey), unit: hPa, for the sounding from Schleswig, 12 hours intervals from 12UTC, 28th of August 2014 to 12UTC 31st of August 2014.

It is now examined how the soundings have changed during the development period for the low with selected parameters from the sounding in Schleswig to gain a better understanding of why the air mass in the low had cloudburst potential. Figure 77 shows the changes of CIN, CAPE and w_{max} during the period. The first few days indicate absence or only a small value of CAPE from 28th of August 12UTC to 29th of August 00UTC, which according to figure 69A corresponds to a high ridge that passed over Schleswig during this period. From 29th of August 12UTC Schleswig begins to be in the air mass of the low and CAPE grows to a maximum on 30th of August 12UTC. In the surrounding times (± 12 hours) there are slightly lower CAPE values, but CIN is approximately $-\frac{1}{5}CAPE$. Falling surface temperatures during these periods due to the nighttime contribute to a stable stratified air layer which can result in these negative CIN values.

In figure 78, LCL, LFC and EL are shown for Schleswig. During the period of absent CAPE values, the values for LCL, LFC and EL are almost the same, which means that there is no possibility of the formation of showers. The acceleration path that is the distance between LFC and EL, reaches a maximum on 30th of August 12UTC - the same time where w_{max} has its highest values in figure 77. A sounding in Copenhagen would have had the longest acceleration path as well as the largest values for CAPE and w_{max} on 31st of August 00UTC due to higher temperature and dew point temperature.

It can be argued that a self-organization takes place based on the clumping of echoes in the radar images after midnight. In figure 77 for CAPE and CIN, it was argued that Copenhagen, 31st of August 00UTC probably reminded of Schleswig, 30th of August 12UTC. A self-organization among the showers means that new showers occur along the gust fronts of old cells (see section 2.3.3 for a description of gust fronts).

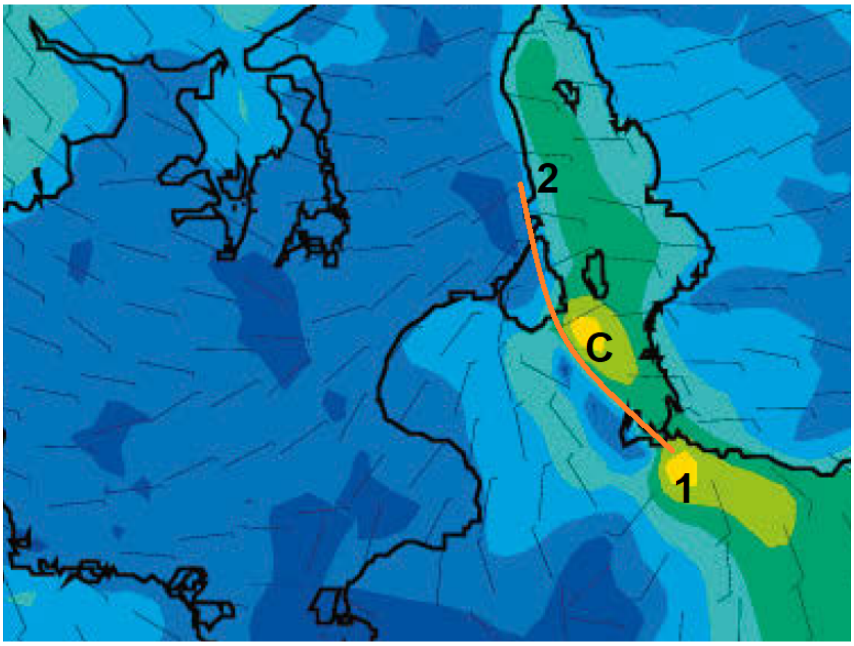

Figure 79: 10 m wind (m/s), 02UTC 31st of August 2014, from DMI's operational model. The orange line "C" is the convergence line and "1" and "2" are the convergence zones. Dark blue: 0-1 m/s. Yellow: 6-7 m/s. [47]

The sounding from Schelswig gave an impression of a humid troposphere with a relatively weak wind shear. These conditions will not immediately provide favorable conditions for lifting surface air along gust fronts. Nevertheless, based on the numerically small CIN, one can argue that self-organization of new cells has been possible. Self-organization also causes the precipitation band to grow in width over time and helps to shield from the ingress of dry and cool air, which increases the precipitation intensity.

A possible reason for the formation of the multicell cloudburst over Copenhagen and later also Malmö is the formation of a convergence line along the shower line. Figure 79 shows 10m wind from DMI's operational weather model, 02UTC 31st of August, where the convergence line (see section 2.1.2 for the theory for this) is drawn as the orange line. Southeast of Amager, several cells are formed at this time in convergence zone 1, which move towards Copenhagen and produce considerable amounts of precipitation. The reason for these showers is, as men-

tioned earlier, the relatively warm seawater in Køge Bay as well as a land breeze circulation that has developed this pattern.
Convergence zone 2, in the northern part of the convergence line in figure 79 arose over the western suburbs (see the early radar images) and drifted over Copenhagen where it became quasi-sationary along the Øresund coast. Based on the wind model, convergence along the coast and the land breeze circulation have played a role in this convergence zone becoming stationary. As can be observed in the radar images, the cells move north along the headwind.
The cloudburst over Copenhagen this late summer evening and night had several factors contributed to high precipitation intensities and precipitation amounts recorded. A humid and unstable troposphere with high PW values, a weak wind as well as a weak wind shear, the presence of CAPE, the stationary nature of the precipitation band and the fact that the precipitation band was self-organized, where new cells arose upstream of the old ones and thus passed over the same area, have all caused the multicell cloudburst to become as powerful as it was. Self-organization could also shield against the intrusion of drier and cooler air at the same time as more thunder cells could pass across Copenhagen.
According to SVK's records, the fourth highest precipitation intensity in Denmark in 2014 was measured this summer night with an intensity of 33 $\mu m/s$ at Træholmen in the southwestern part of Copenhagen. The records also show that the largest total rainfall during a day in 2014 was accumulated at Delfinen[11] with 102.8 mm on 31st of August.

[11] See figure 107 in appendix D for the location

5.6 Case 6: 4th of September 2015: A Morning Cloudburst in Copenhagen, 06UTC to 08UTC

In the early autumn of 2015, the southern part of Scandinavia was hit by heavy rain and cloudbursts in several places. One of the most significant cloudbursts in Denmark was the morning cloudburst in Copenhagen, 4th of September 2015, which is the focus in this section. Around Hellerup in the northern part of Copenhagen, 30 to 40 *mm* fell in a short amount of time. Where some of it fell as hail, afterwards cascades of hail could register in several places well into the day [49].

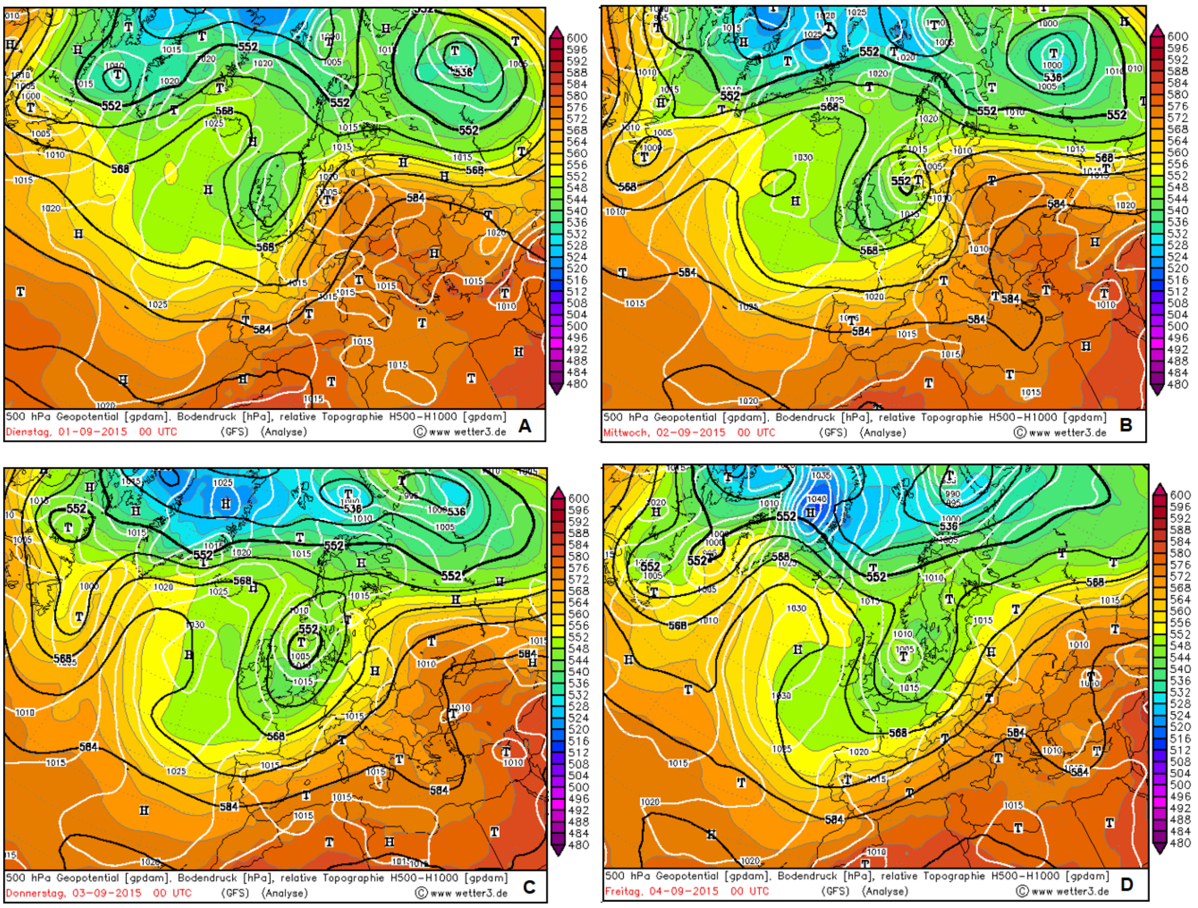

Figure 80: GFS 500 *hPa* geopotential, black curves [*gpdam*] and surface pressure, white curves [*hPa*]. H is high pressure and T is low pressure. 00UTC, 1st of September 2015 (A), 00UTC, 2nd of September 2015 (B), 00UTC, 3rd of September 2015 (C) and 00UTC, 4th of September 2015 (D). [34]

The precipitation episodes, which were registered in Denmark and southern Scandinavia, originated from a low circulation, that increased in strength from 31st of August until 2nd of September in the morning (see figure 81 for full development). Figure 80 shows the course of the low circulation, which can be divided into 3 phases.

In the first phase, the low is located on the warm air side of the upper jet in the troposphere (80A). The low circulation is located over northern Germany around Schleswig. A sounding from Schleswig (figure 84A, p. 82) shows a relatively warm and humid air mass with a high tropopause. A frontal zone is located across Denmark (see water vapor figure 82A). There is also a relatively large distance from the low to the jet core which lies across Great Britain and bends anticyclonally over Central Scandinavia and ends up at southern Finland, figure 85A (p. 83). Phase one can be called the start of a deepening period of the low, which is also shown in figure 81.

The sequences in figure 80 and 85 show how the jet axis in the upper troposphere moves to the east, while the low moves to the northwest. There is thus a change in the location of the low in relation to the jet stream which can be described as phase 2. The low moves into the jet stream sometime during the evening, 1st of September (in figure 80B, the crossing has just happened). The small bump in the graph in figure 81 is a signal that the low is beginning to cross the jet stream axis and is now continuing into its maximum deepening period. During the maximum deepening period which lasts until 06UTC 2nd of September, the low moves under the trough axis and the jet axis is now on the east side of the low. During the deepening period, the low creates a characteristic spiral pattern (see figure 82A).

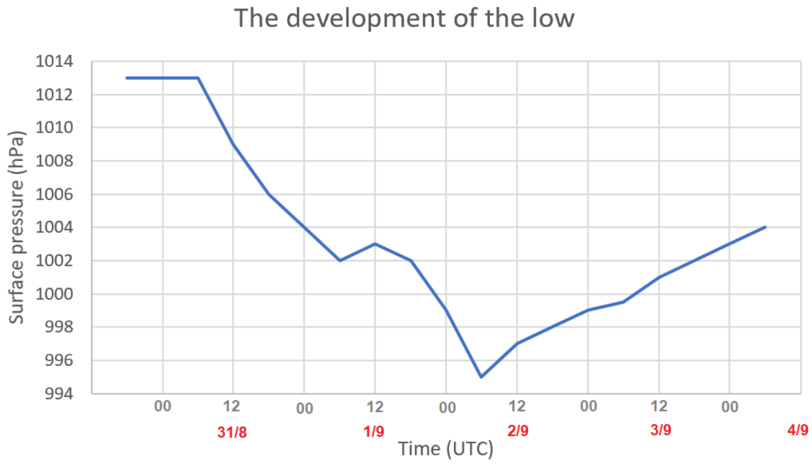

Figure 81: Graph showing the development of the low that dominated the weather in the southern Scandinavia. The pressure values are center air pressure at sea level (hPa). [49]

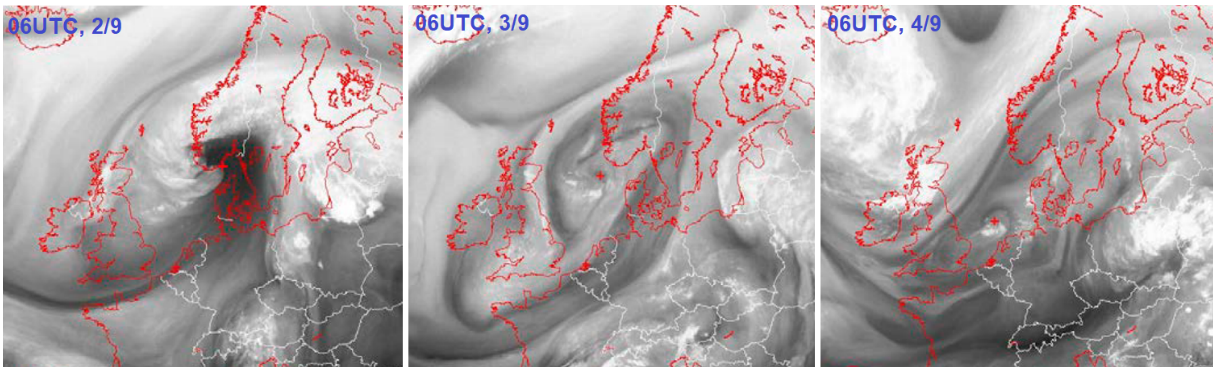

Figure 82: Water vapour images, channel 5, from the geostationary MSG satellite. White colours is water vapour and darker areas are drier. 06UTC, 2nd of September 2015 (A), 06UTC, 3rd of September 2015 (B) and 06UTC, 4th of September 2015 (C). [49]

In phase 3 (figure 80D), the low is now on the cold cyclonic side of the jet core in the left exit area of the jet which is a characteristic of extratopical cyclones as indicated in the analysis of case 2 (see appendix F and G for jet streaks and extratopical cyclones). At this point, the low has been under filling for about 2 days according to figure 81. In phase 3, the low has moved a short distance from southern Norway to the south of the North Sea. Throughout the phase, the low circulation ensures that the atmosphere is homogeneous and almost equalizes the amount of water vapor in the atmosphere (see figure 82C). The frontal zone that previously lay across Denmark on 31st of August has almost disintegrated, where the warm and free air has now been mixed with the dry and cool air. Each phase has its own precipitation events, where the cloudburst in Copenhagen takes place in phase 3.

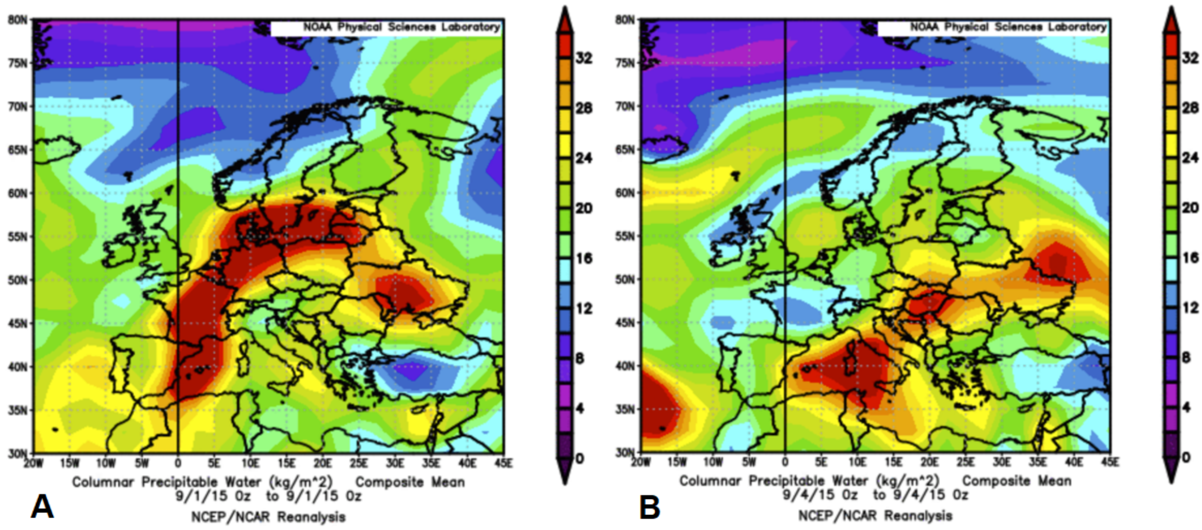

Figure 83: Columnar precipitable water, composite mean in the units of kg/m^2, 1st of September 2015, 00UTC (A) and 4th of September 2015, 00UTC (B). [35]

Figure 83 shows PW values for 1st of September, 00UTC and 4th of September, 00UTC, resp. which support evident from the water vapor images. In figure 83A, there is a large difference in PW across the frontal zone. In the warm air, the PW values are somewhat higher than they are on the cold side of the frontal zone.
In figure 83B, there is a slight difference and PW is almost equalized. From being two different air masses in the deepening phase, the low circulation in the filling phase has now ensured that the air mass is homogeneous with significantly lower PW values. The lower values of PW are a result of mixture of warm and humid air with cold and dry air.
In a low circulation like this, the most favorable conditions for cloudbursts are downstream of the trough where there is ascent of air. In the filling phase, the low has a vertical temperature profile that is almost moisture diabatic as the sounding from Schleswig (figure 84) indicates.
There is no sounding close to Copenhagen on this day, which makes an analysis considerably more challenging, but the sounding from Schleswig on 4th of September, 00UTC, figure 84B, it strikingly similar to the sounding that represented Schleswig from 2014, figure 76. The dew point and surface temperature are quite similar, where in the sounding from 2015 it is 9°C and 10°C resp. The course of the temperature profiles is almost the same, as is the dew point. The most remarkable difference is a dry intrusion around 450 hPa in the sounding from 2015. It is a light wind shear in both cases, where 0-6 km wind shear in 2015 is around 10 m/s (indicate the possibility of multicells, see figure 7) while the wind at the tropopause is around 15 m/s. This weak wind shear may as noted be a contributing reason to why the showers over Copenhagen became so strong as noted in the analysis of case 5.
Of the indices from the method section, only the TOTL-index indicates that there may be scattered thunder cells during the day. The others report a stable troposphere with no CAPE, so the Schleswig sounding does not appear to say anything about how the preconditions for the formation of cloudbursts are present in Copenhagen this morning.

In the satellite images from EUMETSAT's visible channel 0.6 μm, figure 87 (p. 85), it can be seen from the sequence that the showers in the green ring are formed over the Øresund region before they move to Sweden around 08UTC. Furthermore, the location of the low is located in the North Sea, where the spiral pattern is felt. There are no fronts close to Denmark. It also appears that the formation of the showers is under very local conditions. The only other places where heavy rain were formed, without registered cloudbursts are in Kattegat and in the western part of Jylland around Esbjerg on this day. This area is seen as a greater radar reflectivity in figure 89 (p. 87), but also with higher content of water vapour than in Copenhagen in figure 82C. The same area is also brushed out as the orange ring in the satellite images in figure 87. The area is almost an extension of the spiral of the low circulation. At first, it seems that it is more powerful than in Copenhagen, but the intensity was actually strongest in Copenhagen this morning.

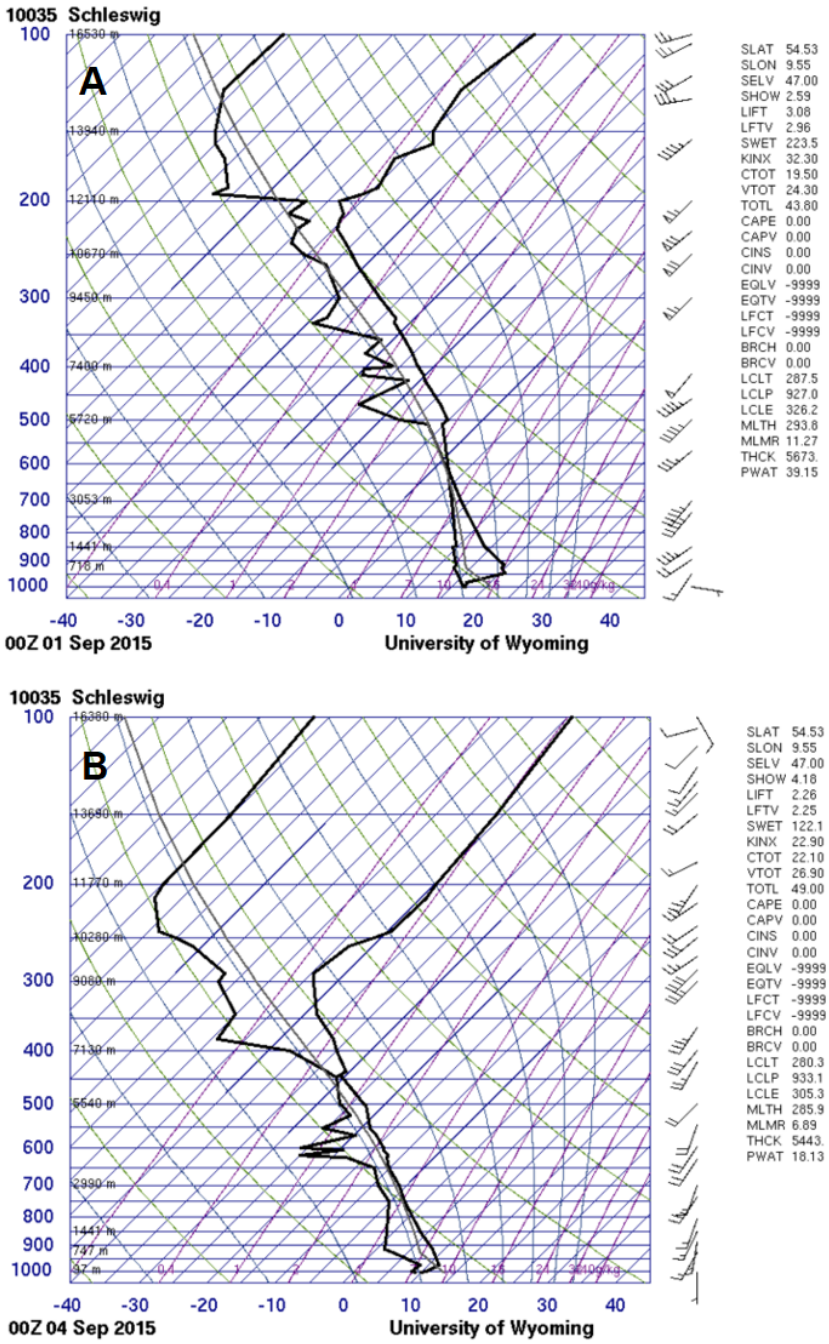

Figure 84: Sounding from Schleswig, Germany, 00UTC, 1st of September 2015 (A) and 00UTC, 4th of September 2015 (B). Same description as figure 39. [36]

According to SVK, Esbjerg had a single extreme rain event (rain uninterrupted) at Esbjerg Renseanlæg of 69 mm for several hours, where no cloudburst intensity were recorded under this event at no time. It was however in Copenhagen. 4 measurements from the capital are in the top 10 for the most intense measurements of 2015. This applies to 28.67 $\mu m/s$ at Hellerup Cemetery, 27.00 $\mu m/s$ at Lygten, 25.67 $\mu m/s$ at Delfinen and 25.33 $\mu m/s$ at Søborg Vandværk. Hellerup had the highest intensity, having measured a double cloudburst.

Figure 86 might explain the circumstances of the heavy rainfall events is. 850 hPa temperature advection (A) and 500 hPa vorticity advection (B) are shown here. This morning in 2015 there

was weak warm advection above especially Jylland. The wind at Scleswig supports this as it is veering in the sounding in figure 84B. The heavy rain at Esbjerg could have developed due to rising air during warm advection according to the qausi-geostrophic omega equation (14).
In Copenhagen, on the other hand, it is more on the border between cold advection and warm advection. It looks like there is slight cold advection, which could indicate that the wind is backing with the altitude as stated in the theory in section 2.3.1 - e.g. in relation with a weak cold front.
In figure 86B, there is a weak PVA at both locations which may indicate that there is an upper level divergence and thus rising air at the surface (described in section 2.2.3). The highest PVA values are found above Copenhagen, which may be a contributing factor to the intensities in Copenhagen becoming stronger than in Esbjerg. This means that at Copenhagen there is the possibility of convergence and thus the rising of air, which may have been the necessary trigger for the cloudburst event. At the same time, there are many indications that the water off Køge Bay has once again been an important initiator as in case 5.

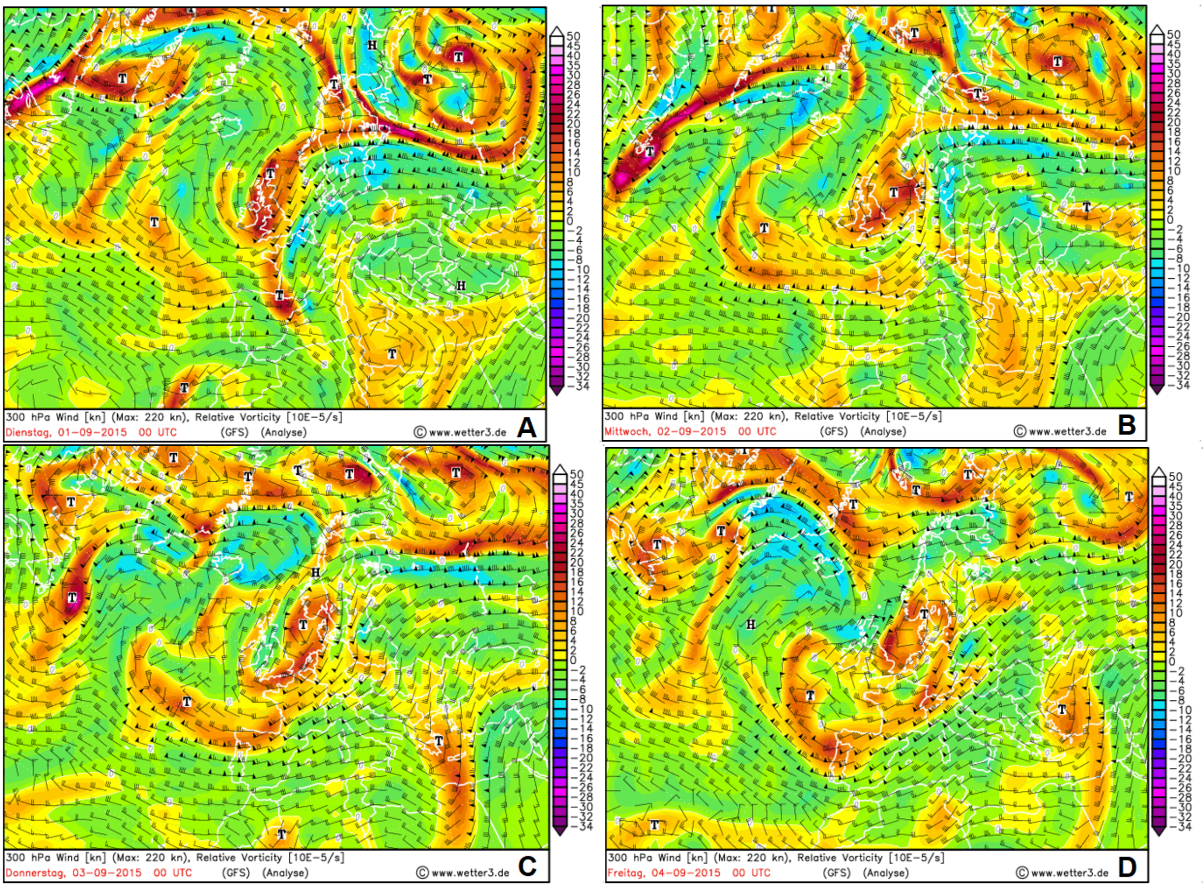

Figure 85: GFS 300 hPa wind [kn] and relative vorticity [$10^{-5}s^{-1}$]. H is high pressure and T is low pressure. 00UTC, 1st of September (A), 00UTC, 2nd of September (B), 00UTC, 3rd of September (C) and 00UTC, 4th of September (D). [34]

The satellite images are supported by the radar images in figure 88, which show reflectivity in the period from 05.25UTC where the first showers are formed until 09.05UTC when the showers are drawn over Sweden. The radar images have similarities with the cloudburst in 2014. The first cells appeared west of Copenhagen and moved north and northeast across the central part of the capital. Furthermore, it is noted that in both cases showers are formed in an area extending from Amager to Møn which once again resembles a convergence line in the

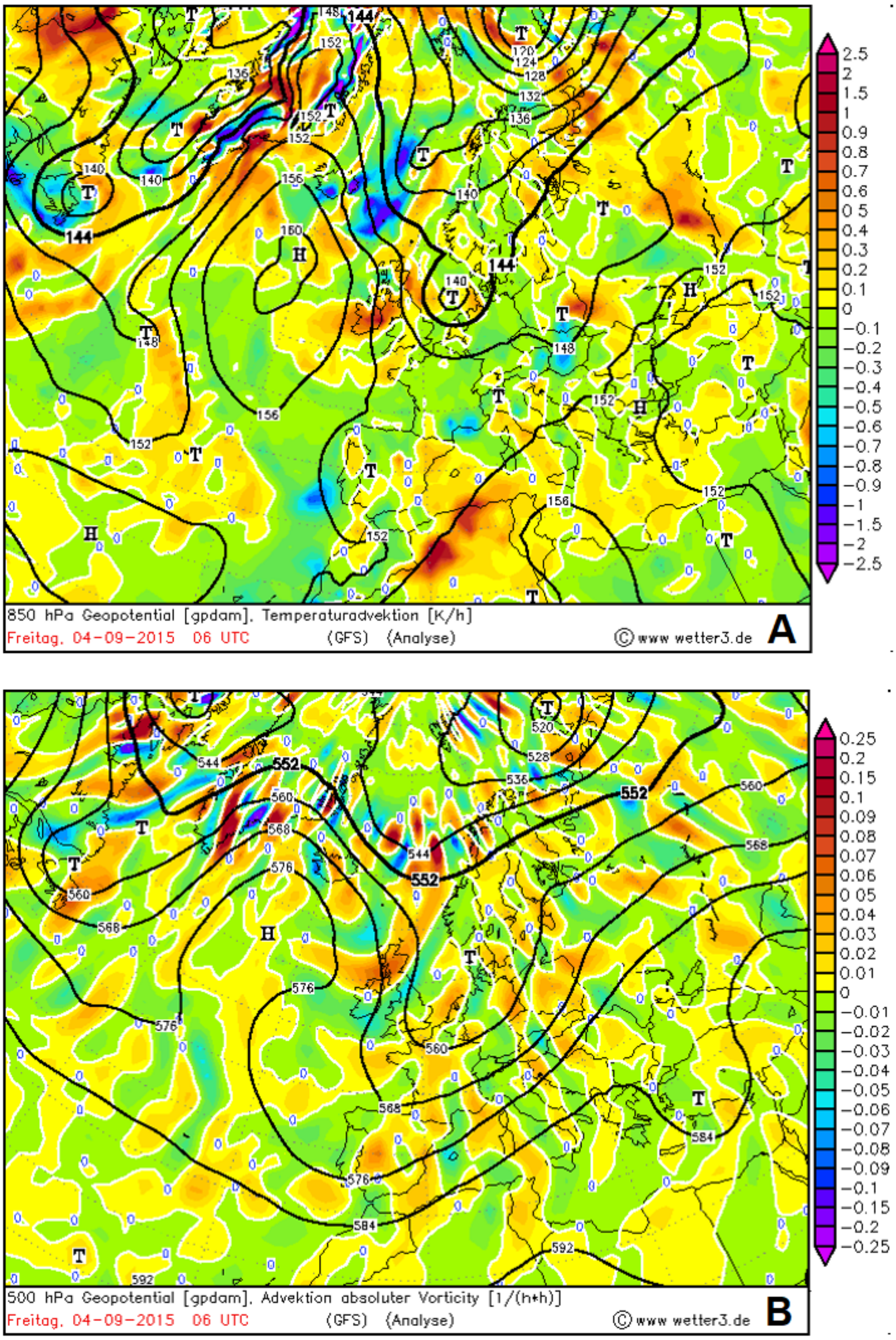

Figure 86: GFS 850 *hPa* geopotential, black curves [*gpdm*] and temperature advection, 06UTC, 4th of September 2015 (A) and absolute vorticity advection, 06UTC, 4th of September 2015 (B). H is high pressure and T is low pressure. [34]

same area. In both cases, the precipitation area drifted over Malmö and Skåne.
The most significant difference between the two cloudbursts is the duration. The cloudburst in 2014 had a duration of about 3 hours from approximately 22.55UTC to 01.55UTC, while the cloudburst in 2015 only has a duration of give or take 1 hour. For case 5, new cells were formed upstream of older cells in a reverse wind shear. That does not seem to be the case for the 2015 case where new cells, according to figure 8 in section 2.3.1, must be formed in a forward wind shear. However, the cloudburst was severe. An official measurement from DMI measured

34.7 *mm* in 22 minutes between 07UTC and 08UTC. An intensity that is more than twice the defined intensity (15 *mm* / 30 min) for a cloudburst in Denmark. Another difference is that the cloudburst in 2014 took place at night, while the one in 2015 took place in the morning.

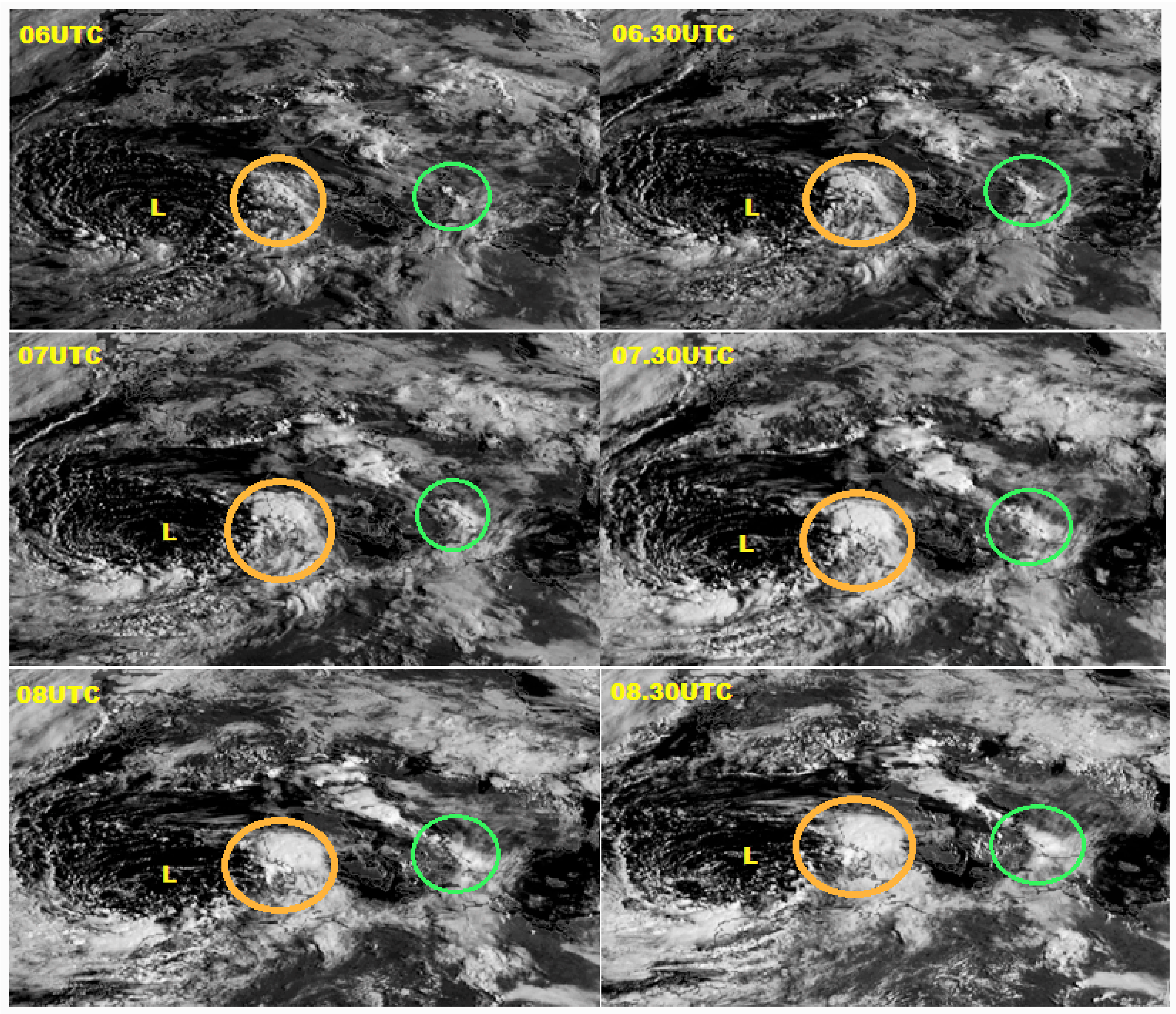

Figure 87: HRI Level 1.5 Image Data - MSG - 0 degree, EUMETSAT [31]. Visible, channel 0.6 μm. 04 Septebmer 2015, 06UTC to 08.30UTC. The analysis are based on 15 minute intervals - in the figure are the intervals 30 min. The green ring is the location of Copenhagen and the cloudburst area and the orange ring is the extreme rain above Esbjerg. A low is marked by the "L".

In Figure 90 (p. 87), CAPE from the GFS model is shown for 06UTC, 4th of September. It immediately shows there is some CAPE in the area above Copenhagen that may have given a sufficiently unstable troposphere. The CAPE values agrees with the sounding from Schleswig in figure 84 with no CAPE values. On the contraryis the CAPE values in Copenhagen at the given time is approximately 200 Jkg^{-1}. A sounding from Greifswald, in northern Germany, 12UTC, figure 91, actually has a similar amount of CAPE. Around noon the same day as the cloudburst, heavy showers formed southeast of Greifswald, which lies in a line that reaches the southern Sweden with the showers that previously ravaged Copenhagen. It is not inconceivable that the air mass in Copenhagen may have resembled the air mass in Greifswald. In the sounding, there is only a very small value of CIN, which might mean that the showers can be formed spontaneously. The convective temperature in the sounding is around 18°C. It does not take much for showers to form if air temperature is rising. A moderate 0-6 *km* wind shear of about 15 m/s gives indications that multicells can form (see figure 7), while for the entire troposphere there is a wind shear of about 20 m/s. LCL is present at an altitude of 900 hPa while LFC is at around 890 hPa. EL is at an altitude around 470 hPa, which is a little distance from the tropopause at around 250 hPa. Just like 2014 as well was a distance away. The indexes in Greifswald indicate a marginally unstable troposphere with widely scattered thunder cells. Hypothetically, a sounding in Copenhagen could have looked like this in Greifswald.

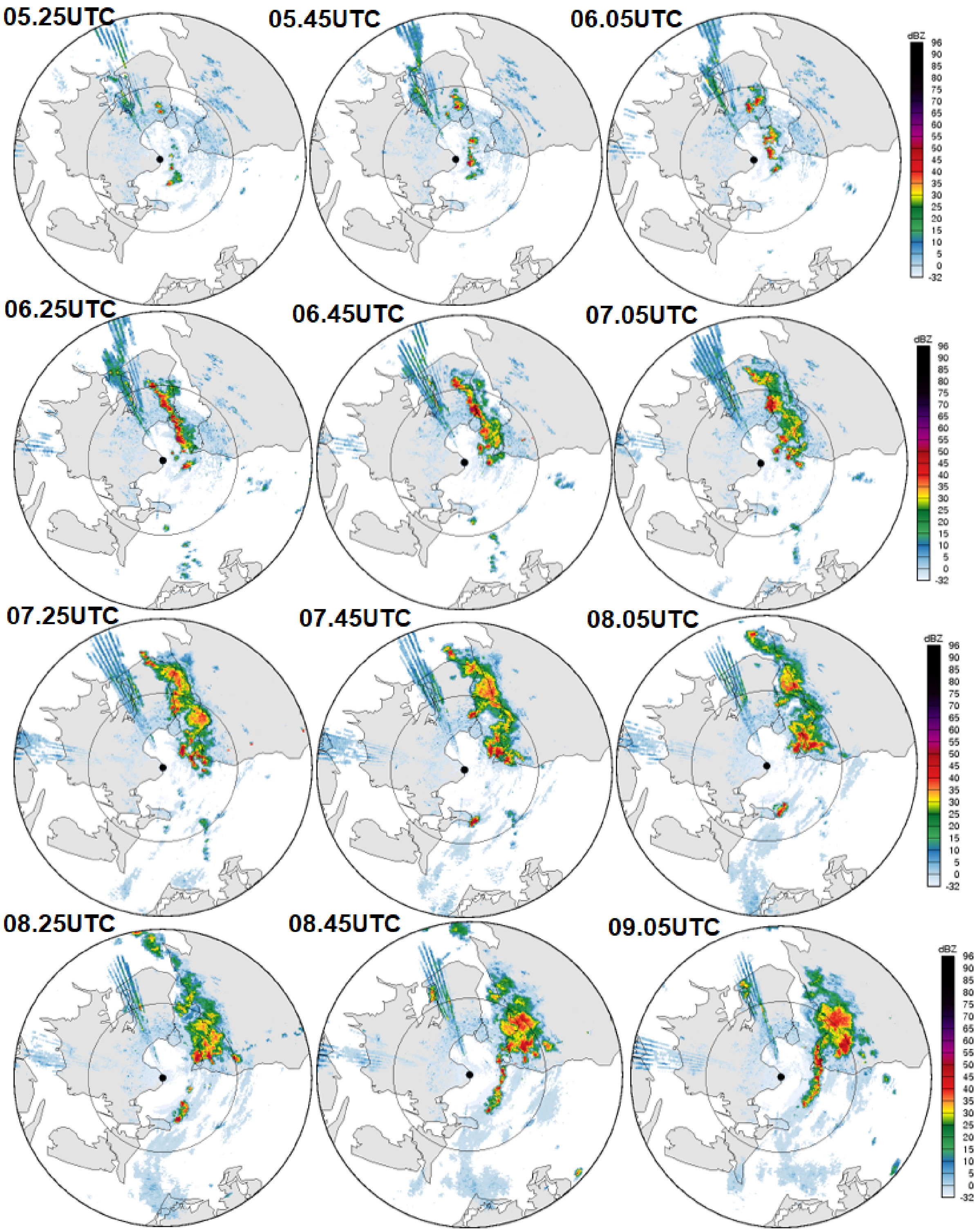

Figure 88: Reflectivity (dBZ) from the radar at Stevns in the period 05.25UTC to 09.05UTC 4th of September 2015. The radar images are generated by Thomas Bøvith, DMI.

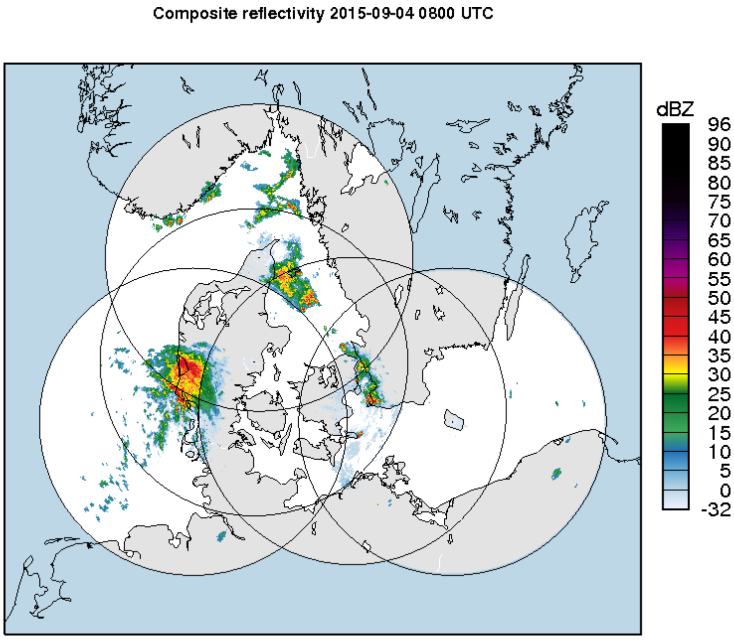

Figure 89: Reflectivity (dBZ) from the Danish radar network 08UTC 4th of September 2015. The radar image are generated by Thomas Bøvith, DMI.

It can be assumed, as in the case from 2014, that there have been local trends that led to forming of cloudbursts over Copenhagen this early autumn. This case shows a greater low circulation during deepening on the anticyclonic side of the jet stream and later during filling in the North Sea on the cyclonic side of the jet stream. Here strong showers were formed downstream in the filling phase. It resembles a multicell system, but where the showers were not formed upstream on the gust front of the old cells as the system was relatively fast. Since the propagation vector and the cell motion vector (see figure 21 for the idea behind these vectors) have had the same direction related to a forward wind shear. But despite that, there was a heavy cloudburst event several places over Copenhagen this autumn day.

This cloudburst is an example that cloudbursts in certain circumstances can occur in a low pressure during filling, which is otherwise mostly seen in winter, and that cloudbursts often happen very locally. Based on radar images, it was assumed that the heaviest precipitation was measured at Esbjerg due to warm advection, but it turns out that cloudburst intensity was only measured at Copenhagen, which can be attributed to CAPE and PVA, but also a weak wind shear in the troposphere.

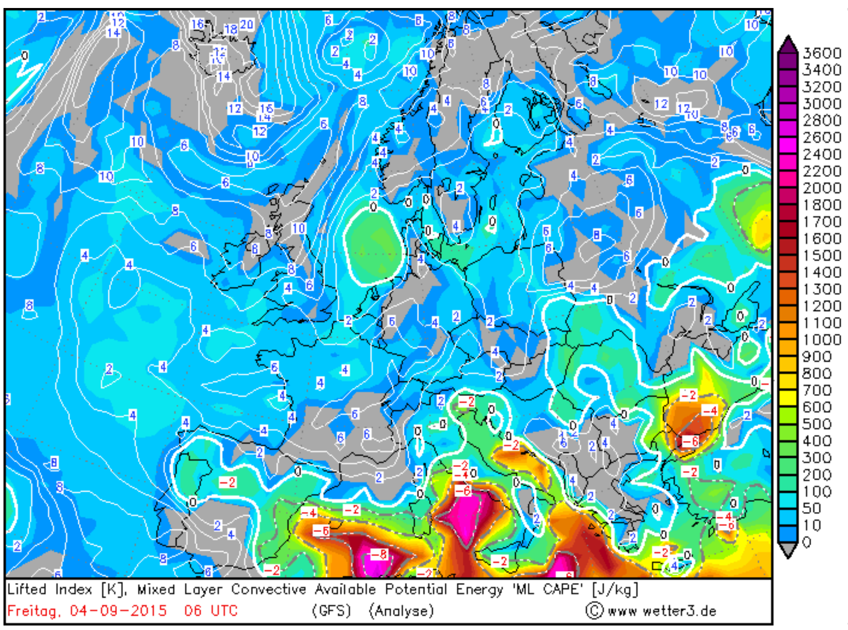

Figure 90: GFS CAPE [Jkg^{-1}] and lifted index [k]. 06UTC, 4th of September 2015. [34]

In addition, the cloudburst in 2015 differs from the other cloudbursts. Where the 6 other cases happen during the afternoon and late evening, this cloudburst event happens in the morning - and as the only one in September. In the table in appendix C of the strongest cloudbursts registered by SVK in Denmark in the period 1984-2019, there are only two that fall outside the summer months - one in May and one in September (see figure 32).

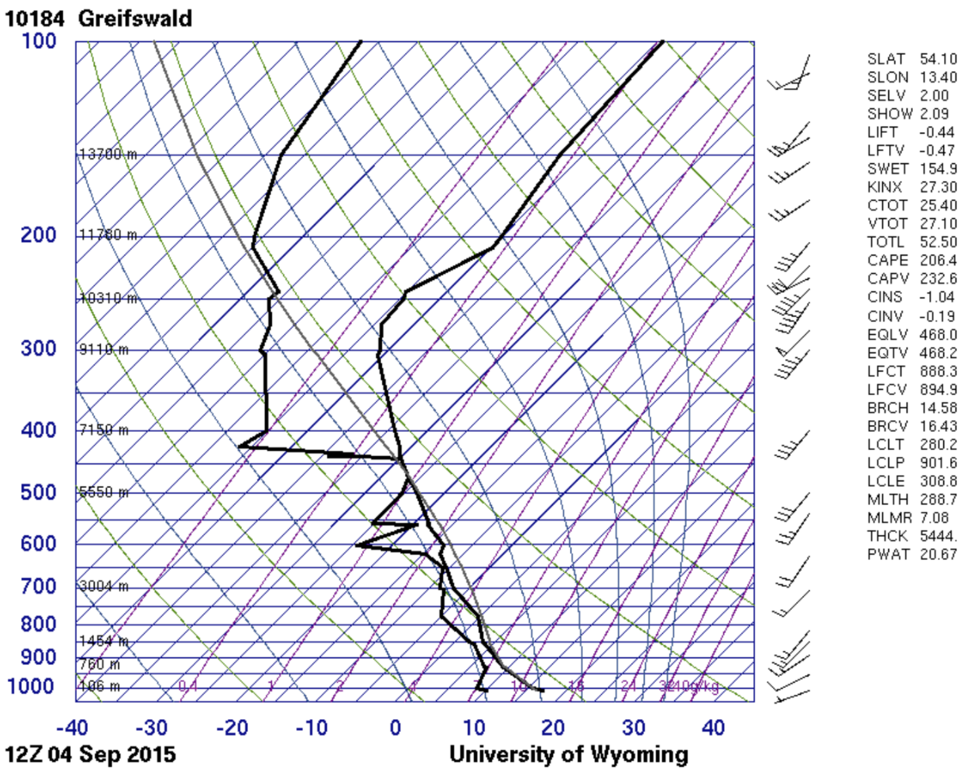

Figure 91: Sounding from Greifswald, Germany, 12UTC, 4th of September 2015. Same desription as figure 39. [36]

Unfortunately, it is probably impossible to pinpoint the exact circumstances for the cloudburst in 2015, as well as in 2014, when the lack of soundings makes it difficult to describe the right circumstances, but there has probably been - just like in 2014 - a convergence line and orographic conditions, such like the land/sea distribution for Copenhagen, that have caused cloudburst events this morning to occur.

Overall, the same low circulation causes a series of incidents in both Holbæk on the 31st of August, floods in southern Norway as well as the heavy rain in Jylland and the cloudburst in Copenhagen on 4th of September.

5.7 Case 7: 14th of June 2019, the Tornado in Aabenraa, 14.30UTC

On Friday 14th of June 2019, Denmark was hit by a severe thunderstorm that swept over large parts of the country. Especially one place in the country, the situation developed into something that is very rare in Denmark. In a parking lot at Aabenraa Hospital, cars were reported to have flipped. The messages sounded on a landspout, but previous analyses describe this phenomenon as a real tornado [13] [22].

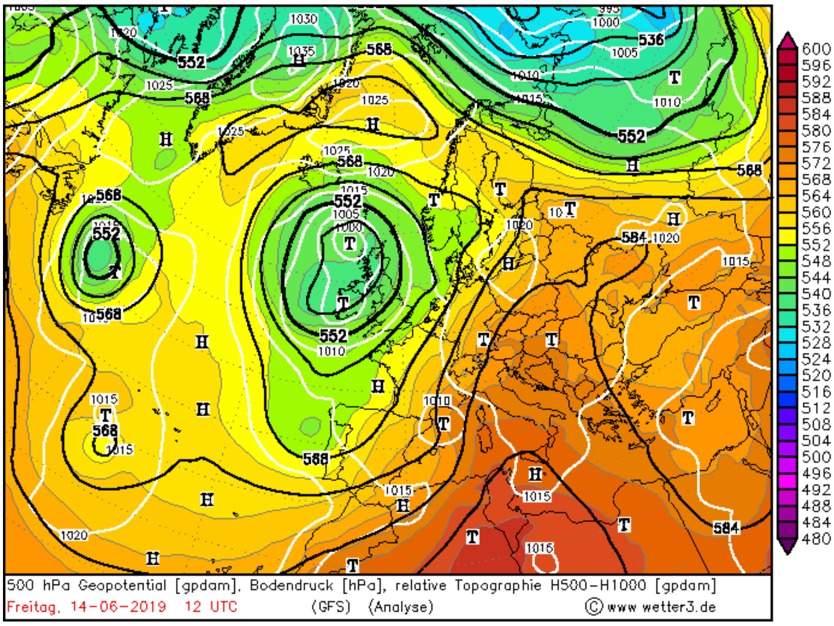

Figure 92: GFS 500 hPa geopotential, black curves [$gpdam$] and surface pressure, white curves [hPa]. H is high pressure and T is low pressure. 12UTC, 14th of June 2019. [34]

The weather map from 14th of June, 12UTC, figure 92, shows the weather situation on this summer day. A greater low circulation west of Scotland dominates the weather in northwestern Europe, while a secondary low in the south of France helps to establish a frontal zone marked in the satellite images (figure 94) as a warm front, separating the cool air from the low circulation to the west-northwest and warm air to the southeast. Furthermore, there is a high east of Denmark over the Baltic Sea. Between the two pressure systems, warm and humid air flows from the south and southeast above Denmark, while in the height there is a south-westerly flow which will be described later. The satellite sequence in figure 94 shows cumulonimbus clouds above Denmark to the southwest, which are constrained to the northeast by less convective showers of clouds over Sweden. A high over the Baltic Sea contributes to the fact that the warm air mass has a movement to the northwest, where it collides with the air mass from the low. To the east of the frontal zone, the high forms a cloudless belt, which is replaced even further to the east by unsettled air with numerous CBs, some of them can be sensed rightmost in the satellite images and in appendix H (figure 111).

Figure 93: Screenshot of a video of the tornado taken by Christian Fredsholm.

Figure 94 and the radar image in figure 98 (p. 89) there is shown thunder cells in most of Jylland, but it appears that the potential for cloudbursts is smaller in the northern part of Jylland than in the southern part of Jylland. A hook echo-like structure can be sensed in

Aabenraa in figure 98, where tornadoes are often formed according to [22].
The radar images in figure 97 (p. 92) shows radar images in a 10-minute resolution, with the shower area pulling up from the southwest. From 13.35UTC, the intensity increases in the south-eastern corner of the precipitation field, where the satellite image at 14UTC shows that an anvil[12] is being formed in relation with the cell development in southern Jylland. In the period 14.15UTC to 14.25UTC, the thunder cell almost splits in two and forms, as mentioned before, a hook echo-like structure. The precipitation is heaviest above Aabenraa at 14.35UTC. During this time a tornado was filmed by a motorist, depicted in figure 93. Shortly after, the cell structure is about to disintegrate.

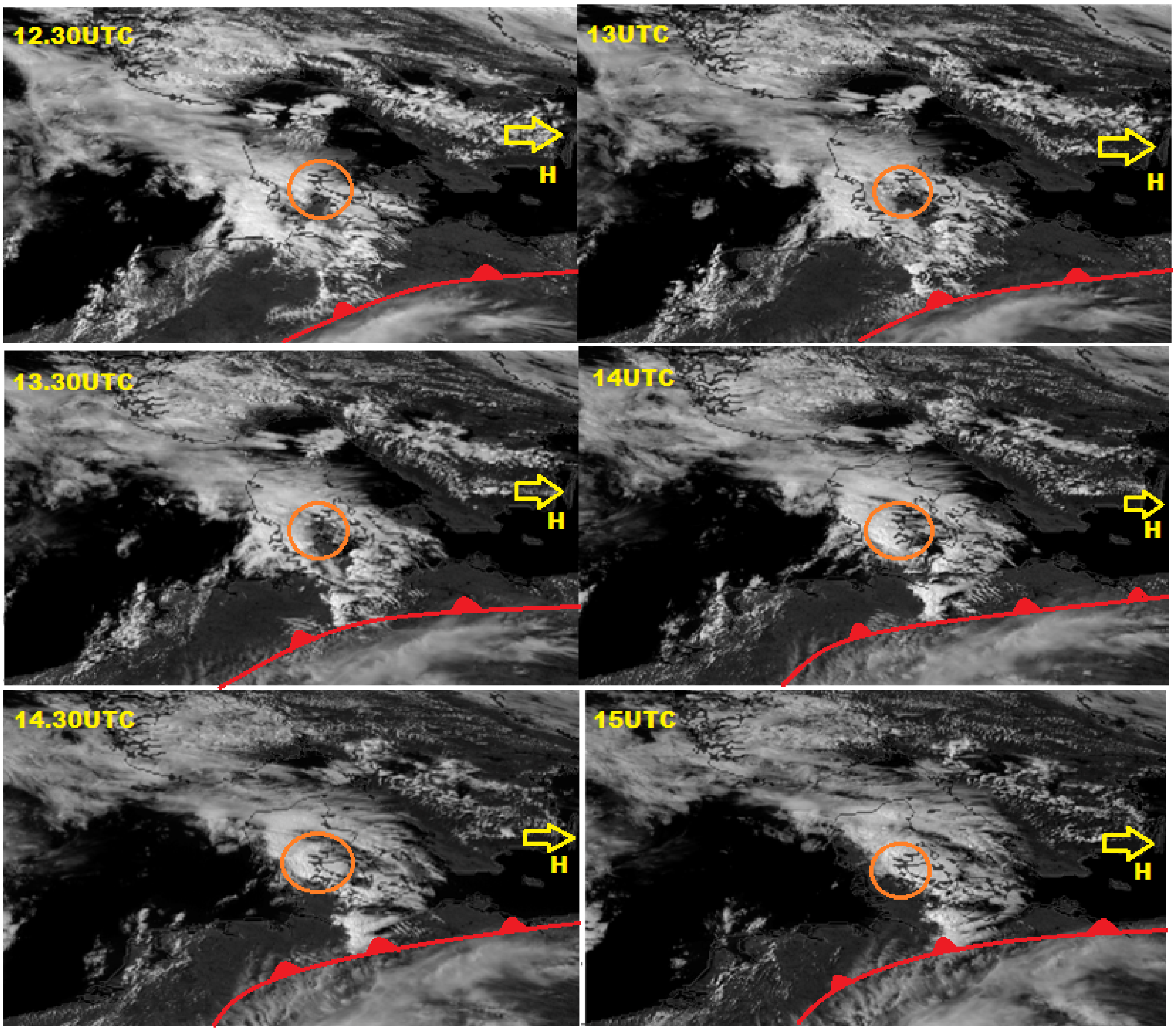

Figure 94: HRI Level 1.5 Image Data - MSG - 0 degree, EUMETSAT [31]. Visible, channel 0.6 μm. 14th of June 2019, 12.30UTC to 15UTC. The analysis is based on 15 minute intervals - in the figure are the intervals 30 min. The orange ring is the location of Aabenraa. A high is marked by the "H", but is found a little bit out of the images indicated by the yellow arrow. The red line are the warm front.

[12]See section 2.3.3 for a description of an anvil

In figure 95, the PW values for 14th of June, 18UTC are shown. The figure shows high values of PW from Germany and over France. That day, there was actually a streak of powerful thunder cells in the area. Meanwhile, radar images also show powerful thunder cells in the eastern Europe in the area with high PW values. Both situations are indicated in figure 111 in appendix H. However, there are not as high values of PW in Denmark. This may be because the air is colder in Denmark due to the colder and drier air from the low circulation above Scotland in figure 92 and thus the air mass must contain less moisture than further south. It can be sensed in figure 95 there is a tongue of humid air above Denmark, while the clear and dry high pressure weather over the Baltic Sea is quite clear, cf. the satellite images. The PW values thus show that there is potential for strong thunder cells to be formed above Denmark this day.

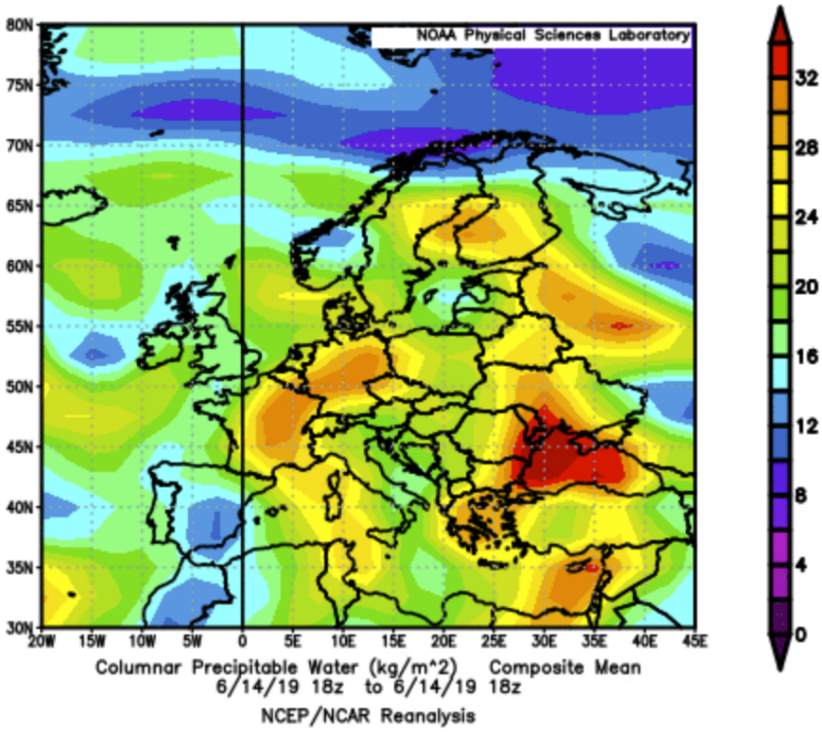

Figure 95: Columnar precipitable water, composite mean in the units of kg/m^2. [35]

Compared to the other cases described in the previous analyses, the precipitation is not as remarkable as when there were no floods or definite damage apart from the cars mentioned in the parking lot. A raingauge from Kliplev registered 10.6 mm measured in 11 minutes (see figure 96), which is actually an intensity equivalent to twice as much as a Danish cloudburst (15 mm in 30 minutes). This shows that there was heavy rain in relation with the thunder cell, but the thunder cell itself was like a ”sprinter”, which did not result in large amounts of precipitation.

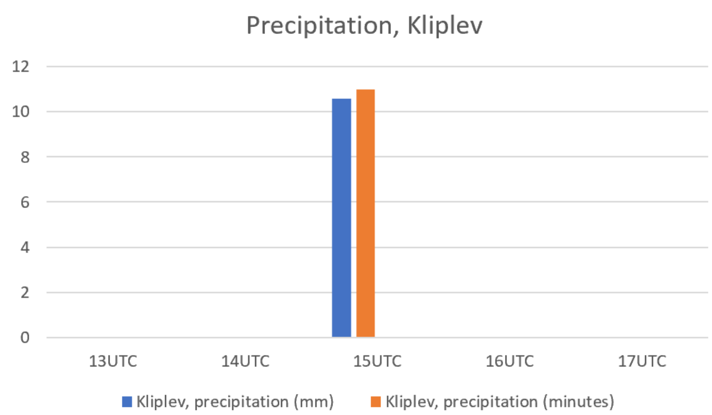

Figure 96: Precipitation (mm), blue bar. Minutes of rain, orange bar. Data: DMI.

Figure 99 (p. 93) depicts a sounding from Schleswig displaying a saturated layer from 700 hPa to 630 hPa before a rapid drying around 630 hPa occurs. It can be argued that the troposphere is convective unstable at that time because the troposphere is dry in the middle layer from 630 hPa to 425 hPa due to the dry intrusion.

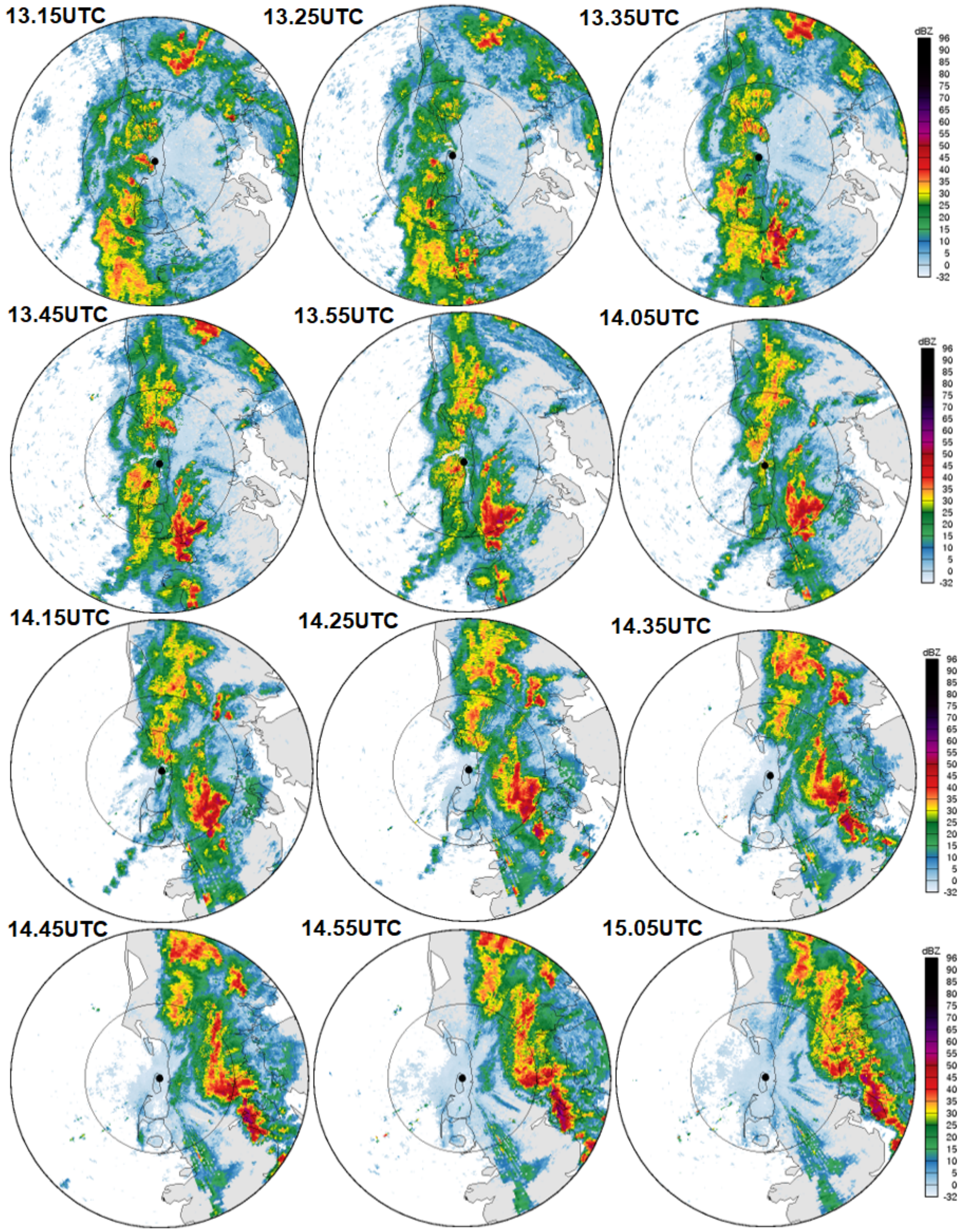

Figure 97: Reflectivity (dBZ) from the radar at Rømø in the period 13.15UTC to 15.05UTC 14th of June 2019. The radar images are generated by Thomas Bøvith, DMI.

The lifting curve for the Schleswig sounding has a surface temperature of 22.8°C, where the LCL is found at 826.8 hPa and the LFC at 729.1 hPa. This means that CIN is a necessity to create the necessary lift according to the theory in section 2.2.3, but at the same time you can see that it does not require much for spontaneous showers to occur in the area, as the convective temperature is around 24°C.

EL is at a height of about 614.4 hPa where a dry intrusion occurs, which in this case does not give much more than cloud tops at an altitude of 4 km.
The indices LIFT, SHOW, KINX and TOTL in fiugre 99 show only a marginal unstable atmosphere with a small chance of the formation of scattered thunder cells. A more pronounced factor in this case is the presence of a significant vertical 0-6 km wind shear of about 23 m/s which meets a necessary condition for the formation of supercells as stated in figure 7. At the same time, the sounding shows that the wind is veering with the height, which indicates the presence of warm advection (see section 2.3.1).

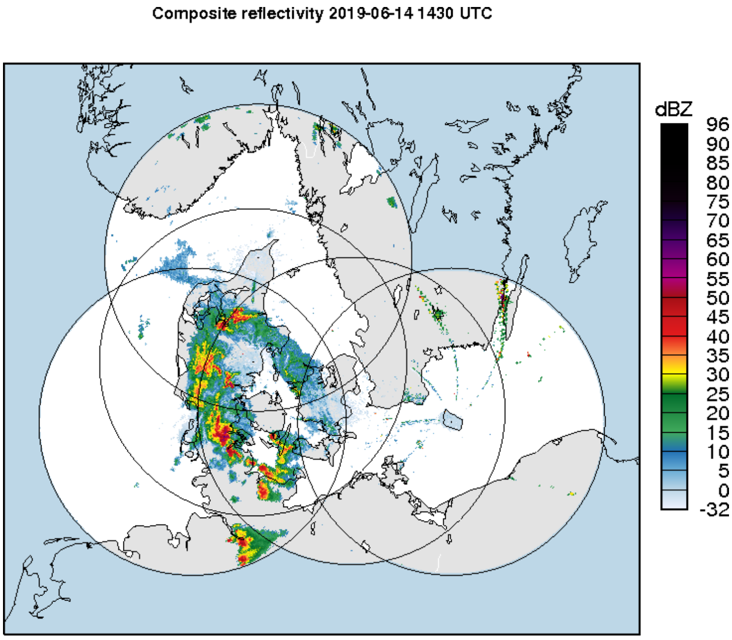

Figure 98: Reflectivity (dBZ) from the Danish radar network, 14.30UTC, 14th of June 2019. The radar image are generated by Thomas Bøvith, DMI.

The total wind shear in the entire troposphere is registered to be between 40 to 45 m/s, which is underlined by figure 100 which shows the forecast for 14UTC for winds in 500 hPa (A) and 300 hPa (B) as well as the air pressure at sea level. In the model, the most significant wind shears are in a band from western Jylland to Schleswig, where the mentioned 23 m/s is the wind speed at 6 km altitude above Schleswig. There is warm advection above Denmark as seen in figure 101, 12UTC. The directional shear that occurs in relation with the warm advection can in special cases lead to the formation of a rotating buoyancy - a mesocyclone [22] which is also described in section 2.3.1.
In figure 100B, there are two currents in particular that are worth noting. One is an elevation trough across the North Sea that is upstream of the large low circulation over Scotland (figure 92) and through extends southeast to the northern Germany.

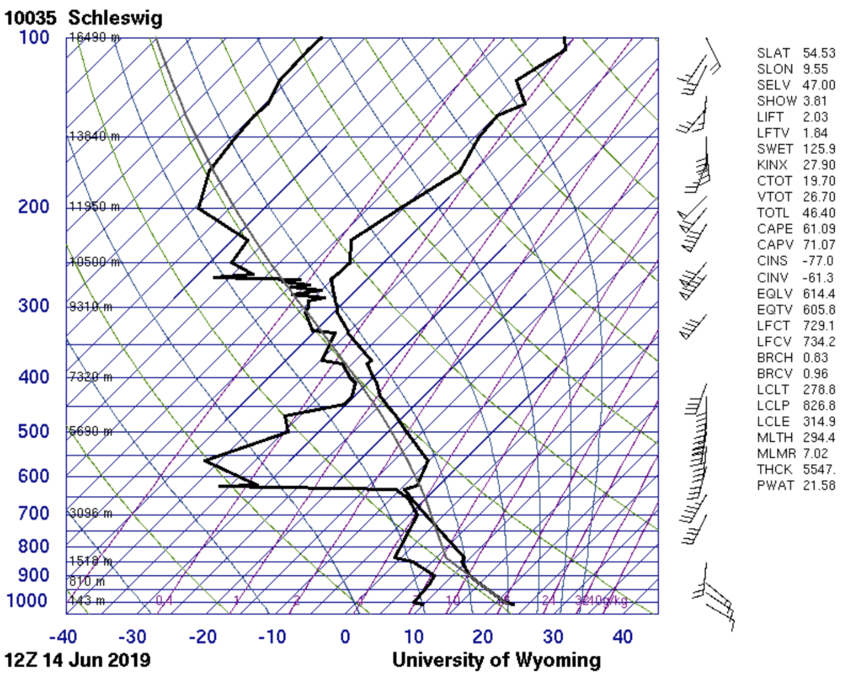

Figure 99: Sounding from Schleswig, 12UTC, 14th of June 2019. Same description as figure 39. [36]

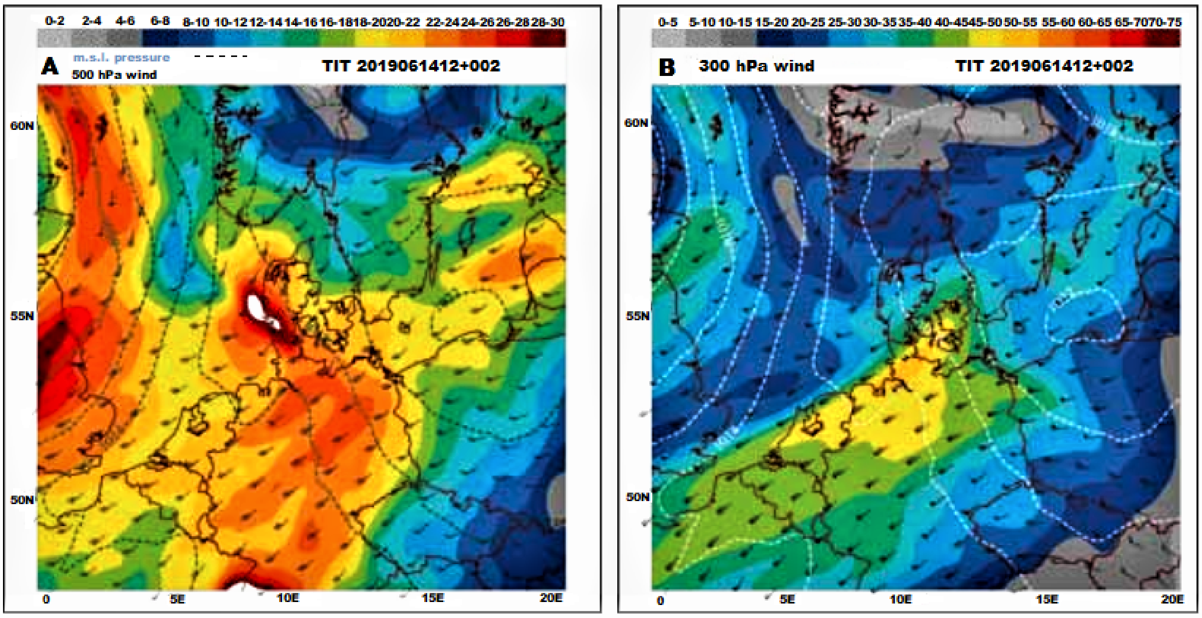

Figure 100: (A) Forecast 14UTC from the weather model TIT, 14th of June 2019. Dotted lines show air pressure at sea level with 2 hPa intervals. The colors show wind in 500 hPa and wind barbs are WMO standard. (B) As figure A but for 300 hPa. [13]

The second is a jet streak that stretches from the North Sea coast of the Netherlands to Sjælland with a wind maximum over the northern part of Germany. The mentioned wind maximum seen in A is located downstream of the axis of the ridge. In both the height trough and the jet streak, the wind is sheared more than 20 m/s - which characterizes the formation of supercells (figure 7).

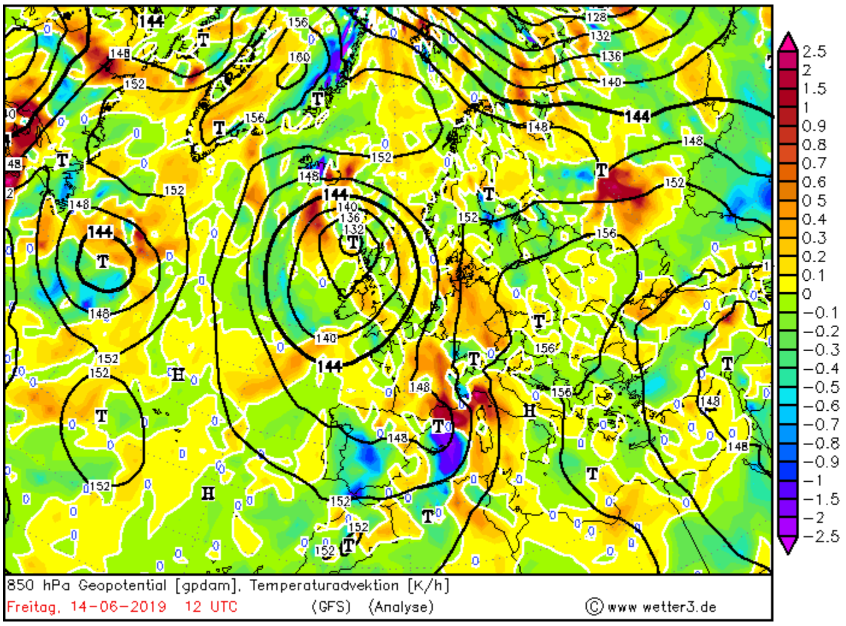

Figure 101: GFS 850 hPa geopotential [$gpdam$] and temperature advection. H is high pressure and T is low pressure. 12UTC, 14th of June 2019. [34]

Figure 102 shows the relative vorticity in 300 hPa, where relative vorticity values higher than 2 indicate stratospheric air. It means that the trough is probably located around the tropopause or in the stratosphere. In addition, around the jet axis figure 100B there is a shift from stratospheric air on the north side to tropospheric air on the south side of the jet axis. The dry intrusion from the Schleswig sounding is probably of stratospheric origin in relation with a tropopause fold.

A cross section perpendicular to the jet axis in figure 103 from an analysis made by Niels Woetmann Nielsen [13] confirms this hypothesis of a tropopause fold. In figure 103 the tropopause fold is seen as the blue area that is dry and cold air from the stratosphere that penetrates into the troposphere, where the tropopause can be described as the boundary between blue and yellow. The jet core is seen at 300 hPa at a speed of 51 m/s around 54.25N and 10.38E. It appears that the troposphere is lower in the trough to the left of the jet core than to the right of the jet core, where the troposphere is considerably deeper due to a warmer air mass.

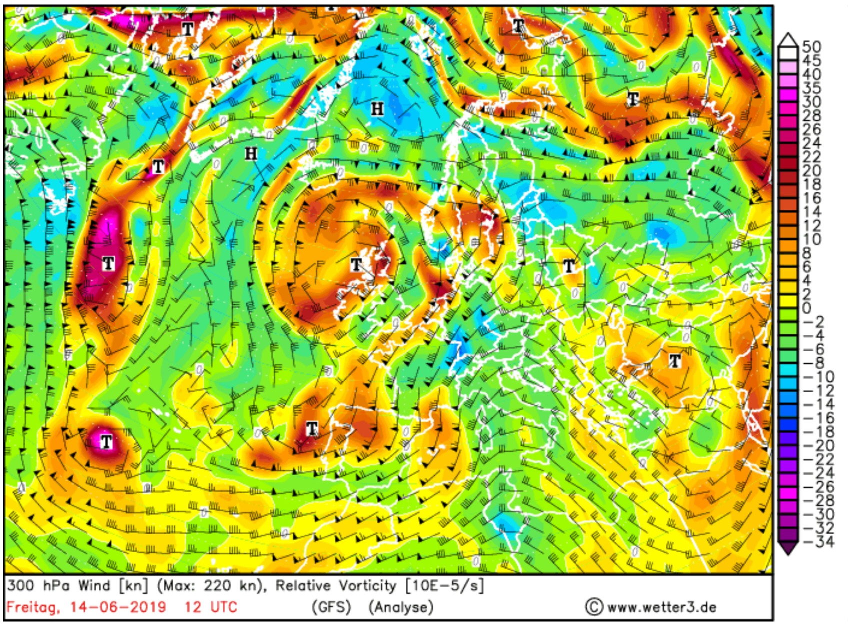

Figure 102: GFS 300 hPa wind [kn] and relative vorticity [$10^{-5}s^{-1}$]. H is high pressure and T is low pressure. 14th of June 2019, 12UTC, 1st of September [13]

The fact that a tornado was formed, cf. the eyewitness account in figure 93, emphasizes that it may be that a supercell was formed over Denmark on this summer day. The collision of warm and humid air form southeast and dry and cold air from west, provided favorable conditions for an unstable air mass with the possibility of strong thunder cells over Denmark and where a jet streak was formed on the jet stream axis in the boundary zone of the two air masses. The largest chance for the development of a supercell was in the left exit area of the jet streak in the southern part pf Jylland, where a dynamic lift in the form of low level warm advection, relatively high PW-values and a strong vertical wind shear have been contributing factors to the formation of what was probably a low-topped supercell. The radar images makes the developmental stage of a low-topped supercell likely to be in the left exit area of the jet streak and furthermore shown a hook echo like structure, which is characteristic of supercells. A low-topped supercell is a miniature ver-

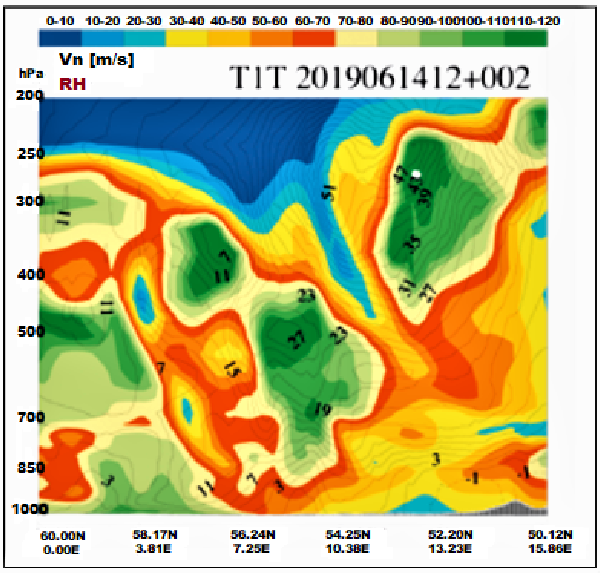

Figure 103: Forecast 14UTC from the weather model TIT, 14th of June 2019. A vertical cross section perpendicular to the jet axis at 300 hPa. Shows the relative humidity (colors) in %. The wind component is perpendicular to the cross section in 2 m/s intervals. [13]

sion of supercells as seen in the USA and where the cloud top does not reach the same height due to a lower troposphere, see section 2.3.4 for a more detailed description of low-topped supercells. The EL in the sounding in figure 99 underlines this statement, where the EL is at a height of approximately 4 km and cut off the buoyancy and then give a low-topped supercell. Due to a strong vertical wind shear over the southern parts of Denmark is likely that a tornado (see section 2.4.1 for the theoretical background for tornadoes in a strong wind shear) has been able to develop in a low-topped supercell. In figure 93, a photo of a rotating trunk is shown at the same time as heavy precipitation in the supercell. Therefore, it is highly probable that there was a mesocyclonic tornado in Aabenraa, which is an extremely rare case in Denmark. This tornado event is included in the analysis due to the cloudburst intensity in figure 96 - despite the more sparse amounts of precipitation.

6 Discussions and Conclusions

The analysis of section 5 shows that cloudburst events in Denmark do not always occur under the same conditions. Local conditions are often the decisive trigger for cloudburst. Nevertheless, there are in the analysis some common characteristic for cloudburst formation in Denmark. Including the instability in the troposphere, the amount of water vapor in the troposphere and quasi-geostrophic forcing.
All cases are phenomena in the summer season primarily due to the higher content of water vapor and high temperature differences up through the troposphere. The high water vapor content, represented by high PW-values in the analysis, provides better conditions for the formation of convective clouds and subsequently cloudburst. The trends of table 3 in appendix C with the 43 most powerful cloudbursts in Denmark from SVK, show that heavy rainfall in Denmark is associated with the summer season. This agrees with figure 32 that shows that there is a predominance of cloudbursts in June to August, with May and September on the flanks and where August has the most cases.
Typically, cloudbursts in Denmark occur in the late afternoon or evening hours due to the phase shift. This means that as the sun rises higher in the sky, the showers can start to bloom due to convection, and then reach maximum intensity at the end of the day. A cloudburst will typically occur in relation with two different air masses. From the case analysis, we can see that in Denmark this is happen with warm and humid air (associated with high values of CAPE) from east and southeast due to a high pressure system over the eastern part of Europe, and a flow from the North Sea with cold and dry air coupled with a low pressure system on synoptic plane. The transition zone between the cold air mass from the through and the warm air mass from the ridge is associated with potential or conditional instability in the troposphere. The instability in combination with quasi-geostrophic forcing such like differential advection of relative vorticity, warm advection, diabatic heating, jet streaks or/and orography forcing are favorable triggering parameters for cloudbursts in Denmark.
Thus cloudburst events are formed in the boundary zone between the air masses, i.e. the cloudbursts seem to organize themselves in bands in the warm air along frontal zones, including convergence zones which is also an option cf. case 5 or in the WCB in case 2. These frontal zones occur in most of the cases in connection with a low pressure west of Denmark, which during deepening creates favorable conditions for thunder cells to develop downstream of the trough.
Once the cells are formed, the wind conditions play a decisive role in how the cells move and in how severe the rainfall is. A classic example is case 4, when the cells were almost stationary over Copenhagen due to a reverse wind shear. Also case 5 and 6, which in many aspects are similar to each other with a presumably orographic forcing with the land/sea distribution and the showers were formed out over the sea off Køge Bay and along a convergence line drifted over Copenhagen. However, they became very different in time, as a reverse wind shear made the system almost stationary across Øresund in case 4, while it drifted faster in case 5 due to a forward wind shear.
Case 6 is different from the others, as this one occurs in the morning. The fact that there are generally more cloudburst events in the afternoon is because the temperature in the afternoon hours more easily reaches the convective temperature and thus there is a greater probability that cloudbursts can occur spontaneously.

In addition, the cases confirm that severe rainfall events require a moderate to strong wind shear according to figure 7, with the strongest events in Denmark on the border between a moderate wind shear and a strong wind shear. The only low-topped supercell in the thesis in case 7 in the southern part of Jylland was formed during a strong wind shear along a triggered jet streak. This case shows that a strong wind shear provides favorable conditions for tornadoes to form, which is what the theory tell us in section 2.4.1.
The connection between the various events is thus a moderate wind shear that helps forming multicell systems which can be stationary under the right conditions, including wind conditions (reverse wind shear) in combinations with forcings and then cause thunder cells with cloudburst intensity. Incidentally, none of the cases were designated as a single cell.
Copenhagen and southern Jylland looks like two particularly vulnerable places due to the location of the 7 cases. It must be noted here that e.g. in Copenhagen there is a much larger network of raingauges that can distort the picture, but looking at the climate atlas from DMI, which will be briefly put into perspective in the next section, Copenhagen is actually one of the places where the amount of cloudbursts will have the largest increase with a high CO_2 level in the future.
An important tool in analysis of cloudburst cases is the local soundings, because they provide valuable measurements for vertical profiles of the troposphere, so that better criteria for cloudburst potential can be established. To formulate an overall description for the formation of cloudbursts in Denmark, analysis of all cloudburst events would be required, which there was neither time or space for in this thesis. With that said, the analyses in this thesis can help provide insight in how cloudbursts are formed and develop.
All in all, the conclusion for cloudburst formation in Denmark is that the right conditions must be met at a synoptic level with two different air masses meeting, which under the right stability conditions and wind conditions in combination with quasi-geostrophic forcing in connection with forcing in extratropical cyclogenesis can develop into cloudburst. The classic example derived from the analyzes is a low pressure system over the North Sea or the British Isles and warm and humid air from a high pressure ridge east of Denmark, where in a frontal zone associated with the low there can be thunder cells which later can be a cloudburst. However, it is local conditions that become the decisive trigger, e.g. the convective temperature, a jet streak, ocean/land distribution or convergence zones. Precisely these local conditions make it difficult to predict these events, but just as much to make completed analyzes.

7 Perspective Words About Cloudburst in a Future Climate

The analyzes in section 5 show that local circumstances are the decisive trigger for the formation of heavy rainfall events. In a warmer future climate, cloudburst incidents in Denmark will become more frequent - and this is despite the fact that the summers will be drier [52]. This is shown by DMI's climate atlas, which makes an overall data base for the future climate in Denmark.

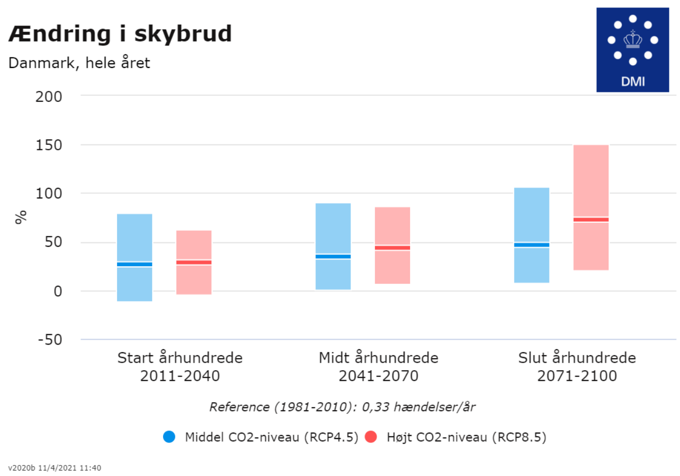

Figure 104: Percentage change in the frequency of cloudbursts in Denmark with the reference period 1981-2010 and the future periods 2011-2040, 2041-2070 and 2071-2100 in the scenarios RCP4.5 and RCP8.5. The expected change at the end of the century for RCP8.5 is 70 % (20 to 150 %). [52]

In figure 104, the percentage change of cloudburst is shown by a medium CO_2 level (blue) and a high CO_2 level (red) resp.. The reference period is 1981-2010 and the future periods are 2011-2040, 2041-2070 and 2071-2100 scenarios RCP4.5 (medium CO_2 level) and RCP8.5 (high CO_2 level), where RCP stands for Representative Concentration Pathway, which are realistic proposals for the development of the future global concentration of greenhouse gases in the atmosphere.

At the end of the period, 2071-2100, RCP8.5 expects a percentage increase in cloudburst events of 70 % with an uncertainty of 20 to 150 %, while RCP4.5 expects an increase of 44 % with an uncertainty of 7 to 106 %. There are thus clear indications that the number of cloudbursts per. years will increase on average. The uncertainty is very high in the different scenarios. Thus, the future scenarios have that there may be more cloudbursts in 2040 at a medium CO_2 level than can be done in the year 2100 at a high CO_2 level, if the uncertainties are kept in mind. Therefore, one must be careful when looking at these values. However, it can be argued that the major changes do not occur at a medium CO_2 level, while there are slightly clearer trends for more cloudbursts at a high CO_2 level.

The fact that there will be more cloudbursts in the future is not surprising, as studies show that the intensity of extreme rainfall will increase remarkably at higher temperatures, partly because convective plumes can receive more moisture from the surrounding atmosphere when the temperature rises [50].

However, there are variations nationwide. Figure 105 shows the change in the number of cloudburst incidents in the municipalities. At RCP4.5 (A), the largest changes are expected to occur in the southern part of the country and especially in the western part of Jylland, while at RCP8.5 (B) it is especially the capital area and areas in northern Jylland that can change in the number of cloudbursts with an increase of 80 %. What is behind these differences is a bit unclear - and statistically, according to DMI, there is no basis for saying that cloudbursts hit one place more than others.

Therefore, it may be questioned how well the climate atlas works. An example is two neighboring municipalities. As concluded in section 5, cloudbursts hit very locally. But as can be seen from figure 104A, there may be a difference between two municipalities that border on each other. E.g. has the climate atlas that at a medium CO_2 level there is a greater increase in the number of cloudbursts in Herning municipality in Jylland than there is in Viborg municipality, which are border municipalities to Herning. Why this difference? And why are the large differences almost offset national by a high CO_2 level? There is not much evidence to say where more cloudbursts immediately hit than elsewhere.

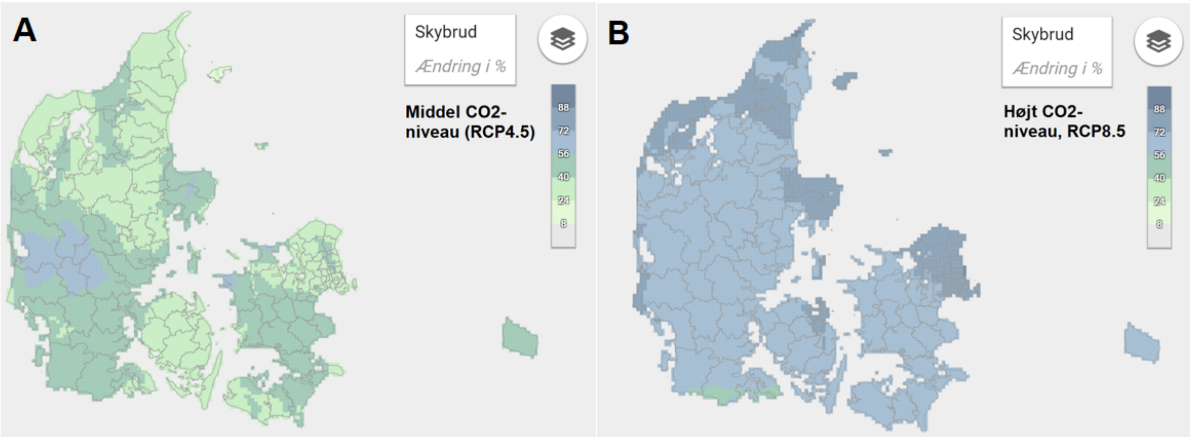

Figure 105: The percentage change between 1981-2010 and the future period 2071-2100 in the frequency of cloudburst precipitation over the year for the whole of Denmark in the scenario RCP4.5 (A) and RCP8.5 (B). Background map © The Danish Agency for Data Supply and Efficiency. [52].

However, there may be something about Copenhagen being additionally exposed to cloudbursts, as was mentioned in the conclusion. Near Copenhagen, there is a significant sea-land distribution, where the wind meets different resistance depending on whether it is above water or above a large urban area as Copenhagen where there is greater resistance due to buildings. Additionally, Copenhagen has a heat island effect that makes it easier to trigger cloudbursts over the capital than anywhere else in the country, but it requires a larger database and a different project focus to reach conclusions on this subject.

Taking the change in cloudburst events into account, there is a basis for addressing analysis in the future within the topic of cloudbursts, so that we will have an easier way to adapting to the climate which will offer more extreme cloudburst events.

8 Appendix

8.1 Appendix A: Abbreviations

CAPE	Convective Available Potential Energy
CAPPI	Constant Altitude Plan Position Indicator
CIN	Convective inhibition
DMC	Deep Moist Convection
DMI	Danish Meteorological Institute
EL	Equilibrium Level
EUMETSAT	European Organization for the Exploitation of Meteorological Satellites
GFS	Global Forecast System
HRV	High Resolution Visible
HRI	High Resolution Image
IR	InfraRed
KINX	K-index
LCL	Lifted Condensation Level
LFC	Level of Free Convection
LIFT	Lifted Index
LPP	Linear Perturbation Pressure
MCS	Mesoscale Convective System
MFG	Meteosat First Generation
MSG	Meteosat Second Generation
NCEP	National Centers for Environmental Prediction
NCAR	National Center for Atmospheric Research
NPP	Non-linear Perturbation Pressure
PVA	Positive absolute Vorticity Advection
PW	Precipitable Water
RHS	Right Hand Side
RCP	Representative Concentration Pathway
SEVIRI	Spinning Enhanced Visible and InfraRed Imager
SHOW	Showalter Index
SMC	Shallow Moist Convection
SVK	Spildevandskomiteen
TOTL	Total Total Index
VIS	Visible
WCB	Warm Conveyor Belt
WMO	World Meteorological Organization
WV	Water Vapour

8.2 Appendix B: Low-Topped Supercell

Figure 106: Low-topped supercell north of Topeka, close to Kansas City, USA. A tornado was produced to the left. Photo: James Wilson, `https://stormtrack.org/community/threads/low-topped-supercell-produces-tornado.30748/`

8.3 Appendix C: The 43 Largest 10-minutes Intensities, 1984-2019

$\mu m/s$	mm/min	Date	Locality
52.00	3.12	02-07-2011	Ishøj Varmeværk
48.67	2.92	23-06-2016	Ærøskøbing Renseanlæg
45.00	2.70	27-08-2011	Måløv Renseanlæg
42.33	2.54	11-07-2008	Copenhagen
41.67	2.50	22-05-2014	Jelling
41.33	2.48	15-07-2009	Sulsted
40.67	2.44	21-08-2006	Nørresundby
40.33	2.42	02-07-2011	Lygten
39.67	2.38	02-07-2011	Delfinen
38.00	2.28	02-07-2011	Avedørelejren
38.00	2.28	26-08-2011	Odense Korup
38.00	2.28	09-06-2017	Vejle Pumpestation
37.33	2.24	02-07-2011	Lygten
37.00	2.22	29-07-2016	Odense NV Renseanlæg
36.67	2.20	07-08-2019	Vejle Centralrenseanlæg
36.67	2.20	02-07-2011	Kløvermarksvej
36.67	2.20	21-06-2005	Skive
36.00	2.16	14-07-2012	Holbæk Renseanlæg
35.67	2.14	02-07-2011	Brøndbyvester Vandværk
35.67	2.14	02-07-2011	Elmegården
35.48	2.13	23-09-1988	Viby, Jylland
35.33	2.12	07-08-2019	Vodskov
35.33	2.12	18-06-2012	Rønne C
34.67	2.08	11-08-2007 + 14-06-1997	Brøndby + Sønderborg
34.33	2.06	11-08-2007	Copenhagen
33.67	2.02	30-07-2017	Slagelse Centralrenseanlæg
33.33	2.00	10-08-2019	Kalundborg + Hornbæk
33.33	2.00	07-08-2005 + 10-12-1987	Tårnby + Herning
33.00	1.98	10-08-2009	Gistrup
32.67	1.96	01-08-2002 + 02-08-2000	Mosede + Slagelse
32.33	1.94	30-07-2019	Viborg + Horsens
32.33	1.94	04-07-1988 + 01-08-1996 + 04-08-1997	Sulsted + Holbæk + Ishøj
32.00	1.92	29-07-1986 + 23-06-2007 + 19-07-2012 + 25-07-2016	Copenhagen + Vejle + Jyllinge + Frederikssund

Table 3: The 43 largest mean intensities over 10 minutes, 1984-2019, calculated for all stations from SVK [1]

8.4 Appendix D: Locations

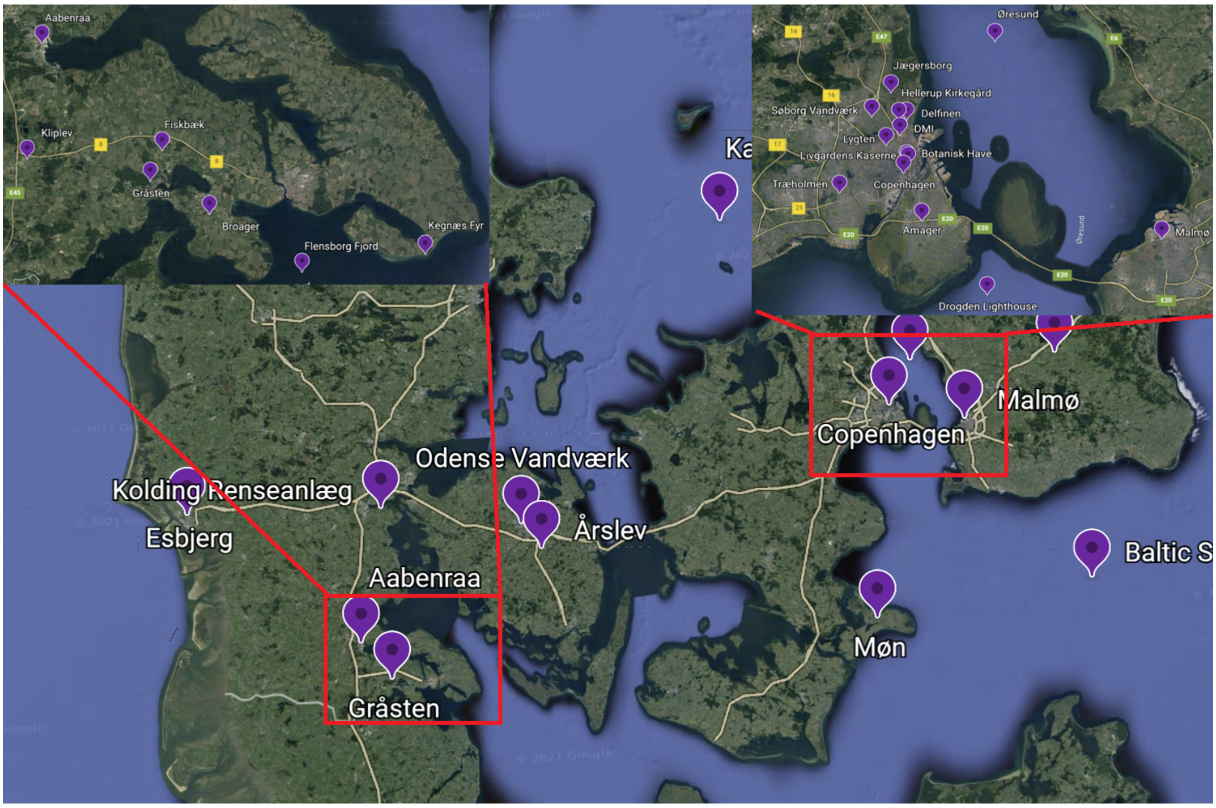

Figure 107: Different locations in Denmark mentioned in the analysis. The map is from Google Earth.

8.5 Appendix E: Sounding in the warm air, 1997

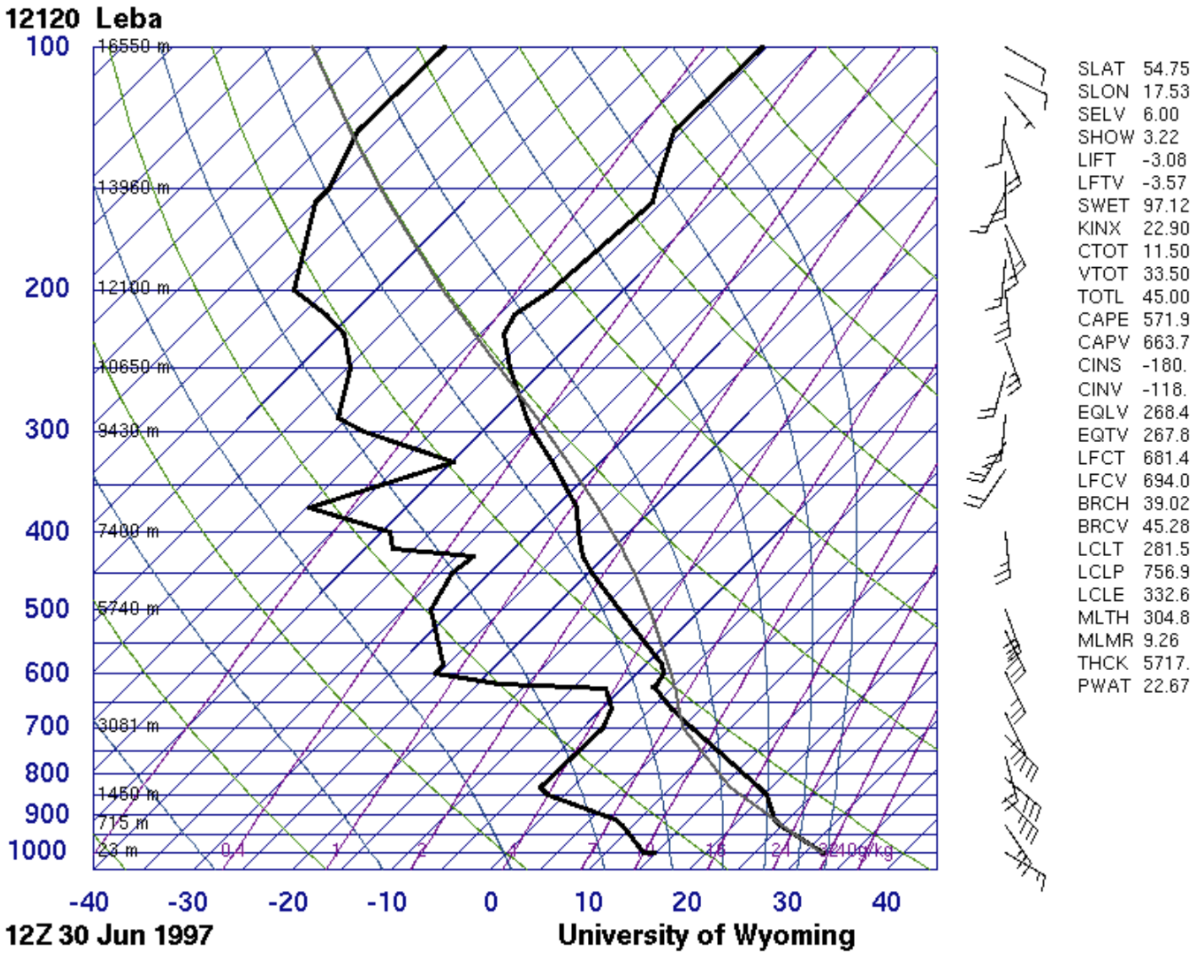

Figure 108: Sounding from Leba, Poland, 12UTC, 30th of June 1997. Same description as figure 36. This sounding was farther inside the warm air this day and thus had higher values of CAPE than the sounding in Jægersborg (figure 36).

8.6 Appendix F: Jet Streaks

Jet streaks are a local wind maximum on the jet stream. Jet streaks can be a contributing factor to trigger severe thunderstorms and are often associated with troughs or ridges. Jet streaks can have wind speeds of more than 50 m/s.

The reason why a jet streak may be a favorable condition for thunderstorms to develop is the rising air associated with the jet streak. Somewhere in a jet streak is more favorable for the rising or sinking of air. Upper level convergence results in sinking motion and upper level divergence results in rising motion. Convergence and divergence are the results of an imbalance of forces when an air parcel accelerates in a jet streak and later accelerate out of the jet streak again. Figure 109 shows divergence and convergence below a stragiht jet streak (A), cyclonically jet streak (B) and anticyclonically jet streak (C) respectively.

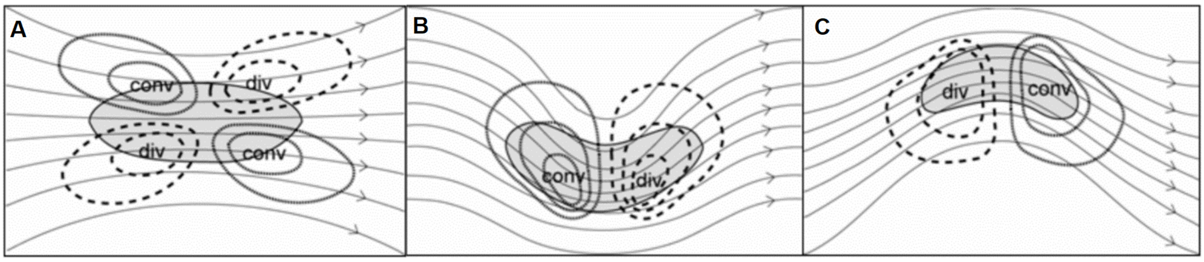

Figure 109: Divergence and convergence for a straight jet streak (A), a cylonically curved jet streak (B) and a anticyclonically curved jet streak (C). Photo: `https://www.estofex.org/guide/1_3_2.html`.

Based on quasi-geostrophic arguments, it can be argued that in a jet streak, air rises in the right entrance area and left exit area, while air sinks below the left entrance area and right exit area. During temperature advection, the ascent areas during warm advection will move closer to the jet axis and further away from the jet axis during cold advection. The opposite applies to the subsidence areas. The result is that thunderstorms will most often occur in the right entrance region.

8.7 Appendix G: Extratropical Cyclones

Extratropical cyclones (also called mid-latitude cyclones) are a large low-pressure system with clouds, rain and strong winds. in contrast to DMC, the vertical motion in an extratropical cyclone is much weaker. Typically air parcels enter at the surface and reach the top of the cyclone at the tropopause [51] after 1000 km.

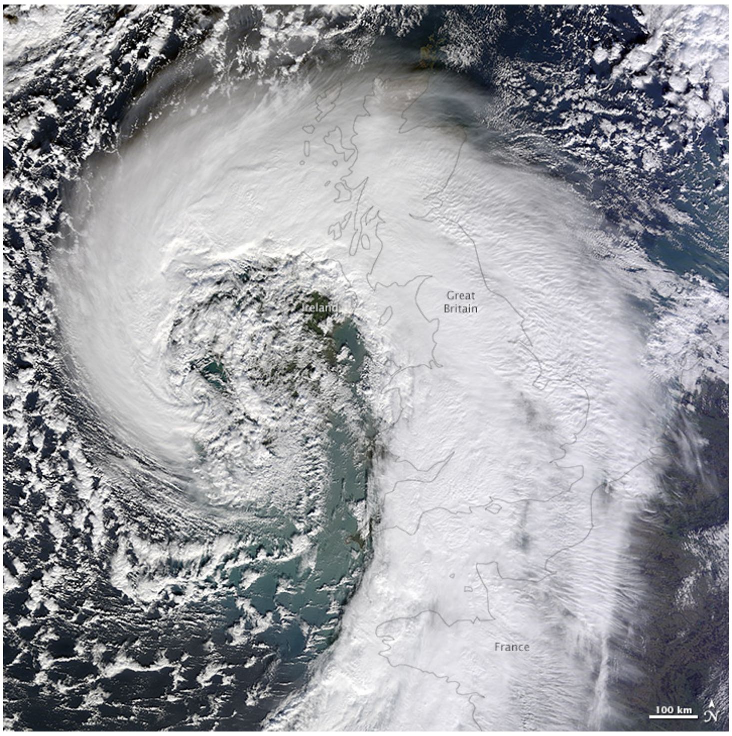

Figure 110: Extratropical Cyclone over the United Kingdom. Photo: NASA Earth Observatory image by Jesse Allen, using data from the Land Atmosphere Near real-time Capability for EOS (LANCE).

Extratropic cyclones are divided into primary and secondary cyclones. The primary lows occur in large baroque zones and have a slow development from 2 to 4 days. They have a large horizontal scale. The secondary lows occur along fronts and develop faster, typically within 1 to 3 days and have a small horizontal scale, about 1000 km. Ie. extratropical cylones is a shallow phenomenon with a vertical to horizontal dimension of 10^{-2} ($10\ km/1000\ km$), whereas e.g. cumulosnimbus clouds are of the order of 1 ($10\ km/10\ km$).
The deepening of an extratropical cyclone is a result of the conversion of available potential energy into kinetic energy. This conversion leads to a lowering of the center of the air mass involved in the extratopical cyclogenesis. Intensification of extratopical cyclogenesis can occur by release of latent heat in the rise of warm and moist air. Extratopical cyclogenesis is a type of instability that involves positive feedback mechanisms between advective and diabatic processes in the atmosphere and can be described with the quasigeostrophic approximations [51].

8.8 Appendix H: Thunder cells in Europe on 14th of June 2019

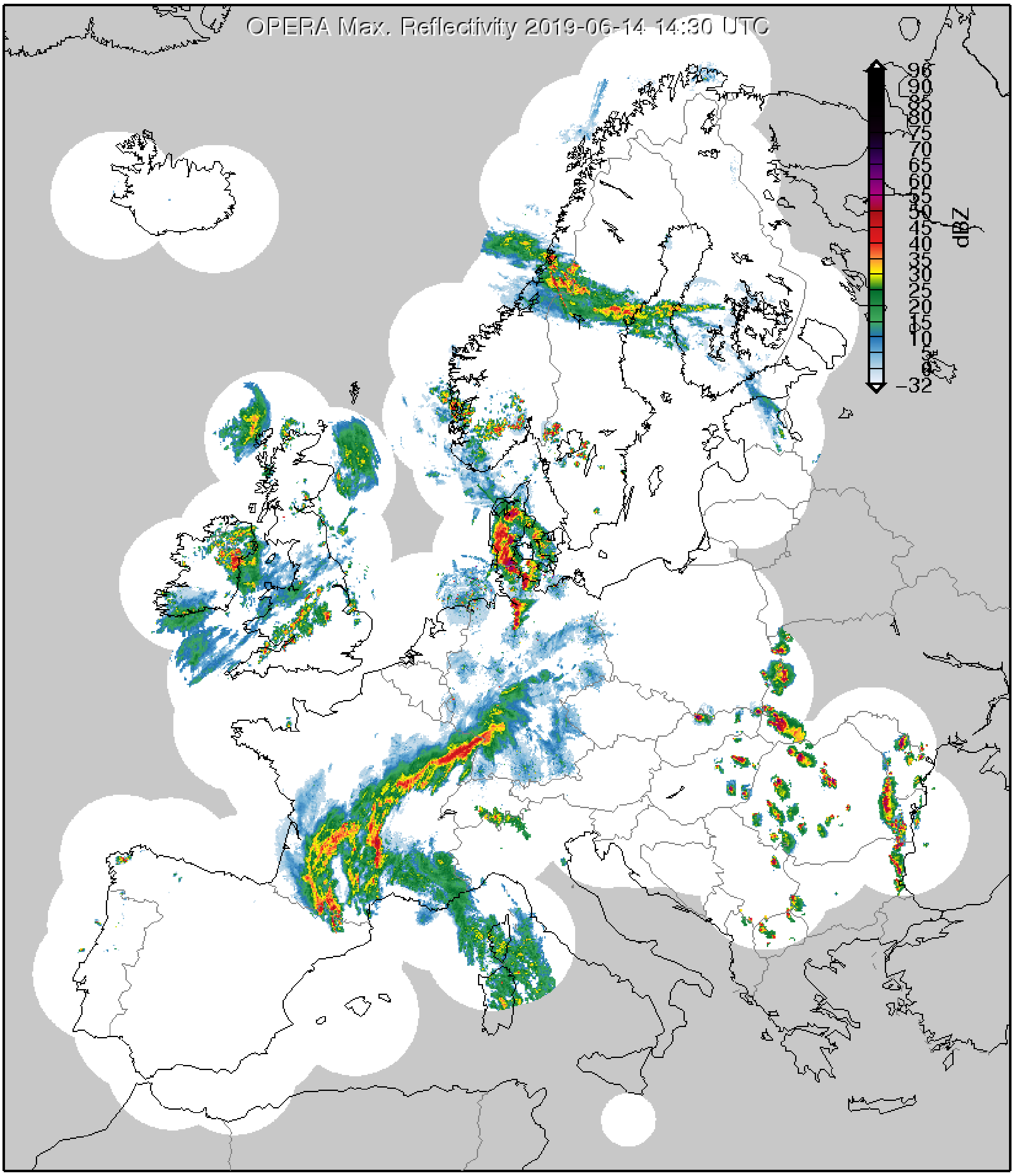

Figure 111: Reflectivity (dBZ) from the European radar netowork, OPERA, 14th of June 2019, 14.30UTC. The radar image are generated by Thomas Bøvith, DMI.

References

[1] John Cappelen *Ekstreme nedbørhændelser i Danmark - opgørelser og analyser til og med 2019*. DMI Rapport 20-06, Copenhagen 2020.

[2] Allen, M.R., O.P. Dube, W. Solecki, F. Aragón-Durand, W. Cramer, S. Humphreys, M. Kainuma, J. Kala, N. Mahowald, Y. Mulugetta, R. Perez, M.Wairiu, and K. Zickfeld *Global Warming of 1.5 °C. An IPCC Special Report on the impacts of global warming of 1.5 °C above pre-industrial levels and related global greenhouse gas emission pathways, in the context of strengthening the global response to the threat of climate change, sustainable development, and efforts to eradicate poverty*. IPCC, 2018: Framing and Context.

[3] *Visible*. Future Learn. `https://www.futurelearn.com/info/courses/learn-about-weather/0/steps/28922`. Visited 14-04-2021.

[4] Chris Webster. *Convergence lines and sea breezes*. MetService Blog. `https://blog.metservice.com/SeaBreezes`. 17-10-2012. Visited 02-04-2021.

[5] Man Kong Yau. *Perturbation Pressure and Cumulus Convection*. Journal of the Atmospheric Sciences, volume 36, April 1979.

[6] Ted Funk. *A Practical, Basic Guide to Quasi-Geostrophic Theory Response to Geostrophic Deformation Ageostrophic Motion Jet Streask* . Science and Operations Officer, National Weather Service, Louisville, Kentucky February 2011.

[7] T. Weidauer, C. Junghans, O. Pauluis, M. Pütz and J. Schumacher. *Shallow Moist Convection*. February 2010.

[8] Jessica Vial, Sandrine Bony, Bjorn Stevens and Raphaela Vogel *Mechanisms and Model Diversity of Trade-Wind Shallow Cumulus Cloud Feedbacks: A Review*. Surveys in Geophysics, volume 38, 14-07-2017.

[9] *Cumulus humilis*. International Cloud Atlas. `https://cloudatlas.wmo.int/en/cumulus-humilis.html`. 2017 edition. Visited 24-01-2021.

[10] Chien-Ming Wu, Bjorn Stevens and Akio Arakawa *What Controls the Transition from Shallow to Deep Convection?*. Journal of the atmospheric sciences, volume 66, June 2009.

[11] Howard B. Bluestein. *Synoptic-Dynamic Meteorology in Midlatitudes*. Oxford University Press, volume 2, first edition, 1993.

[12] Paul Markowski and Yvette Richardson. *Mesoscale Meteorology in Midlatitudes*. Wiley-Blackwell, first edition, 2010.

[13] Niels Woetmann Nielsen, DMI. *Aabenraa tornadoen*. Vejret, p. 21-31, volume 41, no. 4, November 2019.

[14] Jeremy Kappell. *Types of Thunderstorms and the Dangers they Pose*. WDRB.com. `https://fox41blogs.typepad.com`. 28-05-2014.

[15] Herman F. Fuglestvedt and Jan O. Haerter. *Cold Pools as Conveyor Belts of Moisture*. Geophysical Research Letter, Volume 47, June 2020.

[16] Christopher Moseley, Cathy Hohenegger, Peter Berg and Jan O. Haerter. *Intensification of convective extremes driven by cloud-cloud interaction*. Nature Geoscience, October 2015.

[17] R. Jeffrey Trapp, National Oceanic and Atmospheric Administration. *Thunderstorms, Severe*.

[18] Wikipedia *Supercell*. `https://en.wikipedia.org/wiki/Supercell`. Last edited 13-05-2021. Visited 14-05-2021.

[19] National Weather Service. *Mini Supercell Thunderstorms*. `https://www.weather.gov/lmk/mini_supercell`. NOAA Visited 14-04-2021.

[20] Robert A. Houze. *Cloud Dynamics*. Academic Press, first edition, page 349, 1993.

[21] Richard H. Johnson and Paul J. Hamilton. *The Relationship of Surface Pressure Features to the Precipitation and Airflow Structure of an Intense Midlatitude Squall Line*. Monthly Weather Review, volum 116, page 1468, 1988.

[22] Sebastian Pelt and Andreas Nyholm, TV 2 Vejret. *Tornado over Aabenraa den 14. juni 2019*. Vejret, p. 16-20, volume 41, no. 3, August 2019.

[23] Thomas Mørk. *Særlig skypumpe set i Nordjylland*. `https://vejr.tv2.dk/2019-09-28-saerlig-skypumpe-set-i-nordjylland`. TV 2, 28-09-2019. Visited 15-04-2021.

[24] Sebastian Pelt. *Se videoen: Her bliver have raseret af kraftigt uvejr*. `https://vejr.tv2.dk/2019-06-20-se-videoen-her-bliver-have-raseret-af-kraftigt-uvejr`. TV 2, 20-06-2019. Visited 15-04-2021.

[25] *Downburst*. Wikipedia. `https://en.wikipedia.org/wiki/Downburst`. Visited 15-02-2021.

[26] Thomas Mørk. *Husker du vejret den 2. juli 2011: Historisk skybrud ramte København*. `https://vejr.tv2.dk/2016-07-02-husker-du-vejret-den-2-juli-2011-historisk-sky\brud-ramte-koebenhavn`. TV 2, 02-07-2016. Visited 15-04-2021.

[27] Aalborg Universitet: *AAU weather radar nowcast* `http://www.vejrradar.dk/radar/`. Visited 28-12-2020.

[28] Shoichiro Fukao and Kyosuke Hamazu, consulted by Richard J. Doviak. *Radar for Meteorological and Atmospheric Observations*. Springer, 2014.

[29] Flemming Vejen, DMI. *Ekstrem regn i Sønderjylland 20-21. August 2007 belyst med radardata*. Vejret, p. 38-48, volume 30, no. 1, February 2008.

[30] C. G. Collier. *Applications of Weather Radar Systems: A Guide to Uses of Radar Data in Meteorology and Hydrology*. Ellis Horwood, 1989.

[31] Satellite images are ordered from the open source, EUMETSAT data centre archive: `https://www.eumetsat.int/eumetsat-data-centre`.

[32] *Meteosat Second Generation - The Satellite Development*. Europena Space Agency, November 1999.

[33] Kim Sarup. *Drift af Spildevandskomitéens Regnmålersystem*. Årsnotat 2018, DMI Report 19-03. København 2019.

[34] Wetter3: *Die ganze Welt in Wetterkarten* http://www1.wetter3.de/

[35] NOAA, Physical Sciences Laboratory: *6-Hourly NCEP/NCAR Reanalysis Data Composites* https://psl.noaa.gov/data/composites/hour/

[36] Larry Oolman, University of Wyoming: *Atmospheric soundings* http://weather.uwyo.edu/upperair/sounding.html. Visited 30-01-2021.

[37] Niels Woetmann Nielsen, Bjarne Amstrup and Claus Petersen. *Construction of a cloud burst index in numerical weather prediction*. DMI report 17-16, Copenhagen 2017.

[38] Thomas Mørk. *Husker du uvejret den 2. juli 2011? Historisk voldsomt skybrud ramte København*. https://vejr.tv2.dk/2018-07-02-husker-du-uvejret-den-2-juli-2011-historisk-voldsomt-skybrud-ramte\-koebenhavn TV 2, 02-07-2018. Visisted 05-05-2021.

[39] Henrik Vedel, DMI: *RainGate*. Power Point.

[40] Herdis Preil Damberg, DMI: *Skybrudssæsonen er begyndt* https://www.dmi.dk/nyheder/2019/skybrudssaesonen-er-begyndt/. 23-05-2019. Visited 17-04-2021.

[41] Niels Woetmann Nielsen and Leif Rasmussen, DMI. *Tordenstormen over København den 30. juni 1997*. Vejret, p. 1-14, volume 19, no. 3, August 1997.

[42] Niels Woetmann Nielsen, DMI. *Uvejret Skt. Hans Aften 2003*. Vejret, p. 10-21, volume 25, no. 3, August 2003.

[43] *National Meteorological Library and Archive*. Fact sheet No. 10 – Air masses and weather fronts, Met Office.

[44] Niels Woetmann Nielsen, DMI. *Et regnskyl af dimensioner: Skybruddet ved Gråsten i Sønderjylland den 20. august 2007*. Vejret, p. 24-32, volume 30, no. 1, February 2008.

[45] Anders Brandt, TV2 Vejret. *Uvejret den 20. august 2007*. Vejret, p. 33-36, volume 30, no. 1, February 2008.

[46] Niels Woetmann Nielsen, DMI. *Skybruddet over København den 2. juli 2011*. Vejret, p. 12-22, volume 33, no. 3, August 2011.

[47] Niels Woetmann Nielsen, DMI. *Multi-skybruddet over København og Malmø den 31. august 2014*. Vejret, p. 7-18, volume 36, no. 4, November 2014.

[48] K. A. Browning. *The Structure and Mechanisms of Hailstorms*. American Meteorological Society, Meteor, volume 16, page 1-43, 1977.

[49] Niels Woetmann Nielsen, DMI. *Skybrud og kraftig regn i Sydskandinavien på tærsklen til efteråret 2015*. Vejret, p. 27-37, volume 37, no. 4, November 2015.

[50] Peter Berg, Christopher Moseley and Jan O. Haerter. *Strong increase in convective precipitation in response to higher temperatures*. Nature Geoscience, p. 181-185, volume 6, March 2013.

[51] Niels Woetmann Nielsen. *Quasigeostrophic interpretation of extratropical cyclogenesis*. Danish Meteorological Institute, Copenhagen, August 2003.

[52] Peter L. Langen, Fredrik Boberg, Rasmus A. Pedersen, Ole B. Christensen, Alan Sørensen, Marianne S. Madsen, Martin Olesen, Max Darholt. *Klimaatlas-rapport Danmark*. DMI, June 2020.